

Exoskeletons in construction and their role in the Future of Work*

Sean T. Bennett, Peter G. Adamczyk, Fei Dai, Dharmaraj Veeramani, Michael Wehner, and Zhenhua Zhu

Abstract— The construction trade requires repetitive, physically demanding manual tasks which can over time pose severe risks for work-related musculoskeletal disorders (WMSDs) [1]. Exoskeletons and exosuits (collectively called “EXOs” in this work) have substantial potential to protect workers and to increase worker productivity by reducing exertion and fatigue. Despite these potential benefits, EXOs are uncommon in the construction industry. We present preliminary results from a pilot study investigating the knowledge gaps and barriers to EXO adoption.

The overall objective of this work is to establish a foundational understanding of how EXOs can transform the future of construction trade work. The described work focuses on industry collaboration and field-based kinematic evaluation of four subjects performing a real-world construction task, namely dumping a gondola of refuse into a bin. Our preliminary findings build a foundation of understanding of EXO-enabled construction tasks. This will foster EXO adoption and yield benefits including but not limited to improving the productivity of construction trades, reducing the risks of WMSDs and injuries of trade workers, broadening the workforce participation in construction trades, and extending the career life expectancy of existing trade workers.

I. INTRODUCTION

The context for our research is the construction industry, specifically the occupation categories within Construction Trades Workers (“47-2000”), with a focus on “47-2061.00 - Construction Laborers”, “47-2031.00 - Carpenter”, “47-2111.00 - Electricians”, “47-2152.00 - Plumber, Pipefitter, and Steamfitter”, and “47-2171.00 - Reinforcing Iron and Rebar Workers”. These trades represent around 2.76 million workers under the occupation category of Construction and Extraction (“47-0000”) [1]. Workers in these trades are typically required to perform physically demanding job tasks, such as digging holes or trenches, loading/unloading materials, removing debris and garbage, installing doors and windows, building frameworks, installing plumbing or piping, etc. These common tasks require sustained and repeated extreme postures (kneeling, crouching, stooping),

which exposes them to a severe risk for WMSDs resulting in occupational injuries and illnesses [2]. According to the reports from the Bureau of Labor Statistics (BLS), the average injury and illness incidence rate in 2011-2018 reached up to 50.7 cases per 10,000 full-time construction workers [3]. This statistic is a conservative estimate since it excludes unreported cases and incidents not resulting in loss of working days.

On the other hand, although the trades workers primarily do physical work, they continually solve unique challenges while performing highly varying tasks in dynamic, unstructured, and unpredictable work environments. As a result, much of their work has a low potential for automation and is infeasible to be replaced entirely by robots [4]. In this regard, EXO technology shows great promise for making construction tasks more efficient, safer, and accessible to a broader set of workers.

The benefits envisioned with EXO-enabled construction work are manyfold. First, it can extend the career span of existing midcareer tradespeople, protecting them from potential WMSDs and/or acute injuries resulting in loss of working days. Second, it can expand the skilled trades workforce by attracting candidates into the trades who may otherwise not consider such jobs due to their physically demanding nature. Women represent only about 2.5% of tradespeople [5], which could be greatly increased by the adoption of EXOs in trade jobs. Third, the performance gains achieved by EXO-enabled work can help increase productivity in the construction industry. Over the past two decades, global productivity has grown by 2.8% annually; the construction industry, however, has only grown by 1% [6]. The construction industry accounts for a significant portion of the economy and it is still booming. Growth of nearly 35% to \$5.8 trillion worldwide by 2030 is anticipated despite the coronavirus pandemic, and the U.S. would contribute ~12% of that growth [7]. The construction industry faces an increasingly severe shortage of qualified workers against a rapidly increasing demand. 44% of construction firms reported that projects have taken longer than originally anticipated, and 43% reported that costs have been higher due to workforce shortages [8]. Also, many current skilled workers were asked to work more, increasing their risk of WMSDs, injury, and illness [9]. In a recent survey conducted by McKinsey & Company, 87% of the respondents believed that the shortage of skilled workers had a high impact on the construction industry, and almost 50% of respondents expected this to worsen over the next decade [10]. With the passing of the \$1 Trillion Infrastructure Bill in 2021 [11], it has become imperative that we address the need for growing the trades workforce and improving industry productivity.

Although EXOs promise many significant benefits, their adoption currently in the construction industry is minimal,

*Research supported by the National Science Foundation.

Z. Zhu is with the Civil and Environmental Engineering Department, University of Wisconsin, Madison, Madison, WI. 53706 USA (corresponding author: (608) 265-3228; zzhu286@wisc.edu).

S. T. Bennett, P. G. Adamczyk, M. Wehner, are with the Mechanical Engineering Department, University of Wisconsin, Madison, Madison, WI. 53706 USA (e-mails: stbennett2@wisc.edu, peter.adamczyk@wisc.edu, wehner2@wisc.edu respectively).

F. Dai is with the Civil and Environmental Engineering Department, West Virginia University, Morgantown, WV. 26506 USA (e-mail: fei.dai@mail.wvu.edu).

D. Veeramani is with the Industrial and Systems Engineering Department, University of Wisconsin, Madison, Madison, WI. 53706 USA (e-mail: raj.veeramani@uwebc.wisc.edu).

primarily due to a lack of understanding of how EXOs can transform construction tasks and the associated benefits and broader impacts. Our research based on field experiments at construction sites aims to address this critical knowledge gap, and thereby help improve EXO-worker partnership and promote EXO usage in construction.

II. METHOD

A. Defining EXOs

This work describes a task performed unassisted and assisted using a passive lower-back EXO (HeroWear, Apex, passive lower-back exosuit), more suited for the construction industry, compared with active EXOs [12]. Through these experiments, our aim was to gain insights into how EXOs impact the task and the worker and to develop a deeper understanding regarding incompatibility between construction task requirements versus EXO form factor and capabilities. Most existing EXOs rely on the fixed-axis rotation hinges for joints, which do not accurately mimic how worker limbs move in construction settings. As a result, the worker's mobility in an EXO does not reflect natural movement and has limited versatility. Both discomfort and limited range of motion can make some EXOs unappealing to workers for some tasks, and therefore pose a barrier to EXO use by construction trade workers [13, 14].

B. Defining the Task

Previous EXO evaluation studies in construction have focused primarily on EXO functionalities to reduce muscle fatigue, perceived exertion, and metabolic cost. They measured test subjects' oxygen consumption, muscle activities, etc., when subjects wear EXOs and perform simple tasks (e.g., static holding and lifting) in controlled laboratory environments (e.g., [15, 16]). In these studies, test subjects are typically not professional workers with years of working experience, and the test period is short. Therefore, the process of executing construction tasks and the postures assumed during these tasks are not representative of the real workplace. Field-based evidence is critical to support the safe adoption and use of EXOs in practice, as it provides an understanding of EXOs' true effectiveness, practicality, safety, and user acceptance [17, 18]. However, existing EXO field tests are limited to automotive assembly (e.g., [19 – 22]), manufacturing (e.g., [23]), warehousing (e.g., [24, 25]), and agriculture (e.g., [26, 27]) settings. Compared with these field test settings, construction workplaces are more cluttered, unstructured, and dynamic.

C. Experimental Procedure

We partnered with an industry-leading construction contractor to evaluate workers as they performed a typical construction task with and without an EXO. The task consisted of dumping a loaded gondola (wheeled cart) from an elevated platform into another cart. The loaded cart had a mass of 120 kg (265 lb), and the unloaded cart had a mass of 64kg (140 lb). This task required repetitive high-force operations on the lower back. This task is common on construction sites, as gondolas loaded with construction refuse are dumped into trash receptacles throughout the construction process.



Figure 1. Worker wearing the Hero Wear Apex EXO (Left), pushing then dumping (middle), screen capture from video of motion capture (Right).

Four workers (male, age 25 to 61 with 4–35 years in their current jobs) participated in the task. Workers performed their tasks in an unassisted state (no EXO) and with an EXO for assistance (Fig. 1). To reconstruct full-body kinematics, the test subject donned a suite of wearable movement sensors (XSens MVN Awinda). Videos were also recorded. For the dumping task, each subject performed ten full cycles over roughly 15 minutes without EXO. Next, the subject donned the EXO and performed an additional ten cycles. All subjects were requested to complete a survey on comfort, pain, and perceived effectiveness of using EXOs.

III. RESULTS

Results from these tests suggested changes in body kinematics from using the EXO while performing the dumping task versus performing the same task without EXO assistance. The results are summarized with mean \pm SD in Table 1. Pelvic forward inclination data for four subjects is shown in Figure 2. Angle is presented as pelvis deviation from vertical (0°), viewed in the sagittal plane. Forward bending is positive and leaning backwards is negative. These are roughly equivalent to trunk flexion and extension if the legs were constraint to a neutral posture. While the mean pelvic angle during the dumping process showed little change (19° for both Herowear and no Exo cases), standard deviation was greatly reduced for workers wearing the Herowear EXO (8° vs 4°). Inner quartile range (IQR) and 5–95% range of motion (ROM) data similarly show sizeable drops in standard deviation while workers wore the Herowear EXO. This preliminary data suggests that wearing the EXO may not reduce the mean trunk incline angle. However, the preliminary results suggest that wearing the Herowear EXO may reduce the occurrence of very extreme postures during the dumping task.

Further, the EXO enabled three of four subjects to reduce their mean forward trunk lean angle during the dumping activity (Fig. 2). Reduced forward trunk lean may indicate reduced exertion of the hip and lower back muscles, consistent with the EXO's intended effect. Because the EXO also provides a hip extension moment to assist the lift, the reduced exertion may be further compounded.

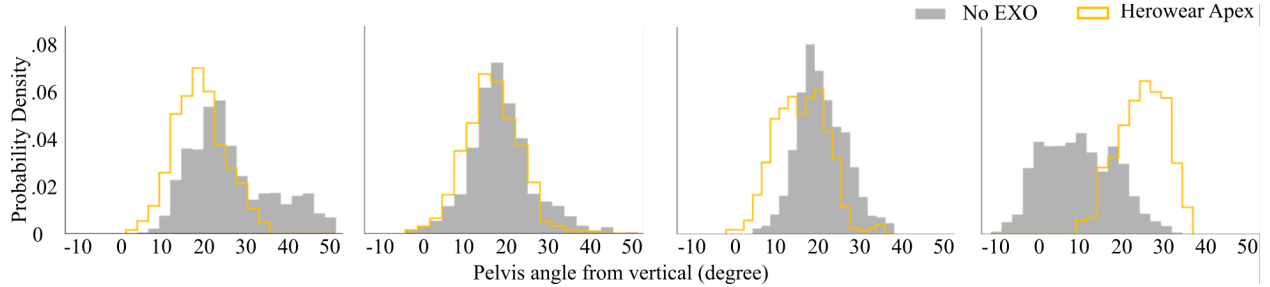


Figure 2. Results for 4 subjects. Changes in movement kinematics, unassisted and while wearing an exoskeleton while dumping a gondola of refuse into a larger cart.

These results validate the approach of using wearable movement sensors to evaluate the effects of EXOs during in-field construction tasks. These effects should be evaluated using task-specific metrics, such as trunk lean in lifting or pushing and shoulder flexion and abduction for overhead work, to minimize the presence of non-targeted movements in the data. Because our approach uses whole-body movement reconstruction along with task video, we can isolate specific portions of a task for analysis. Similar approaches for assessing specific tasks captured in long-term real-world monitoring have proven to reduce variability in the data and strengthen results [28].

TABLE I. RANGE OF MOTION

Condition	Pelvis Angle from Vertical (degree)		
	Mean \pm S. D.	IQR (25-75%)	ROM (5-95%)
No EXO	19 \pm 8	11 \pm 3	27 \pm 6
HeroWear Apex	19 \pm 4	8.7 \pm 0.3	19.9 \pm 0.8

The workers completed a survey asking on a scale of 1 (strongly disagree) to 5 (strongly agree) regarding satisfaction with the EXO and intent to use the EXO in the future. Satisfaction yielded an average score of 2.4, and intent to use in the future yielded a score of 2.2 (Table 2). No worker answered 5 for either question, and one worker responded 1 to each question. The workers most liked the support provided by the EXO when performing the task. They mentioned that the EXO helped them keep their backs aligned and under less perceived stress. On the other hand, the workers disliked the movement restraints imposed by the EXO as well as uncomfortable feelings due to the tightened straps on legs when wearing EXOs. One worker reported pain, soreness, or discomfort when wearing the EXO.

TABLE II. SURVEY RESULTS

	Number of Responses	
	Satisfied	Intend to use
(Strongly Disagree) 1	1	1
2	0	0
3	1	2
4	2	1
(Strongly Agree) 5	0	0
Mean Score:	2.4	2.2

IV. DISCUSSION

Preliminary results have established the feasibility of executing a quantitative assessment of the effects of EXOs through controlled observational field testing in real construction tasks. Hence, in our future work, we plan to execute such tests in a variety of construction settings and tasks and evaluate outcomes measuring the effects of EXOs on biomechanics, performance, and productivity, in conjunction with traditional user experience outcomes. Potential tasks may include installation or removal of carpet squares or framing of wall segments laid on the floor. Finally, we will explore ways to instrument the EXOs themselves to further clarify their function. For example, we may measure the displacement of the clutched cable in the HeroWear Apex lower-back EXO with a string potentiometer, to understand how the user uses its locking/unlocking feature. Further instrumentation, such as instrumented insoles and electromyographic (EMG) sensors, can be employed to obtain valuable force and muscle activation data. Results from these further tests will serve as valuable tools for EXO manufacturers and construction organizations for improving future EXO designs and for planning EXO-enabled tasks.

ACKNOWLEDGMENT

This research was supported by the National Science Foundation via grants #CNS-2128823 and #CNS-2128716. The authors also acknowledge M.A. Mortenson Company for their collaboration on this research.

REFERENCES

- [1] U.S. Bureau of Labor Statistics (BLS) (2020). "Occupational Employment and Wage Statistics." <https://www.bls.gov/oes/current/oes_nat.htm#47-0000> (Feb. 07, 2022).
- [2] Zhu, Z., Dutta, A., and Dai, F. (2021). "Exoskeletons for manual material handling – A review and implication for construction applications", Journal of Automation in Construction, Vol. 122, February 2021, 103493, doi.org/10.1016/j.autcon
- [3] U.S. Bureau of Labor Statistics (BLS) (2020). "Nonfatal Occupational Injuries and Illnesses Requiring Days Away from Work." <<https://data.bls.gov/PDQWeb/cs>> (Jan. 12, 2022).
- [4] McKinsey & Company (2017). "Jobs lost, jobs gained: workforce transitions in a time of automation." McKinsey Global Institute, <<https://www.mckinsey.com/featured-insights/future-of-work/jobs-lost-jobs-gained-what-the-future-of-work-will-mean-for-jobs-skills-and-wages>> (Feb. 6, 2022).
- [5] BigRentz Inc. (2022). "Women in construction: the state of the industry in 2022." <<https://www.bigrertz.com/blog/women-in-construction>> (Feb. 9, 2022).

- [6] McKinsey & Company (2017). "Reinventing construction: a route to higher productivity." <<https://www.mckinsey.com/business-functions/operations/our-insights/reinventing-construction-through-a-productivity-revolution>> (Feb. 25, 2022).
- [7] Condon, M. (2020) "Global construction sector to grow 35% to 2030 on urbanisation, softer pandemic impact" <<https://www.icis.com/explore/resources/news/2020/09/11/10551509/global-construction-sector-to-grow-35-to-2030-on-urbanisation-softer-pandemic-impact>> (March 07, 2021).
- [8] Associated General Contractors (AGC) (2019), "2019 Worker Shortage Survey Analysis" <<https://www.agc.org/sites/default/files/Files/Communications/2019%20Worker%20Shortage%20Survey%20Analysis.pdf>> (Mar. 05, 2021).
- [9] Engineering News Record (ENR) (2016), "Labor gaps bring steady pay raises" <https://www.enr.com/ext/resources/Issues/National_Issues/2016/Oct-2016/10-Oct/ENR1010_QCR3.pdf> (Mar. 02, 2020)
- [10] McKenzie & Company (2020). "The next normal in construction: How disruption is reshaping the world's largest ecosystem" <<https://www.mckinsey.com/business-functions/operations/our-insights/the-next-normal-in-construction-how-disruption-is-reshaping-the-worlds-largest-ecosystem>> (Mar. 10, 2020).
- [11] New York Times (2021). "Senate Passes \$1 Trillion Infrastructure Bill, Handing Biden a Bipartisan Win." <<https://www.nytimes.com/2021/08/10/us/politics/infrastructure-bill-passes.html>> (Feb. 20, 2022).
- [12] Trimble Inc. (2019). "Exoskeletons for Construction Workers Are Marching On-Site", <<https://constructible.trimble.com/construction-industry/exoskeletons-for-construction-workers-are-marching-on-site>> (Feb. 11, 2022)
- [13] Kim, S., Moore, A., Srinivasan, D., Akanmu, A., Barr, A., Harris-Adamson, C., Rempel, D., Nussbaum, M. (2019). "Potential of exoskeleton technologies to enhance safety, health, and performance in construction: industry perspectives and future research directions", IIE Trans. Occup. Ergon. Human Fact. 7 (3–4) (2019) 185–191. doi.org/10.1080/24725838.2018.1561557
- [14] Koopman, A., Kingma, I., de Looze, M. van Dieën, J. (2019). "Effects of a passive back exoskeleton on the mechanical loading of the low-back during symmetric lifting", J. Biomech. 102 (2019) 109486, <https://doi.org/10.1016/j.jbiomech.2019.109486>.
- [15] Antwi-Afari, M., Li, H., Anwer, S., Li, D., Yu, Y., Mi, HY., Wuni, I. (2021). "Assessment of a passive exoskeleton system on spinal biomechanics and subjective responses during manual repetitive handling tasks among construction workers," Safety Science, Volume 142, 2021, 105382
- [16] Gonsalves, N., Omobolanle, O., Abiola A. and Chukwuma, N. (2021). "Assessment of a passive wearable robot for reducing low back disorders during rebar work." J. Inf. Technol. Constr. 26 (2021): 936-952.
- [17] Howard J, Murashov VV, Lowe BD, Lu M-L. (2020). "Industrial exoskeletons: need for intervention effectiveness research," Am J Ind Med. 2020; 63(3):201-208.
- [18] Nussbaum MA, Lowe BD, de Looze M, Harris-Adamson C, Smets M. (2019) "An introduction to the special issue on occupational exoskeletons," IIE Trans Occup Ergon Hum Factors. 2019;7(3–4):153-162.
- [19] Kim S, Nussbaum MA, Smets M, Ranganathan S. (2021). "Effects of an arm-support exoskeleton on perceived work intensity and musculoskeletal discomfort: An 18-month field study in automotive assembly," Am J Ind Med. 2021 Nov;64(11):905-914.
- [20] Kim S, Nussbaum MA, Smets M, (2021). "User Acceptance, and Health Outcomes of Arm-support Exoskeleton Use in Automotive Assembly: An 18-month Field Study," J Occup Environ Med. 2021 doi: 10.1097/JOM.0000000000002438.
- [21] Hefferle M, Snell M, Kluth K. (2021) "Influence of two industrial overhead exoskeletons on perceived strain—a field study in the automotive industry," In: Zallio M, (Ed.). Advances in Human Factors in Robots, Drones and Unmanned Systems. Cham: Springer; 2021:94-100.
- [22] Gillette J. and Stephenson M. (2019). "Electromyographic assessment of a shoulder support exoskeleton during on-site job tasks," IIE Trans Occup Ergon Hum Factors. 2019;7(3–4):302-310.
- [23] Amandels S, Eyndt HOH, Daenen L, Hermans V. (2018). "Introduction and testing of a passive exoskeleton in an industrial working environment," In Bagnara S, Tartaglia R, Albolino S, Alexander T, Fujita Y, (Eds.). Proceedings of the 20th Congress of the International Ergonomics Association (IEA 2018). Springer International Publishing; 2019:387-392.
- [24] Motmans R, Debaets T, Chrispeels S. (2018). "Effect of a passive exoskeleton on muscle activity and posture during order picking," In Bagnara S, Tartaglia R, Albolino S, Alexander T, Fujita Y, (Eds.). Proceedings of the 20th Congress of the International Ergonomics Association (IEA 2018). Springer International Publishing; 2019:338-346.
- [25] de Bock S, Ghillebert J, Govaerts R, et al. (2021). "Passive shoulder exoskeletons: more effective in the lab than in the field?," IEEE Trans Neural Syst Rehabil Eng. 2021;29:173-183.
- [26] Omoniyi A, Trask C, Milosavljevic S, Thamsuwan O. (2020). "Farmers' perceptions of exoskeleton use on farms: finding the right tool for the work(er)," Int J Ind Ergon. 2020;80:103036.
- [27] Thamsuwan O, Milosavljevic S, Srinivasan D, Trask C. (2020). "Potential exoskeleton uses for reducing low back muscular activity during farm tasks," Am J Ind Med. 2020;63(11):1017-1028
- [28] Wang, W. and Adamczyk, P. (2019). "Analyzing Gait in the Real World Using Wearable Movement Sensors and Frequently Repeated Movement Paths," Sensors, vol. 19, no. 8, p. 1925, Apr. 2019, doi: 10.3390/s19081925.

Vision-based Automated Flagging System in Construction*

Wei Han and Zhenhua Zhu

Abstract— Flaggers are a high-risk profession. They are always required to work closely with the open traffic lanes. Any distracted, speeding or intoxicated drivers might hit them, leading to their injuries and fatalities. From 1980 to 1992, a total of 54 fatalities involving flaggers in the construction industry have been reported. To protect flaggers and reduce their exposure to potential vehicular traffic, previous studies proposed and implemented the Automated Flagger Assistance Devices (AFADs). However, the AFADs have not been widely used in practice due to their costs. In addition to hiring a flagger to remotely operate an AFAD, the cost of an AFAD system alone ranges from \$25,000 to \$30,000 without the consideration of device maintenance. Instead of creating an assistance device, this paper proposed an automated flagging system (AFS) that can guide the traffic without the need for a flagger available on the site. The proposed system is composed of two modules: information capturing and decision-making. The information module is to monitor traffic conditions and retrieves useful information for the decision-making module to decide which sign (STOP or SLOW) to display in the LED panel. So far, a prototype was developed and tested in a laboratory environment. A vehicle detector was trained and integrated into the prototype. The laboratory test results indicated that the prototype could correctly show the STOP or SLOW sign based on the detection of simulated traffics.

I. INTRODUCTION

The United States roadway system contains around four million miles of roads [1]. The system is important in economics for communication and transportation. To keep the roads in a functional condition, the roads cannot be entirely closed for construction activities in most cases [2]. Thus, the workers in the work zones are in high-risk situations. From 2011 to 2015, a total of 279 fatalities related to vehicles were reported by the U.S. Bureau of Labor Statistics [3].

The use of flaggers on multi-lane highway work zones is a requirement of standard specifications for road construction in many State Departments of Transportation (DOTs) [4]. This makes flaggers becomes one of the most dangerous professions. They are required to work closely with the open traffic lanes, where physical barrier protections are not set up in most cases. They might be hit by any distracted, speeding, or intoxicated motorist, leading to injuries and fatalities. From 1980 to 1992, 54 fatalities involving flaggers were reported; and they were hit by

vehicles on the construction sites [5].

As a result, the concept of automated flagger assistance devices (AFAD) has been proposed to protect the safety of the flaggers. An AFAD aims to be operated remotely by a flagger positioned outside the traffic lanes. This way, it could reduce the exposure of the flagger to vehicular traffic. The AFADs developed in the early time were remotely controlled to switch between the stop and slow signs or between red and yellow lenses to alternate the right-of-way [6]. Recently, the AFAD developed by the Missouri Department of Transportation combined signs and lenses; and the device could be further mounted on a truck to increase its mobility [7].

Although the concept of AFADs has been proposed and developed for a while, they have not been widely adopted in practice. One possible reason behind this is that the device is not cost-effective at the moment. Although a flagger does not have to stay close to the traffic lane to guide the traffic with an AFAD, he or she is still required and gets paid to operate the device remotely. On the other hand, the price for purchasing or renting an AFAD did not drop significantly in the market. It was noted that the cost of a single AFAD system could range from around \$25,000 to \$30,000 or \$3,000 to \$3,200 per month [8]. As a result, construction contractors or project managers prefer flaggers rather than the use of AFADs.

Compared with AFADs, this paper proposed the concept of creating an AFS that can guide the traffic without the need or aid of a flagger. The system is composed of two modules, i.e., the information capturing module and the decision-making module. First, the information capturing module is responsible to monitor the traffic through visual object detection, tracking, and distance estimation. Based on the traffic information captured, the decision-making module determines which sign (STOP or SLOW) should be shown on an LED panel for the traffic guidance.

So far, the main hardware of the proposed system has been assembled into a prototype. A vehicle detector was trained and integrated into the prototype. The prototype was tested in a laboratory environment. The test results showed that the vehicle detector could detect 7 classes of vehicles commonly seen on road, such as trucks, dump trucks, motorcycles, and buses. Also, the prototype could determine which sign (STOP or SLOW) to show based on the detection of simulated traffics.

II. AUTOMATED FLAGGER ASSISTANT DEVICES

There are several AFAD products available in the market. They can be remotely operated by flaggers, keeping them away from the traffic lanes and reducing their possibility of being struck by vehicles. Virginia, Missouri,

*Research supported by Wisconsin Alumni Research Foundation.

Wei Han is with the Department of Civil and Environmental Engineering, University of Wisconsin – Madison, Madison, WI 53706 USA (e-mail: whan59@wisc.edu).

Zhenhua Zhu is with the Department of Civil and Environmental Engineering, University of Wisconsin – Madison, Madison, WI 53706 USA (corresponding author, phone: 608-265-3228; fax: 608-262-5199; e-mail: zzhu286@wisc.edu).

and Maine DOTs started to evaluate and deploy them to the field [9 - 11]. AFADs were added in the 2009 edition of the Manual on Uniform Traffic Control Devices (MUTCD) for the use of controlling traffic in temporary traffic control zones [12]. The standards of AFAD applications have been listed in the MUTCD Section 6E.04. For example, if the AFAD is operated at nighttime, it should be illuminated. Additionally, different states may adopt more strict AFAD application policies or standards. For instance, MUTCD does not have any limitation in average daily traffic (ADT) in general; however, Virginia Department of Transportation only allows AFADs to be applied when ADT is below 12,000 vehicles [8].

In MUTCD, AFADs have been divided into two types. The device in the first type only contains a remotely controlled STOP/SLOW sign. The STOP sign is designed to inform drivers to stop in front of the sign and wait for the next instruction. The SLOW sign means that drivers can pass through with caution. It was pointed out that approximately 25 percent of the drivers might misunderstand the meaning of STOP signs, and they just stop their vehicles for a moment and then proceed [13]. Therefore, it was recommended to put on additional explanations, such as “wait on stop” and “go on slow”, to help the drivers understand the actual meaning of the signs [13].

The device in the second type is equipped with a Red/Yellow light remotely controlled and a gated arm. When the light turns red, the gated arm would be lowered to stop the traffic. When the light turns yellow, the gated arm would rise to let vehicles pass. Existing studies [13,14] showed that most of the drivers could understand the operation of the AFAD with the gated arm.

In addition to these two types of AFAD devices, the Missouri DOT proposed the AFADs that could be truck-mounted on trucks. The AFADs are equipped with STOP/SLOW signs, Red/Yellow lights, and a changeable message sign (CMS) [9]. The lights and CMS could make the drivers spot the AFAD far away and facilitate their understanding so that they could slow their vehicles earlier.

III. PROPOSED SYSTEM

A. System Overview

The proposed system is composed of two modules, i.e., the information capturing module and the decision-making module. To monitor the traffic conditions, the information capturing module collects and processes the video streams into objects with information on categories and actions. The action information of the objects is presented as approaching or leaving. Once the object information is obtained, the module leverages object tracking and action detection. Then, the object category and action information are fed to the decision-making module. The module gives a SLOW or STOP signal to the sign controlling module to show “STOP” or “SLOW” in the sign display panel.

B. Information Capturing

The information capturing module is to monitor traffic conditions on lanes and retrieves useful information as inputs to the decision-making module. Here, the traffic

information of interest includes vehicle categories, quantities, and actions. The vehicle categories and quantities are retrieved through the detection and tracking of construction and non-construction vehicles, such as dump trucks, motorcycles, and buses. This way, the proposed system could know how many and what kinds of vehicles tend to go through. The vehicle actions include approaching, leaving, and idling, where the approaching is further identified as to whether the vehicle intends to enter the construction site.

C. Decision Making

The decision-making module determines which sign (STOP or SLOW) to show in the sign panel to guide and control traffic. Here, two scenarios are defined. The first scenario is referred to as the non-shared lane (NSL) scenario. It means that the vehicles in different directions do not need to share the same lane, as shown in Figure 1(a). The second scenario is the shared lane (SL) scenario. It indicates that a lane is temporarily closed and the vehicles in different directions need to share one lane, as shown in Figure 1(b).

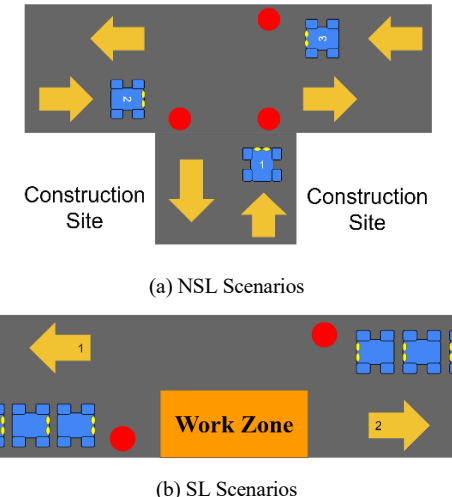


Figure 1. Examples of NSL and SL Scenarios

To guide the construction vehicles (e.g., trucks, excavators, backhoes, and loaders) that tend to enter or leave the construction site, three conditions in the NSL scenario are analyzed in general. When there are no vehicles in all the directions, all the devices show SLOW. When construction vehicles are coming from one direction, the device responsible for monitoring that direction shows SLOW, and others show STOP. When construction vehicles come from multiple directions, it is necessary to prioritize them and determine which one goes first. Here, the vehicle leaving the construction site is always given the highest priority. As for the vehicles in other directions, the vehicle turning left should always yield the right of way. Take Figure 1(a) for an example. Vehicle 1 that is leaving the construction site owns the highest priority; thus, it goes first. Then, vehicle 2 waits for vehicle 1 to go, because vehicle 1 turns right to enter the construction site. After vehicles 1 and 2, vehicle 3 can enter the construction site.

In the SL scenario, four conditions are analyzed in general to guide the vehicles in both directions to pass by the

work zone safely. When no vehicles are coming from both directions, two devices show STOP. When vehicles are coming from one direction, the device responsible for monitoring that direction shows SLOW, and the other shows STOP. When vehicles come from both directions, it is necessary to prioritize them and determine which one goes first. Here, the vehicles that are not on the same side of the work zone are given higher priority. To prevent the vehicles with a lower priority from infinite waiting, the priorities between two directions will be swapped after a predefined duration (e.g., 40 seconds). Take Figure 1(b) for an example. The vehicles in direction 1 get the higher priority because they are on the opposite side of the work zone. Thus, they go first. After a predefined duration, if those vehicles are not yet finished passing, the priorities of directions 1 and 2 will be exchanged. Then, direction 2 now owns the higher priority. Thus, vehicles in direction 1 stop for letting vehicles in direction 2 pass. The priorities keep exchanging until all the vehicles pass by the work zone.

IV. IMPLEMENTATION AND PRELIMINARY RESULTS

A. Prototype Development

A prototype was assembled as shown in Figure 2. The prototype includes four cameras, a computer, a led panel, and a battery. They are mounted on a cart so that the prototype is movable, self-powered, and without the need for an internet connection. The cameras on the stand can be rotated horizontally according to the needs of monitoring traffic conditions. The led panel is controlled by a Raspberry pi which connects to the computer with an ethernet cable. The IDs of cameras are set up manually and shown on the number tags near the cameras. The prototype requires approximately 300 watts of power supply to operate for one hour without charge. The device will be further improved for energy efficiency. For example, the computer will be replaced with more energy efficient computing device. Also, low-power self-organizing network will be added to the system to reduce the energy consumption of communications between devices.

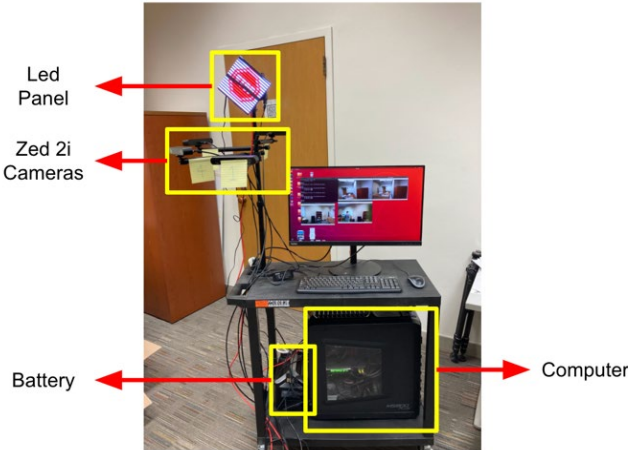


Figure 2. Prototype Development

B. Preliminary Results

So far, a vehicle detector has been trained and integrated

into the prototype. To support real-time detection, the detector relies on YOLOv5, one of the fastest and most accurate object detection models [15]. It was trained to detect 7 vehicle classes, i.e., bicycle, car, motorcycle, dump truck, bus, cement truck, and truck. The dataset for training and validating the detector contains a total of 9,962 images with 32,060 labels, where 8,515 images with 28,030 labels were used for training and 1,447 images with 4030 labels were used for validation. The critical training settings were shown in Table 1. Figure 3 shows that 100 epochs are enough for model training, because the precision curve and loss curve begin to be steady after 160 steps (80 epochs). The detector was evaluated in terms of precision, recall, and mAP₅₀ shown in Table 2.

Table 1. Detector Training Settings

Setting	Value	Setting	Value
epochs	100	Optimizer	SGD
Batch Size	2	Momentum	0.937
Image Size	640x640	Learning Rate	0.01

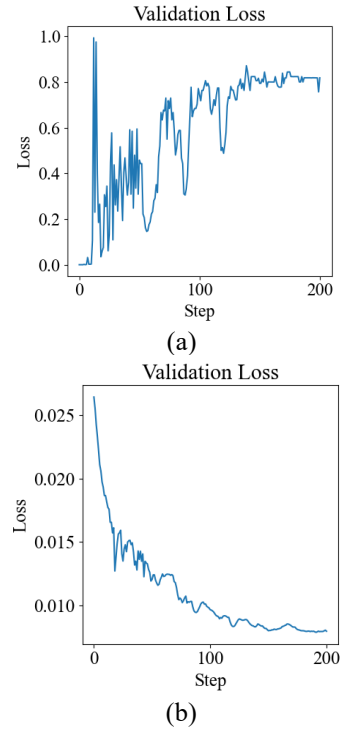


Figure 3. (a) Precision curve and (b) loss curve of training process.

Table 2. Detector Performance

Class	Precision	Recall	mAP ₅₀
Bicycle	0.50	0.45	0.50
Car	0.64	0.61	0.65
Motorcycle	0.65	0.61	0.66
Dump Truck	0.84	0.82	0.53
Bus	0.72	0.71	0.78
Cement Truck	0.92	0.91	0.90
Truck	0.41	0.43	0.47
Overall	0.67	0.65	0.64

Figure 4 showed the STOP or SLOW sign on the prototype's LED panel. Here, the LED panel was set to be associated with the camera on the right side (Camera A). Camera A was manually assigned with the highest priority. The STOP sign was shown when traffics were detected in any other camera views and meanwhile, no traffics were detected in the view of Camera A. No matter whether traffics were detected in the views of other cameras, the SLOW sign was shown as long as there were traffics detected in the view of Camera A.

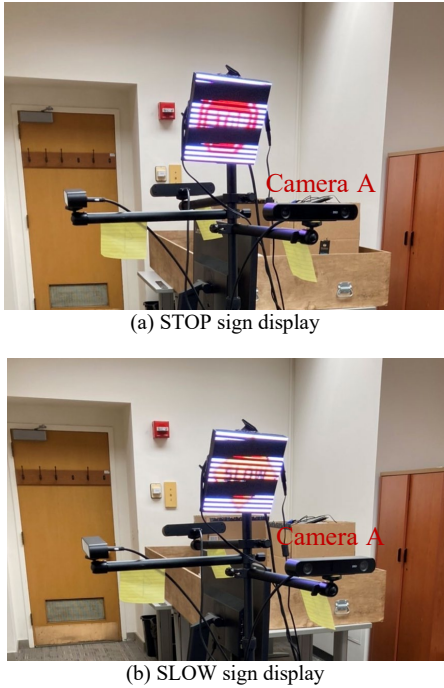


Figure 4. Signs on the LED panel

V. CONCLUSION AND FUTURE WORK

This paper proposed a vision-based flagging system to automatically guide the traffic near a construction site. The system consists of two modules: information capturing and decision making. A prototype built upon the concept of the system was assembled. The prototype is equipped with four cameras, a computer, a led panel, and a battery, all of which were mounted on a cart for mobility. So far, a vehicle detector has been trained and integrated into the prototype. A laboratory test was conducted to illustrate the feasibility of the prototype to show STOP or SLOW signs depending on the detection and tracking results. Future work will focus on implementing the remaining parts of the system and testing it on real construction sites to evaluate the performance of decision-making algorithms.

REFERENCES

- [1] "Highway Finance Data Collection," U.S. Department of Transportation/Federal Highway Administration, 7 Nov. 2014, <https://www.fhwa.dot.gov/policyinformation/pubs/hf/pl11028/chapter1.cfm>.
- [2] Bushe, B., Feraco, T., Forbes, E., Stilwell, I., & Vanscoy, J. (2020). "A Study of a Traffic Controlling Robot for Safer Work Zones."
- [3] "Fatal Injuries at Road Work Zones," U.S. Bureau of Labor Statistics, 5 Apr. 2017, <https://www.bls.gov/opub/ted/2017/fatal-injuries-at-road-work-zones.htm>.
- [4] Ahmed, A., & Liang, L. (2017, January). Impact of flaggers on safety and mobility of highway work zones. In *Canadian Society for Civil Engineering Annual Conference and General Meeting 2017: Leadership in Sustainable Infrastructure* (pp. 264-271). Canadian Society for Civil Engineering.
- [5] Ore, T., & Fosbroke, D. E. (1997). Motor vehicle fatalities in the United States construction industry. *Accident Analysis & Prevention*, 29(5), 613-626.
- [6] Nada D Trout, Melisa D Finley, and Brooke R Ullman. Motorists' understanding of automated flagger assistance devices in work zones. *Transportation research record*, 2337(1):42–49, 2013.
- [7] Zhu Qing, Siyang Zhang, Henry Brown, and Carlos Sun. "Evaluation of truck-mounted automated flagger assistance devices in Missouri: Case study," *Journal of Transportation Engineering, Part A: Systems*, 145(12):05019006, 2019.
- [8] "Guidance on the use of Automated Flagger Assistance Devices," *American Traffic Safety Services Association*, (2012), https://workzonesafety-media.s3.amazonaws.com/workzonesafety/files/documents/training/fhwawz/grant/atssa_afad.pdf.
- [9] Qing, Zhu, et al. "Evaluation of truck-mounted automated flagger assistance devices in Missouri: Case study," *Journal of Transportation Engineering, Part A: Systems* 145.12 (2019): 05019006.
- [10] Cottrell, Benjamin H. "Evaluation of the Autoflagger in Virginia," No. FHWA/VTRC 07-R12. *Virginia Transportation Research Council*, 2006.
- [11] Thompson, Bill. "Field evaluation of automated flagger assistance devices (AFADS)," No. 42959. *Maine. Dept. of Transportation*, 2008.
- [12] FHWA, USDOT. "Manual on uniform traffic control devices (2009)." *Baton Rouge: Claitor's Law Books and Publishing* (2010): 137-179.
- [13] Trout, Nada D., Melisa D. Finley, and Brooke R. Ullman. "Motorists' understanding of automated flagger assistance devices in work zones," *Transportation research record* 2337.1 (2013): 42-49.
- [14] Finley, Melisa D. "Field evaluation of automated flagger assistance devices in work zones on two-lane roads," *Transportation research record* 2337.1 (2013): 1-8.
- [15] Nepal, Upesh, and Hossein Eslamiat. "Comparing YOLOv3, YOLOv4 and YOLOv5 for Autonomous Landing Spot Detection in Faulty UAVs," *Sensors* 22.2 (2022): 464.

Extended abstract: Towards the autonomous underwater construction of cement block structures with free-floating robots

Samuel Lensgraf*, Amy Sniffen*, Alberto Quattrini Li*, Devin Balkcom*
Dartmouth College*

Abstract— This paper presents StoneClaw, our custom-made free-floating autonomous underwater vehicle that plans for an efficient use of two complementary energy sources (battery and compressed air) and exploits self-correcting features on our designed manipulator, for constructing structures with interlocking cement blocks.

I. INTRODUCTION

Infrastructure development in coastal areas has long been essential to supporting the most populous cities on earth. Randomly stacked piles of stone have been used for centuries to create artificial areas of calm. Artificial reefs such as those used in the Grande Anse Artificial Reef Project in Figure 1b have long been built to restore damaged reefs. In the modern age, attention is increasingly paid to offshore infrastructure due to the twin factors of sea level rise and increased need for green energy production. While automation for inspection and intervention tasks has been well explored, little attention has been paid to using autonomous underwater vehicles (AUVs) to directly construct infrastructure.

In this abstract, we present preliminary results on the StoneClaw freefloating AUV construction system shown in Figure 1a. The StoneClaw AUV system is a holistically-designed system featuring a custom designed AUV and error correcting cement blocks. It is, to our knowledge, the first free-floating AUV system for building small-scale structures from practical materials. In addition, it is the first free-floating construction robot to explicitly utilize buoyancy to minimize battery usage.

While free-floating robots on land (e.g., drones) have long been identified as an attractive option for building structures on land, their scale has been limited in practice due to the energy cost required to transport building materials. We exploit the relative ease of changing buoyancy underwater to develop the first planning algorithm for balancing the use of two finite and complementary energy sources while transporting heavy objects: one

This project was partially supported by the NSF GRFP, CNS-1919647.

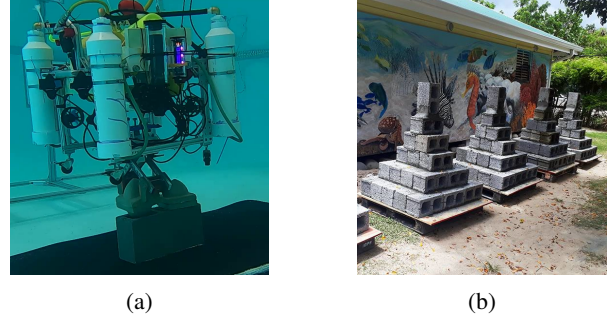


Fig. 1: (a) StoneClaw placing a cone insert. (b) Artificial reefs from the Grande Anse Artificial Reef Project.

for changing buoyancy and one for powering thrusters. We defined a convex program which allocates varying amounts of buoyancy to each block based on a calibrated approximation of the cost to hold a block aloft. Preliminary results suggest that our convex-optimization-based procedure for allocating buoyancy can improve vehicle life as compared to a simpler, naive buoyancy strategy. Buoyancy changing drones which combine air heated by a torch and thruster power to manipulate blocks could utilize the same type of approach on land.

StoneClaw is designed to build structures out of interlocking cement blocks. The bulk of the structure is made up of standard, low-cost cinder blocks. StoneClaw drops molded cement cone inserts into the cores of the cement blocks which allow passive error correction when placing the next layer of cinder blocks. We envision a new class of robust, yet temporary coastal infrastructure enabled by systems like StoneClaw. Fleets of AUVs could be deployed to erect the foundation for a bridge in an emergency, then disassemble it when the emergency has passed.

II. RELATED WORK

A. Underwater Manipulation

Existing underwater manipulation systems used in practice are often tele-operated, but autonomous approaches have been a recent research focus. Existing

approaches tend to use expensive and complex AUV systems mounted with high degree-of-freedom manipulators such as the TRIDENT project in the EU [1]. These AUVs, called “Intervention AUVs”, focus on tasks such as retrieval or turning valves in submerged panels [2]. Our AUV features a relatively simple, passively strong manipulator specifically designed for picking up flat-sided stone blocks which allows simpler control.

B. Autonomous assembly on land

Our work is the closest to initial steps taken on the autonomous assembly of masonry structures with drones [3]. The authors explore the development of drone-compatible masonry units and present non-autonomous tests with a drone. The problem of battery usage for transporting the blocks is left as future work. Robotic dry stacking of found stones has been explored more thoroughly [4]. Our focus on stones of known geometry allows the system to more easily execute assembly operations with imprecise localization and grasping position inherent to a free-floating robot.

C. Energy constrained planning

To our knowledge, our system is the first to explicitly balance two complementary energy sources during manipulation tasks. Minimizing energy consumption by mobile robots has been widely explored. In particular, energy conservation has been explored for robots intended to operate for long missions such as autonomous sail boats [5], or UAVs [6]. Energy constrained planning specifically has received less attention. When it has been explored, it is often in the context of exploration [7], but the robots are limited to a single on board battery.

D. Variable ballasting

Compressed air has been used to accommodate the payload of a ROV for manipulation [8], but the source of compressed air was fed into the robot through an umbilical and the system was designed specifically for a single known manipulation target. Our system focuses on working reliably with major changes in payload and varying amounts of water in its ballast tanks.

III. STONECLAW AUV

The StoneClaw AUV is a tetherless AUV featuring a two power sources: compressed air canister for active buoyancy control, and a LiPo battery to power the thrusters. StoneClaw’s active ballasting system is driven by a 3 liter SCUBA pony bottle pressurized up to 3000psi which feeds four vertical PVC ballast tanks. Using four vertical thrusters, the AUV can supply up to 26.2kg of thrust. The ballast tanks are vertically oriented

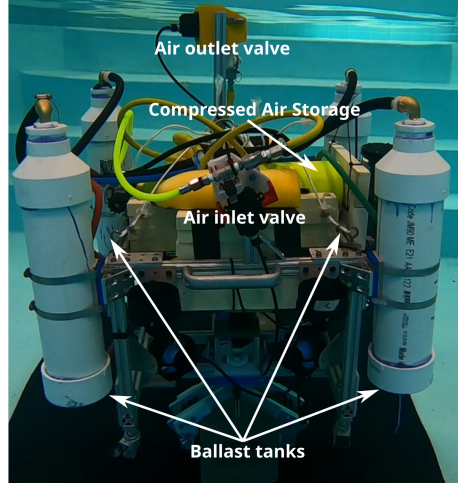


Fig. 2: Active ballasting system.

to limit the effects of sloshing as the AUV positions itself and are located as far apart as possible to limit the pendulum effect created when repositioning with a cinder block.

Instead of directly sensing air flow or pressure changes, StoneClaw uses change in depth to sense its buoyancy. This allows a uniform policy for defining buoyancy in terms of the amount of battery power used to hold the vehicle at depth despite variations in what it grasps. To control buoyancy, we specify $b \in [0, 1]$ which is mapped to an intensity of downward or upward thrust. When increasing buoyancy, b is mapped to a downward thrust applied by the four vertical thrusters. The air inlet valve pulses until the thrust is enough to lift the AUV. When decreasing buoyancy, the thrusters push down while the air outlet valve is pulsed. Figure 2 shows the location of the air inlet and outlet valves.

A. Manipulator

Our primary guiding principles in designing a manipulator for StoneClaw were simplicity and passive strength. This is in contrast to other AUV systems where generality and flexibility are core concerns. Lacking the passive strength present in our manipulator, other more standard manipulators could require large energy expenditures to keep the blocks in hand.

The manipulator’s linkage, based on stone grabbers, uses the weight of the block to draw itself closed passively. No sensing of the position of the fingers is required. Instead, a relay powers the actuating servo down when the fingers are commanded to stop, preventing the stalled servo from consuming power.

The fingers are actuated using a high-torque underwater servo which drives a lead screw. The lead screw

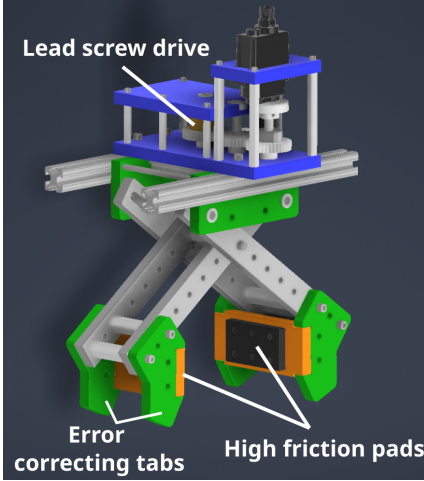


Fig. 3: 3D rendering of 1DOF manipulator.

nut is given room to travel between two spaced plates. When the nut is driven against the top plate, the lead screw extends downwards, preventing opening while preserving a passively strong grip. Tabs on the fingers guide StoneClaw into place as it approaches a block or cone insert. Figure 3 shows the manipulator in detail.

IV. CINDER BLOCKS & CONE INSERTS

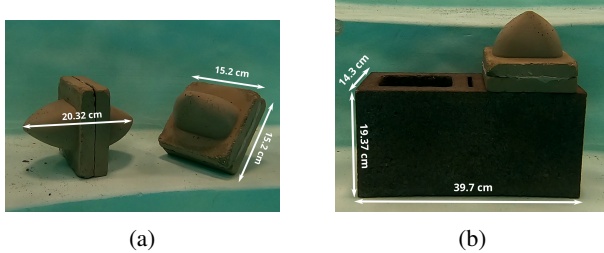


Fig. 4: (a) Cone inserts. (b) Cone insert in block.

We designed our cement building system to help overcome the unavoidable pre-drop and pre-grasp position errors. Standard cinder blocks (9.5kg in water) form the bulk of structures and molded cement cone inserts (3.17kg in water) guide the blocks together. The base of the cone inserts is slightly wider than the cement blocks to facilitate disassembly. To passively correct error while falling, the cone inserts are weighted to bias their center of gravity towards the tip of the bottom cone.

Based on their geometry, the cones can provide up to 4.5cm of error correction along the length of the block and 2cm along its width. Taller, pointer cones with steeper sides can correct more error but are more likely break when dropped or pushed against the sides

of the blocks. We selected our current cone geometry to balance strength and error correction.

V. PLANNING BUOYANCY DURING CONSTRUCTION

Any weight not offset by the vehicle’s positive buoyancy must be made up by the thrusters. When the AUV is not loaded with a block, any positive buoyancy must be overcome by the thrusters on the return trip.

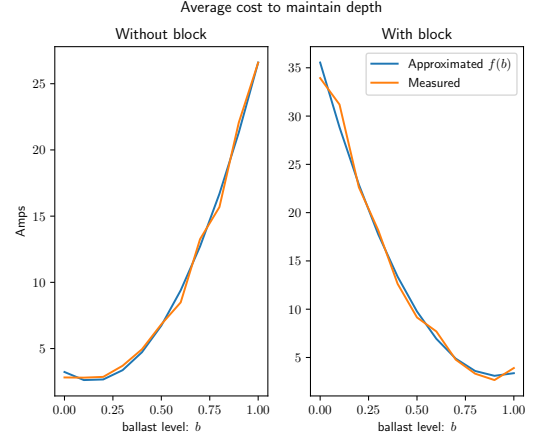


Fig. 5: Calibrated instantaneous cost curves.

For long motions in which the AUV is sufficiently far from neutrally buoyant, we expect that the dominant battery cost will be holding the AUV at depth while moving between points. We model the average instantaneous energy consumption $f(b)$ where f is a polynomial function in the level of buoyancy $b \in [0, 1]$. Figure 5 shows our calibrated instantaneous cost curves with a best fit two-degree polynomial for positive and negative buoyancy changes. The cost of completing a motion is proportional to the distance travelled during that motion. Specifically $\mathbf{E}(\hat{b}) = \sum_{i=2}^n f(\hat{b}_{i-1})||x_{i-1} - x_i||$ where x_i is the i -th location in the construction process and b_i is the ballast level for motion i .

A. Convex Program for Allocation

The AUV first grasps a block, transports it, then deposits it, then moves to grasp the next block. Our goal is to allocate the amount of buoyancy for each hop which minimizes battery consumption while limiting the compressed air use to a reasonable level. Let $\mathbf{x} = [x_1, x_2, \dots, x_n]$ be the set of locations the AUV must travel between in order. The AUV grasps a block at x_1 , transports it to x_2 and deposits it, then travels to x_3 to grasp the next block. Our optimization variable, $\Delta = [\delta_1, \dots, \delta_{n-1}]^T \in [0, 1]^{n-1}$, tracks the changes in buoyancy after each leg of the trip. δ_1 corresponds

to adding air into the ballast tanks and δ_2 corresponds to releasing air. To map Δ into \hat{b} we can define a matrix, $M\Delta = \hat{b}$, a lower triangular matrix composed of columns of ones of alternating sign.

Given M , we can define linear constraints for our convex program. $0 \leq M\Delta \leq 1$ ensures the ballast tanks are never more than completely full or empty. Let M' be M with its negative columns set to zero. $M'\Delta \leq C$ constrains the amount of compressed air used by limiting positive buoyancy changes. Collecting all of these definitions, gives the convex optimization problem in Equation 1.

$$\begin{aligned} \min_{\Delta} \quad & E(M\Delta) \\ \text{subject to} \quad & 0 \leq \Delta \leq 1 \\ & M'\Delta \leq C \\ & 0 \leq M\Delta \leq 1 \end{aligned} \quad (1)$$

VI. PRELIMINARY RESULTS & NEXT STEPS

For preliminary trials of the StoneClaw system, we deployed the AUV in a 1.6 meter deep indoor pool. For localization, StoneClaw utilizes a fiducial marker mounted near a rubber mat. Assembly actions are described in terms of the state machine described in our previous work [9]. Fixed waypoints defined relative to the fiducial marker guide the assembly process.

A. Buoyancy optimization

As a preliminary trial of our ballast optimizer, the AUV grasped a block, moved it 6m, grasped the next block 1m away then carried that block 5m before depositing it. In terms of the convex program in Section V, we set $x = [(0, 0), (0, 6), (0, 5), (0, 0)]$ and $C = 1$. Solving the convex program in Equation 1 yielded $\Delta = [0.73, 0.27, 0.26]^T$. Multiplying out $M\Delta$ gives us $\hat{b} = [0.73, 0.46, 0.72]^T$. To compare the effectiveness of the optimized allocation strategy with the obvious strategy of evenly allocating buoyancy, $\hat{b} = [0.5, 0.0, 0.5]^T$, we used both strategies to move a cinder block. The optimized strategy consumed 1.55 Ah while the naive allocation used 3.54 Ah, showing that preserving air for small motions can increase battery life.

B. Construction trials

In preliminary trials of the construction process, the AUV grasped the cone inserts and moved them to a pre-placed cinder block. With proper tuning of the waypoints, the AUV was able to place the cone inserts 60% of the time in a small scale trial. The AUV was able to place the second cinder block on top of the two cones but failed to detect it should release it.

C. Next steps

a) Compliant insertion behaviors: Noise in the AUV's pre-drop position can cause the cinder blocks to become jammed on the cones as it falls. We plan to develop compliant sliding motions in which the AUV guides the cement blocks into place without dropping, allowing control of falling speed, trajectory, and angle.

b) Full construction planning: The problem of planning the full construction sequence is yet-unaddressed. It is possible that building intermediate structures such as creating a stack near the structure could improve efficiency. To allow the exploration of this problem, we plan to develop a high-level construction planner based on Monte-Carlo Tree Search.

c) Insertion success detection: While the AUV is attached to a block, it forms a single rigid body. This fact could be exploited to indirectly sense the status of the insertion process. For example, using the vehicle's gyroscopes, we could detect whether a block is jammed at an improper angle.

REFERENCES

- [1] P. J. Sanz, P. Ridao, G. Oliver, *et al.*, “Trident: Recent improvements about autonomous underwater intervention missions,” *Proc. IFAC*, vol. 45, no. 5, pp. 355–360, 2012.
- [2] N. Palomeras, P. Ridao, D. Ribas, and G. Vallicrosa, “Autonomous I-AUV docking for fixed-base manipulation,” *Proc. IFAC*, vol. 47, no. 3, pp. 12 160–12 165, 2014.
- [3] S. Goessens, C. Mueller, and P. Latteur, “Feasibility study for drone-based masonry construction of real-scale structures,” *AUTOMAT CONSTR*, vol. 94, pp. 458–480, 2018.
- [4] V. Thangavelu, Y. Liu, M. Saboia, and N. Napp, “Dry stacking for automated construction with irregular objects,” in *Proc. ICRA*, 2018, pp. 4782–4789.
- [5] C. Sauzé and M. Neal, “Long term power management in sailing robots,” in *OCEANS 2011 IEEE - Spain*, Jun. 2011, pp. 1–8.
- [6] D. H. Choi, S. H. Kim, and D. K. Sung, “Energy-efficient maneuvering and communication of a single UAV-based relay,” *IEEE T AERO ELEC SYS*, vol. 50, no. 3, pp. 2320–2327, Jul. 2014.
- [7] Y. Choi, Y. Choi, S. Briceño, and D. N. Mavris, “Energy-Constrained Multi-UAV Coverage Path Planning for an Aerial Imagery Mission Using Column Generation,” in *J INTELL ROBOT SYST*, vol. 97, no. 1, pp. 125–139, Jan. 2020.
- [8] K. Wasserman, J. Mathieu, M. Wolf, A. Hathi, S. Fried, and A. Baker, “Dynamic buoyancy control of an rov using a variable ballast tank,” in *Oceans 2003*, vol. 5, 2003, SP2888–SP2893.
- [9] S. Lensgraf, A. Sniffen, E. Honnold, *et al.*, “Droplet: Towards autonomous underwater assembly of modular structures,” in *RSS*, 2021.

TeleLayering: Teleoperated Construction 3D Printing Using Multimodal Feedback for Extraterrestrial and Terrestrial Construction

Ali Kazemian, Hunter Gilbert, Yimin Zhu, Michael R. Fiske, Natalia Alexandrov

Abstract - In this paper, we propose a teleoperated construction 3D printing technology, called TeleLayering, for planetary and terrestrial applications. The TeleLayering technology is enabled by effective multimodal control and monitoring systems and enhanced construction 3D printing robots to build or repair a variety of structures in extreme environments without the need for human presence on the jobsite. This paper presents a general description, main technical requirements, implementation challenges, and applications of this technology.

I. INTRODUCTION

Reportedly, in the United States alone, over 1100 construction worker fatalities happen each year [1]. Removing human workers from the construction sites can prevent the frequent injuries and fatalities, and can minimize human exposure to dust and other hazards typically present at construction sites. Teleoperation of construction machinery is one approach to achieving this goal. Teleoperation, in general, enables interactions with robotic manipulators remotely, extending human manipulation capabilities to far-off locations to execute complex tasks while avoiding unsafe environments [2]. Teleoperation enables human-robot teams to complete challenging tasks, where robots can be used for labor-intensive, dangerous, and repetitive tasks, while humans with their unmatched cognitive capabilities can engage in supervisory control, such as real-time process modifications due to contingencies. The first bilateral teleoperation system was developed in the 1940s by researchers at the Argonne National Laboratory for remote handling of radioactive materials [2]. The first mechanisms were mechanically coupled, with the slave manipulator mimicking the master motions. The first electrically-coupled master-slave teleoperation system was developed in the 1950s [2, 3]. Since then, a variety of wired and wireless telerobotics systems have been used for different applications such as surgery, underwater operations, maintenance, and space missions [4, 5]. Telerobots have been used in space as early as 1970. The Lunokhod 1 rover landed on the Moon in November 1970 and was followed by Lunokhod 2 in January 1973, both remotely operated from Earth [6, 7].

Teleoperation has the potential to significantly improve worker safety in different domains while offering other

benefits. For example, Khoshnevis [8] proposed a teleoperated manufacturing paradigm for complex manufacturing tasks which cannot be fully automated and require human skills. The manufacturing industry can adopt this new approach to deal with pandemics and other challenges associated with crowded and congested working environments. In the construction industry, teleoperation has been previously used to remotely control heavy machinery for excavation, leveling, and demolition [9, 10]. Kita *et al.* [5], for example, developed and successfully tested a teleoperated underwater excavator, for seabed leveling controlled by a teleoperator on a ship. The developed system includes three major subsystems: underwater information representation, a seabed mapping module, and an easy-to-operate attachment for seabed leveling. In order to calculate and represent the posture of the excavator during underwater operations, the customized underwater excavator was equipped with a variety of sensors such as a gyroscope, a depth gauge, and an underwater acoustic positioning device [5]. These successful experimental efforts, as well as real-life applications of teleoperation in excavation, highlight the great potential of teleoperation for remote operation of construction machinery.

In this paper, we propose a telerobotic infrastructure construction 3D printing (C3DP) technology, called TeleLayering, for extreme environments. Currently the existing C3DP technologies on Earth rely heavily on the human presence on the job site. Manual inspection and process modifications are typically required to ensure the successful completion of the construction process.

Examples of typical manual process modifications during C3DP include nozzle height adjustments and printing speed and extrusion rate modifications. These manual modifications are commonly needed to prevent excessive layer deformations, surface defects, and collapse of freshly printed structures. TeleLayering, however, provides a solution for conditions where human presence on the jobsite is not safe or feasible. The teleoperated C3DP technology for extreme environments, as described in this paper, has not been previously implemented for either terrestrial or extraterrestrial applications. Therefore, the new requirements regarding system design and control schemes for extraterrestrial and terrestrial TeleLayering will be presented in the following sections.

Ali Kazemian is with the Bert S. Turner Department of Construction Management at Louisiana State University, Baton Rouge, LA 70803, USA (Phone: 225-578-3798; e-mail: kazemian1@lsu.edu).

Hunter Gilbert is with the Department of Mechanical and Industrial Engineering at Louisiana State University, Baton Rouge, LA 70803, USA (e-mail: hbgilbert@lsu.edu).

Yimin Zhu is with the Bert S. Turner Department of Construction Management at Louisiana State University, Baton Rouge, LA 70803, USA (e-mail: yimin.zhu@lsu.edu).

Michael R. Fiske is with the Jacobs Space Exploration Group (ESSCA Technical Fellow- NASA Marshall Space Flight Center), Huntsville, AL 35808, USA (e-mail: michael.r.fiske@nasa.gov).

Natalia Alexandrov is with the NASA Langley Research Center, Hampton, VA 23666, USA (e-mail: n.alexandrov@nasa.gov).

II. TELELAYERING: DESCRIPTION AND TECHNICAL REQUIREMENTS

The TeleLayering technology includes four main components: (1) a specialized remotely controlled mobile C3DP robot equipped with onboard sensory, data processing, and control systems as well as a robotic gripper, (2) a bi-directional feedback and control interface which supports multiple control modes, (3) a wireless communication system, and (4) a human teleoperator. The specifications and technical details of each element depends on the application for which the TeleLayering system is designed. The general requirements and considerations for each component is discussed in the following paragraphs.

A **specialized C3DP robot** is one of the most important aspects of TeleLayering, which works in concert with the human teleoperator to complete the construction related tasks in the remote site. There are four main performance requirements for TeleLayering robots: (1) Navigation and operation in unstructured and unknown environments (robustness, reliability, and resilience), including fault and anomaly detection and mitigation; (2) Ability to collect critical process and environment data which could affect the construction process; (3) Ability for local data processing and control for automated completion of sub-tasks; (4) Ability to complete tasks beyond layer extrusion, such as pick-and-place operations.

A bi-directional multimodal **feedback and control interface** is another key component of a TeleLayering system, which realizes a continuous or intermittent information flow between the human operator and the remote robot. The first main requirement for a TeleLayering interface is to facilitate perception of the remote environment by the teleoperator, given the bandwidth and telecommunication limitations. Maintaining a balance between complexity and operability is the main challenge in design of a TeleLayering interface, since a wide range of parameters and data can be presented to the human teleoperator in various modalities (video, augmented reality, digital twin models, quantitative process parameters, etc.).

A related constraint is the bandwidth limitations that commonly limit the amount of real-time data that could be presented to the human teleoperator. With the ongoing advancements in telecommunications networks (e.g., 5G technology), this limitation will not be as significant in the future. Still, the amount of data presented to the teleoperator, and their modalities, need to be carefully determined. Presenting a large amount of data to the teleoperator can result in cognitive overload and fatigue, which in turn can severely impact the teleoperator's performance and decision-making ability [9, 12].

The second main technical requirement for a TeleLayering interface is to support multiple control modes, with the capability of switching between these modes during the operation. We envision a wide range of autonomy levels for TeleLayering. Specifically, we propose two operation modes, a shared autonomy mode and a supervisory control mode, which can be deployed in various scenarios, while some complex tasks may require transition between these operation modes. Table 1 summarizes the automation levels

for several tasks involved in TeleLayering under the two proposed operation modes.

Shared autonomy (shared control) allows the teleoperator to directly guide the nozzle movements within the build envelope to construct different objects layer by layer without the need for a CAD model (on-demand construction) and to install reinforcement or other components during the construction process by directly controlling the robotic gripper. In this operation mode, process parameters such as extrusion rate or temperature are controlled automatically, or with minimal input from the user (such as "material type"). With supervisory control, however, much of the operation is autonomous, and the teleoperator only intervenes when it is necessary, to prevent process failure. This operation mode relies heavily on the advanced sensory systems and edge computing capabilities of the remote TeleLayering robot.

Various automated quality control techniques for conventional C3DP systems have been implemented and studied by researchers. Machine vision, 3D laser scanning, and extrusion monitoring using various inline sensory systems have been investigated [13, 14, 15]. For example, Kazemian *et al.* [16] designed and demonstrated an adaptive extrusion system based on machine vision for automated extrusion rate control during C3DP, using an embedded single-board computer. 2D and 3D vision systems, specifically, hold great promise as tools for non-contact measurements during TeleLayering and for feedback to the teleoperator to enable reliable remote control. In terms of overall productivity and operability, the supervisory TeleLayering mode is preferred. However, its implementation is technically more challenging and requires integration of advanced and reliable sensory and edge computing systems into the remote robotic system. Shared autonomy, on the other hand, is a more practical approach for scenarios requiring human dexterity and creativity, such as emergency construction.

Table 1. Various levels of autonomy with TeleLayering

Task	TeleLayering Operation Modes	
	Shared Autonomy	Supervisory
Robot Navigation	Direct Control, Guided or Automated	Automated
Nozzle Movements	Direct Control	Automated
Extrusion Parameter Selection	Guided or Automated	Automated
Pick-and-place Operations	Direct Control or Guided	Guided or Automated
Real-time Modifications (contingencies)	Direct Control or Guided	Direct Control or Guided

With respect to the **wireless communication system**, the general requirements are similar to other teleoperation systems: high bandwidth and low latency to allow a continuous bi-directional information flow and to reduce the chances of instabilities induced by time delays. Given a reliable and intelligent construction robot, high-latency TeleLayering also seems technically feasible in the future. However, low-latency TeleLayering is a more viable starting point. Implementation of low-latency TeleLayering systems can generate the necessary data (on the process failure modes

and intervention strategies) to design TeleLayering systems with a higher degree of automation which can possibly be teleoperated over high-latency wireless networks.

The **human teleoperator** plays an important role in any telerobotic system, by perceiving the information from the remote site through the interface, and making decisions and sending commands to the remote robot accordingly [17]. Human factors, such as the cognitive capacity to interpret real-time data, and the impact of telecommunication latency levels on the teleoperator's performance, must also be considered during the design process. Examples of quantitative metrics for overall human-robot performance evaluation include task completion time, percentage of overall mission completed, or use of standard surveys to assess situational awareness and cognitive load [18, 19].

Finally, teleoperation functionality will significantly affect TeleLayering hardware design. While different robotic configurations have been used for C3DP in the past, considerations related to TeleLayering control schemes and the required autonomy will give rise to new design requirements. For example, which configurations- robot type and mobility platform- lend themselves more readily to the TeleLayering requirements in extreme environments?

III. APPLICATIONS

TeleLayering systems can be designed for remote operation either with or without direct line-of-sight. The latter has a broader range of applications and is the main focus here. We discuss the applications of this technology in planetary and terrestrial construction, as well as some of the performance requirements in each domain.

A. Extraterrestrial TeleLayering

TeleLayering can be deployed for infrastructure construction, repair, and outfitting on the Moon and Mars. For planetary construction missions, requiring on-site presence of astronauts and assigning manual tasks to them during extraterrestrial construction is inefficient, unsafe, and costly. In addition, the inspection and process adjustments that are commonly done by human workers during C3DP on Earth, cannot be easily carried out by a suited astronaut, as extravehicular activity (EVA) suit systems typically encumber an astronaut's range of motion, reach, and field of view [7]. TeleLayering enables reliable operation of mobile C3DP robots on the planetary surfaces by astronauts who are not present on the job site but remotely monitor and control the process from an environmentally controlled command center. It also eliminates the need for prolonged EVA operations which expose astronauts to harmful radiation and contamination on planetary surfaces during construction. In addition, TeleLayering has great potential to be deployed in precursor missions for Lunar and Martian construction, in advance of crewed missions.

Developing fully autonomous planetary construction systems is highly desired by NASA and other space agencies. However, considering the extreme extraterrestrial conditions, the associated uncertainties, and lack of relevant data, fully autonomous construction does not seem viable in the near future. TeleLayering, on the other hand, can serve as a viable solution that can be used during upcoming Artemis missions

and enable a gradual transition towards fully automated planetary construction. The implementation of the TeleLayering technology can result in valuable sensory and tele-control data from different operation modes, which can be used to design advanced control algorithms and augment the autonomy of C3DP robots over time, and ultimately enable fully autonomous planetary construction.

With respect to system design and implementation, planetary TeleLayering is significantly more challenging compared to terrestrial TeleLayering. Reliable and durable C3DP robots are required to navigate the rough Lunar and Martian terrains and successfully complete the assigned construction or repair tasks in an environment with a high degree of uncertainty. Considering the high costs and limited opportunities for maintenance and repair in planetary environments, these robots must be designed for a longer service life and a higher degree of robustness, compared to terrestrial robots.

Time delay (latency) is another major technical challenge in space telerobotics. In high-latency scenarios such as Mars Exploration Rovers (MERs) with tens of minutes of delay, command sequences are often intermittently uplinked to the robot by mission control. The robot then functions independently for long periods without communication with teleoperators at mission control [7]. As a starting point for technology development, low-latency TeleLayering seems to be more viable. For Lunar construction, the TeleLayering robots on the Moon can be controlled by the crew in the Lunar habitats or crew lander (over-the-horizon commanding), or from Earth-Moon libration point with round trip time latency of approximately 400 ms, or even possibly from the Earth. On Mars, TeleLayering robots can be controlled by human crew in nearby Martian habitats or from vehicles on orbit.

B. Terrestrial TeleLayering

On Earth, TeleLayering can be used for construction and repair of structures in extreme environments, such as the vicinity of active volcanoes, underwater, active war zones, or in areas with high radiation levels due to nuclear accidents. In the case of hazardous chemical leakage or nuclear accidents, TeleLayering robots can be used to construct temporary structures to confine the source of the hazard. In applications where a large number of structural elements and substructures are produced repeatedly (such as prefabrication factories), TeleLayering can improve the construction productivity and reduce the need for laborious manual activities by assigning humans to supervisory and telecontrol roles. By advancing the TeleLayering technology toward supervisory operation mode, it would be possible to assign one teleoperator to multiple remote robots, which will significantly improve the overall productivity.

IV. CHALLENGES AND RESEARCH NEEDS

One of the key aspects of TeleLayering technology is the control and monitoring interface, which provides the necessary situational awareness to the human teleoperator, and sends commands to the remote robot. The requirements for each operational mode must be studied during the design and implementation of a TeleLayering interface. For the shared autonomy operation mode, for example, the interface should be equipped with controllers for capturing the user's

direct spatial inputs for nozzle movements. One possibility is using force and haptic feedback for direct control of nozzle movements within specified boundaries. Extensive research and systematic studies are needed to evaluate the efficiency of different control and feedback interface configurations, considering the relevant human factors. Virtual environments can be used for initial investigations on the performance of various systems and the teleoperator performance in simulated environments (Figure 1). Virtual environments can also be used for training teleoperators, especially in preparation for future space missions.

Figure 1: BIM CAVE facility at Louisiana State University – Using simulated environments for future TeleLayering research



Another area which needs extensive research is the TeleLayering robot design, as well as innovative material delivery systems which can support mobile TeleLayering robots. Depending on the specific application, TeleLayering robots should be able to complete multiple tasks in addition to large-scale 3D printing, including reinforcement installation, outfitting, coating, and pick-and-place tasks. Enhanced C3DP robots equipped with robotic grippers can be used to complete the majority of these tasks. Finally, in future TeleLayering applications, a team of construction and supporting robots are anticipated to work together on a remote site. Planning, coordination, and interoperability protocols and advanced control systems need to be designed to implement an interconnected network of telerobots working in concert with human teleoperators while maximizing the overall productivity and avoiding collision and other issues.

V. SUMMARY AND CONCLUSIONS

In this paper, we proposed a teleoperated construction 3D printing system called TeleLayering to enable safe and efficient infrastructure construction in extreme environments on Earth and beyond. TeleLayering builds upon the existing knowledge and advances in telerobotics, C3DP, telecommunications, machine vision, VR and AR, and several other maturing technologies. A key requirement for implementation of TeleLayering technology, is to design an intuitive and reliable control and monitoring interface to provide the teleoperator with a high level of situational awareness for successful completion of remote construction tasks. Latency is also a related key consideration in design of TeleLayering systems. Low-latency TeleLayering seems to be a more viable starting point for this innovative technology, while high-latency TeleLayering seems possible after higher levels of autonomy are developed within the realm of C3DP technology.

While TeleLayering can directly benefit from several major existing technologies, extensive multidisciplinary research is needed to explore the capabilities and limitations of this construction technology in various domains.

VI. REFERENCES

- [1] United States Department of Labor, [Online]. Available: <https://www.osha.gov/data/commonstats>. [Accessed 15 12 2021].
- [2] L. Basañez and R. Suárez, "Teleoperation," in *Springer Handbook of Automation*, Berlin, 2009, pp. 449-468.
- [3] T. Sheridan, *Telerobotics, Automation, and Human Supervisory Control*, MIT Press, 1992.
- [4] R. Wirz, L. Torres, P. Swaney, H. Gilbert, R. Alterovitz, R. Webster III, K. Weaver and P. Russell III, "An experimental feasibility study on robotic endonasal telesurgery," *Neurosurgery*, vol. 76, no. 4, pp. 479-484, 2015.
- [5] T. Kita, T. Hirabayashi, A. Ueyama, H. Kinjo, N. Oshiro and N. Kinjo, "Sea Experiment on Teleoperation System of Underwater Excavator," in *Proceedings of the International Symposium on Automation and Robotics in Construction (ISARC)*, 2020.
- [6] A. Kemurdjian, V. Gromov, I. Kazhukalo, G. Kozlov, V. Komissarov, G. Korepanov, B. Martinov, V. Malenkov, A. Mitskevich, V. Mishkin, and G. Rogovsky, "Soviet developments of Planet Rovers in Period of 1964-1990," *Journal of the Robotics Society of Japan*, vol. 12, no. 7, pp. 993-1001, 1994.
- [7] T. Fong, J. Rochlis Zumbado, N. Currie, A. Mishkin and D. Akin, "Space telerobotics: unique challenges to human–robot collaboration in space," *Reviews of Human Factors and Ergonomics*, vol. 9, no. 1, pp. 6-56, 2013.
- [8] B. Khoshnevis, "Telefacturing: A New Manufacturing Paradigm for Worker Safety and Other Benefits," *The Bridge*, vol. 51, no. 1, 2021.
- [9] J. Lee, Y. Ham, H. Park and J. Kim, "Challenges, tasks, and opportunities in teleoperation of excavator toward human-in-the-loop construction automation," *Automation in Construction*, vol. 135, 2022.
- [10] M. Tanzini, J. Jacinto-Villegas, M. Satler, M. Niccolini and C. Avizzano, "Embedded Architecture of a Hydraulic Demolition Machine for Robotic Teleoperation in the Construction Sector," in *2018 IEEE 14th International Conference on Automation Science and Engineering (CASE)*, 2018.
- [11] COBOD, [Online]. Available: <https://cobod.com/>. [Accessed 01 04 2022].
- [12] Y. Desai, D. Davis, S. Jiang and A. Ward, "The Effect of Auditory Cues on Haptic-Controlled Excavator Operator Performance," in *Proceedings of IIE Annual Conference*, 2014.
- [13] A. Kazemian and B. Khoshnevis, "Real-time extrusion quality monitoring techniques for construction 3D printing," *Construction and Building Materials*, vol. 303, 2021.
- [14] O. Davtalab, A. Kazemian, X. Yuan and B. Khoshnevis, "Automated inspection in robotic additive manufacturing using deep learning for layer deformation detection," *Journal of Intelligent Manufacturing*, pp. 1-14, 2020.
- [15] R. Buswell, P. Kinnell, J. Xu, N. Hack, H. Kloft, M. Maboudi, M. Gerke, P. Massin, G. Grasser, R. Wolfs and F. Bos, "Inspection Methods for 3D Concrete Printing," in *RILEM International Conference on Concrete and Digital Fabrication*, 2020.
- [16] A. Kazemian, X. Yuan, O. Davtalab and B. Khoshnevis, "Computer vision for real-time extrusion quality monitoring and control in robotic construction," *Automation in Construction*, vol. 101, pp. 92-98, 2019.
- [17] M. Ferre, R. Aracil, C. Balaguer, M. Buss and C. Melchiorri, *Advances in Telerobotics*, Berlin: Springer, 2007.
- [18] A. Kumar, M. Bell, B. Mellinkoff, A. Sandoval, W. Martin and J. Burns, "A Methodology to Assess the Human Factors Associated with Lunar Teleoperated Assembly Tasks," in *IEEE Aerospace Conference*, 2020.
- [19] A. Steinfeld, T. Fong, D. Kaber, M. Lewis, J. Scholtz, A. Schultz and M. Goodrich, "Common metrics for human-robot interaction," in *1st ACM SIGCHI/SIGART conference on Human-robot interaction*, 2006.

Autonomous Excavator System with Real-World Deployment

Liangjun Zhang^{1*}, Xibin Song¹, Liyang Wang¹, Lingfeng Qian¹, Tianrui Guan²
Zhenpeng He¹, Zhixian Ye¹, Ruitao Song¹, Haodong Ding¹, Dinesh Manocha²

¹Baidu Research, ² University of Maryland, College Park

Abstract—Excavators are widely used for material-handling applications in unstructured environments, including mining and construction sites. Workers operating excavators suffer from prolonged working hours and loads, which can result in injuries and fatalities. In this paper, we highlight our recent progress on developing autonomous excavator systems (AES) for material loading tasks. We present an architecture that combines perception, planning and control. We fuse multi-modal perception sensors, including LiDAR and cameras, with advanced image enhancement, material and texture classification, object detection, terrain traversability mapping, motion planning, and terrain navigation algorithms. AES has been successfully deployed in a real-world scenario, where two excavators automatically operate in recycling pipelines and handle hazardous industrial solid waste material. AES can achieve 24 hours of continuous operation for the scenario and has been used by the customer for more than 8,500 hours.

I. INTRODUCTION

Excavators are considered the most versatile heavy equipment and are frequently used in different applications corresponding to construction, mining, exploration, environmental restoration, archaeological investigations, emergency rescue, etc. The size of global market for excavators is predicted to grow to 63.14 billion USD by 2026 [7], and a total of 380,000 new excavators are projected to be sold in 2024 in China [8].

Currently, excavators are mainly operated by human operators. In addition to facing life-threatening incidents or injuries, human operators may have to operate excavators in extremely abominable working conditions, such as working in remote areas, or even in desert, where conditions include heavy dust and extreme high or low temperatures [1]. Furthermore, workers also suffer from prolonged working hours and loads, which can result in fatigue and injuries [2]. Our work deals with developing an autonomous excavator system (AES) [12]. An unmanned excavation system would vastly reduce the number of casualties or injuries during excavation operations. Moreover, such an excavator could conduct tedious and repetitive tasks for extended hours, thereby increasing the overall throughput.

Efficiency, robustness, and generalizability are the three essential requirements in terms of designing an autonomous excavator [3], [5], [9]. To operate robustly in real world scenarios, the system needs to operate under an extensive range of environmental conditions that vary by the terrain types, weather, lighting conditions etc.

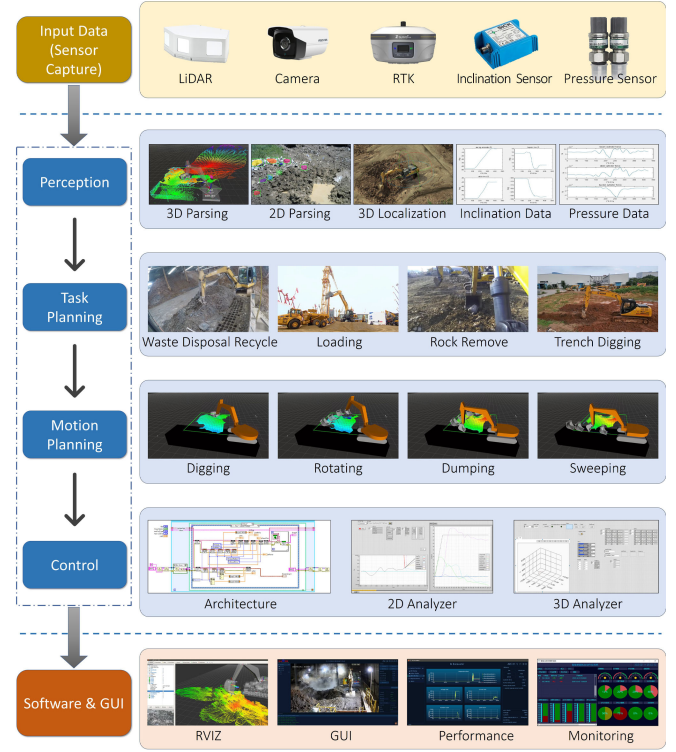


Fig. 1. Overview of Autonomous Excavator System (AES)

Considering these challenges, we develop a set of algorithms and a robust autonomous excavator system (AES) [4], [10], [11], [12], [13]. Our system mainly consists of three main modules: perception, planning, and control together with a HW sensors layer and an application layer. Specifically, we mount LiDAR and cameras on the excavator and employ multi-modal sensor-fusion approaches to perceive the surroundings and the attributes of the target objects, including source material piles, dump trucks, dumping area, impurities, and obstacles. Our perception pipeline follows the “coarse-to-fine” manner, which can not only reduce the overall run-time, but also improve the system performance, enabling prolonged automatic operations without human operator assistance. Based on the perception results, we design a hierarchical planning module composed of a task level planning layer and a motion planning layer for both excavator arm and base movement. For excavator motion control, to overcome the complex non-linearity, large time delay and

*Corresponding author

large disturbances during excavation, we use a hierarchical motion controller.

We have deployed AES in real-world scenarios, where two excavators automatically operate in recycling pipelines and handle hazardous industrial solid waste material produced by various industrial activities. We demonstrate that our system can be seamlessly integrated within the pipelines for loading and dumping industrial waste, which are hazardous for human operators. We have extensively tested AES in different scenarios. AES can achieve 24 hours of continuous operation for this waste material loading scenario and has been used by the customer for more than 8,500 hours.

II. AES OVERVIEW

A. Hardware System

The robot platform is a hydraulic excavator equipped with the drive-by-wire system. Currently, we have developed and tested multiple different sizes of excavators, including 6.5-ton and 7.5-ton compact excavators, 33.5-ton standard excavators, and 49-ton large excavators. These excavation platforms offer enormous output power to conduct various excavation tasks successfully. A control interface through a CAN bus is used so that the entire unit can be controlled by software. To ensure safety, a fallback human control mechanism is implemented in case of an emergency.

To sense the excavator locations and motions, multiple sensors are installed for AES. We use a real-time kinematic (RTK) positioning device to provide the location of the excavator. Inclinometers are used to measure the angles of different joints of the excavator. A combination of light detection and ranging (LiDAR) sensors and RGB cameras collect the environmental information for the perception module to fuse, process, and analyze the surroundings.

B. Software Architecture

There are three software modules in our system. The perception module is designed for sensing various obstacles, modeling the terrain, classifying the material, and locating the dump truck. Based on the perception results, the planning module optimizes the motion trajectories for the excavator arms and base. Then the control module transfers the planning results to the hardware control commands, which are sent to the excavator to track the desired motion. In addition, the application layer of the software adjusts the other modules based on the application.

All modules run simultaneously as nodes under the ROS framework. In the following, we provide more details on the perception and planning modules, which are the key components that enable our system to be deployed in real-world scenarios.

III. COARSE-TO-FINE PERCEPTION SYSTEM

Our perception module focuses on parsing and understanding the surroundings and identifying the target objects in the unstructured working zones. In specific, to handle various challenging scenarios, we perform coarse-to-fine

2D/3D perception for LiDAR point clouds and camera RGB inputs, including:

- 1) Recognizing the texture of the material and modeling the shape of the material pile to perform the loading operation;
- 2) Detecting the impenetrable portion of the material to avoid direct contact between it and the excavator's arm;
- 3) Identifying the blocking obstacles that need to be removed;
- 4) Determining the pose of the trucks for material dumping;
- 5) Constructing the terrain traversability mapping of the environments for the excavator to navigate;
- 6) Enhancing the images through computer vision methods, such as dedusting, which aims to remove the influence of dust in image capturing, thus improving the performance of obstacle identification and texture recognition.

Our perception module works in a “coarse-to-fine” manner and exploits state-of-the art algorithms like semantic segmentation, instance segmentation, texture and material recognition, object detection and dedusting. Taking a stone detection and segmentation task as an example, an image enhancement algorithm is first used. Then a texture and material recognition algorithm is exploited to identify the stone/puddle/pipe area from the whole image. Next, a 2D detection and segmentation algorithm is utilized to segment these objects accurately. Finally, the 2D segmentation and LiDAR’s depth information are combined to fit the 3D bounding box for each detected obstacle.

During the excavation operation, especially for handling stone and soil, dusts often exist in the working area. The dust can considerably affect the recognition of obstacles, such as rocks and trucks. To solve this problem, we propose a deep neural network based dedusting method [10] to generate clean images from dusty input images in closed-loop manner. Taking dust image as input, an encoder and three decoders are used to recover atmospheric light, clean image and transmission map, simultaneously. The encoder is used to extract features, where Dense Feature Fusion strategy and Residual Group are utilized in the encoder process to obtain better feature representation. In the decoder process, deconvolutional layers are used to up-sample the features, then SOS Boosted strategy is employed to enhance the obtained features. Clean loss and reconstruction loss are utilized so that the proposed network can converge well during the training.

IV. HIERARCHICAL PLANNING AND CONTROL SYSTEM

We develop a hierarchical planner architecture for general excavation applications [11]. As shown in Fig. 2, there are two levels of task planners plus one level of motion primitives. From top to bottom, they are high-level task planner layer, sub-task planners layer and motion primitives layer. In most scenarios, the excavator alternates between the motion of its arm to perform excavation operation and the moving of the base to the desired position. Based on this

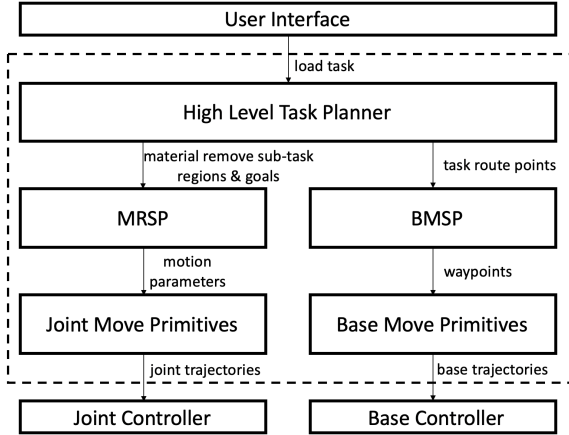


Fig. 2. AES Planning Architecture.

characteristic, our planner currently separates the arm movement and base movement into two planning pipelines. The high-level task planner plays the role of determining which location the excavator needs to move to and which region of material the excavator needs to dig. The sub-tasks planners deals with these types of sub-tasks, namely material removal sub-tasks (MRSP) for completing the sub-region excavation efficiently and accurately, and base move sub-tasks (BMSP) for planning the waypoints for the excavator to move to the desired locations. Finally, the motion primitive layer uses advanced motion planning approaches for generating feasible excavator arm and base motion. Overall, our hierarchical planning system is closely related to the perception module, as shown in Fig. 3. The system can account for the terrain shape as well as the location of obstacles, trucks and other machinery, explicitly. The system architecture and planner algorithms are able to generate effective task and motion plans, which are suitable for various excavation tasks.

Excavator motion control can be challenging because the hydraulic excavator is a complex non-linear system with a large time delay and is subject to large disturbances during excavation. We use a hierarchical motion controller, which consists of a bucket end-effector following controller, an excavator base controller and low-level machine specific look-up tables, which map the command velocity to the hydraulic valve command.

V. TERRAIN TRAVERSABILITY BASED NAVIGATION

To enable the excavator navigating on complex terrain environment, we present a terrain traversability mapping and navigation system for traversability prediction and autonomous navigation. Traversability [6] refers to the capability of a ground vehicle to reside over a terrain region under an admissible state wherein it is able to enter given its current state. Based on the coarse-to-fine perception system, we use an efficient semantic-geometric fusion method to extract a traversability map representation, which leverages the physical and computational constraints of the robot, including maximum climbing degree, width of the body, run-time computational budget, etc. A trajectory is planned

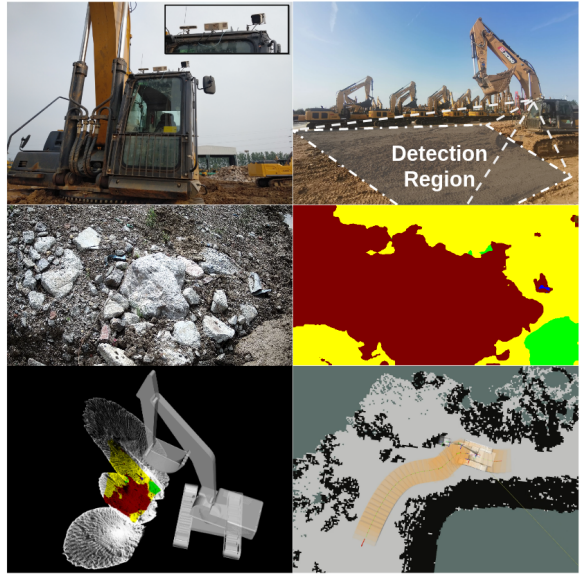


Fig. 3. Terrain Traversability Mapping and Navigation System.

based on this map representation, and the control system ensures that the trajectory is followed in the real-world. In our approach, we first define critical ranges based on the maximum climbing degree of the excavator. Whenever the geometry of the terrain is out of that range, we would assign bad traversability score on that region. When the terrain score is in a reasonable range, we fine-tune the weight for geometry and semantic of the terrain such that the final traversability map is useful for trajectory planning.

VI. EXPERIMENTAL RESULTS

Our autonomous excavation system has been evaluated under multiple controlled, real-world testing scenarios. To thoroughly test the system capability, we set up scenarios in a closed test field, mimicking common real-world use cases for an excavator. Based on the successful test results in these scenarios, we also evaluated the efficiency and robustness of the system in one of our deployment sites, a waste disposal factory.

A. Perception Results

Fig. 4 demonstrates an excavator's process for digging and then loading truck, which is captured in a real-world mining operation scenario. As shown in Fig. 4 (Input dust image), the digging and truck loading process suffer from heavy dust, and camera images for the working areas and the excavator are blurry. In such a process, it is difficult for human eyes to perceive the surrounding and detect objects due to the existed dust. It could be even harder for computer vision technologies to perceive. For instance, the rock areas are difficult to localize even for humans. Therefore, the dust heavily impedes the automation of this process. As shown in Fig. 4 (Results), our approach can remove the influence of dust effectively, and the excavator and rocks areas can be easily detected after the dedusting process.

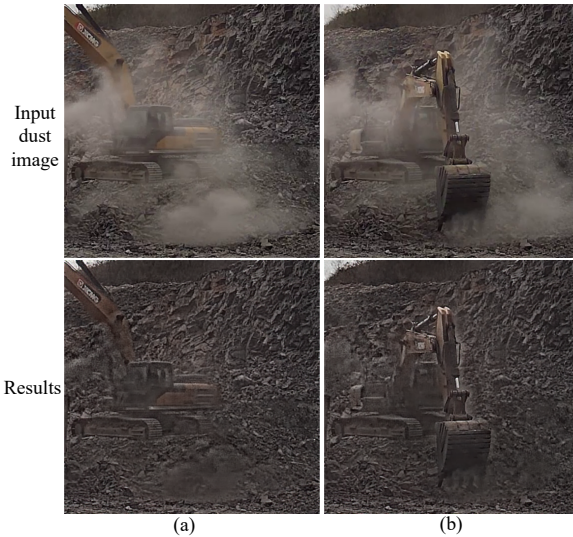


Fig. 4. Dedusting results of real-world captured dust images.

B. Terrain Navigation

Our system is deployed on a actual worksite larger than $200 m^2$. Our robust mapping and navigation system ensures that the excavator is able to reach the given goal in all trials, and maintains the average error under 9 cm overall.

C. AES Deployment for Real-World Scenarios

We have successfully deployed AES to a real-world scenario, where AES can run continuously for 24 hours without any human intervention as shown in Fig. 5. For the waste disposal and recycling applications, the excavator is assigned to load industrial waste material into a designated area. Afterward, the material is transferred and recycled. The material may consist of excessive dust, which is toxic to human beings. The material pile is not stable and could collapse, which is another threat to human operators. The speed of material loading by the excavator must coordinate with the belt conveyor's speed and material processing rate. Hence, there is a high-efficiency requirement for our autonomous excavator. In addition to satisfying the efficiency requirement, our autonomous excavator system can handle both dry and wet material. AES can also function at night. In this scenario, AES can operate a whole 24-hour day without any human intervention. The 7.5-ton excavator can handle as much as $67.1 m^3$ material per hour, which is closely equivalent to a human operator's performance. Furthermore, AES performs consistently over time, while the performance of human operators may vary. Since the deployment, AES system has been used by the customer for more than 8,500 hours.

VII. CONCLUSION

In conclusion, we highlight our recent progress on developing autonomous excavator system and deploying AES to real-world. In future, we plan to extend the system to handling more diverse scenarios, such as excavating fragmented rocks and operating in challenging weather conditions. We



Fig. 5. Robust and non-stop operation of AES in a real-world waste disposal scenario.

also would like to develop approaches for sensing and modeling material physical properties and excavation resistance force for autonomous excavation.

REFERENCES

- [1] Susan Afanuh, Matthew Gillen, and Thomas Lentz. Preventing worker deaths from trench cave-ins. <https://www.cdc.gov/niosh/docs/wp-solutions/2011-208/pdfs/2011-208.pdf?id=10.26616/NIOSH PUB 2011208>.
- [2] Tim Bauerle, Zoë Dugdale, and Gerald Poplin. Mineworker fatigue: A review of what we know and future decisions. *Mining engineering*, 70(3):33, 2018.
- [3] Siddharth Dadhich, Ulf Bodin, and Ulf Andersson. Key challenges in automation of earth-moving machines. *Automation in Construction*, 68:212–222, 2016.
- [4] Tianrui Guan, Zhenpeng He, Ruitao Song, Dinesh Manocha, and Liangjun Zhang. Tns: Terrain traversability mapping and navigation system for autonomous excavators. In *Robotics: Science and Systems*, 2022.
- [5] Dominic Jud, Simon Kerscher, Martin Wermelinger, Edo Jelavic, Pascal Egli, Philipp Leemann, Gabriel Hottiger, and Marco Hutter. Heap - the autonomous walking excavator. *Automation in Construction*, 129:103783, 2021.
- [6] Panagiotis Papadakis. Terrain traversability analysis methods for unmanned ground vehicles: A survey. *Engineering Applications of Artificial Intelligence*, 26(4):1373–1385, 2013.
- [7] Grand View Research. Excavator market size, share trends analysis report by product (crawler, wheeled, mini/compact), by application (construction), by region, competitive landscape, and segment forecasts, 2018 - 2025, July 2018.
- [8] Industry Research. Global excavator market report. <https://www.industryresearch.co-global-excavator-market-15473051>.
- [9] Sanjiv Sing. *Synthesis of tactical plans for robotic excavation*. PhD thesis, Carnegie Mellon University, 1995.
- [10] Xibin Song, Liangjun Zhang, Dingfu Zhou, and Jin Fang. Image dedusting with deep learning based closed-loop network. In *Proceedings of the International Symposium on Automation and Robotics in Construction (ISARC)*, 2021.
- [11] Liyang Wang, Zhixian Ye, and Liangjun Zhang. Hierarchical planning for autonomous excavator on material loading tasks. In *Proceedings of the 38th International Symposium on Automation and Robotics in Construction (ISARC)*, 2021.
- [12] Liangjun Zhang, Jinxin Zhao, Pinxin Long, Liyang Wang, Lingfeng Qian, Feixiang Lu, Xibin Song, and Dinesh Manocha. An autonomous excavator system for material loading tasks. *Science Robotics*, 6(55):eabc3164, 2021.
- [13] Sibo Zhang and Liangjun Zhang. Vision-based excavator activity analysis and safety monitoring system. In *Proceedings of the 38th International Symposium on Automation and Robotics in Construction (ISARC)*, 2021.

Upper extremity exoskeletons in construction, a field-based study

Sean T. Bennett, Peter G. Adamczyk, Fei Dai, Dharmaraj Veeramani, Michael Wehner Senior
Member, IEEE, and Zhenhua Zhu

Abstract— The construction trade requires repetitive, physically demanding manual tasks which can over time pose severe risks for work-related musculoskeletal disorders (WMSDs) [1]. Exoskeletons and exosuits (collectively called “EXOs” in this work) have substantial potential to protect workers and to increase worker productivity by reducing exertion and fatigue. Despite these potential benefits, EXOs are uncommon in the construction industry. We present preliminary results from a pilot study investigating the knowledge gaps and barriers to EXO adoption.

The overall objective of this work is to establish a foundational understanding of how EXOs can transform the future of construction trade work. The described work focuses on industry collaboration and field-based kinematic evaluation of three subjects performing a real-world construction task, removing wooden blocks from a steel-frame wall. We demonstrate the range of motion of the upper extremities of the subjects performing the task unassisted, followed by performing the task wearing two upper-extremity EXOs. This work is presented in parallel with our separate study (evaluating the effects of a lower back EXO while dumping a gondola of refuse) also presented at this workshop. Our preliminary findings build a foundation of understanding of EXO-enabled construction tasks. This will foster EXO adoption and yield benefits including but not limited to improving the productivity of construction trades, reducing the risks of WMSDs and injuries of trade workers, broadening the workforce participation in construction trades, and extending the career life expectancy of existing trade workers.

I. INTRODUCTION

Since the industrial revolution (and arguably long before that), tremendous effort has been made to evaluate work and work tasks, and to present possible improvements for the worker, their productivity, and for the organization as a whole. Ranging from new machinery, to formation of unions, to the widespread incorporation of Personal Protective Equipment (PPE), there have been widespread efforts to make the worker safer, more comfortable, and more productive. Through all of these efforts (and many non-industrial efforts), we have gained great understanding of occupational biomechanics [1], industrial ergonomics [2]–[4], anthropometry[5], [6], and workplace tasks such as symmetric [7] and general lifting [8] in both industrial and general tasks. Gaining this level of understanding took countless studies over many years, yet our knowledge is

incomplete, and workplace musculoskeletal injuries remain the second most common cause of absenteeism after the common cold. There is such a broad range of workers (anthropometry, strength, age), situation (work conditions, survivor bias, external stressors) and tasks (myriad industries requiring countless tasks) that a comprehensive evaluation of industrial work remains essentially impossible. Adding exoskeletons to these work scenarios holds a great deal of promise but makes the problem even more challenging.

Many administrative and engineering solutions have been implemented to reduce workplace injury with varying levels of success. Safety and assistive devices such as overhead supported lifts for tools and packages have been installed in industrial settings such as automobile assembly plants. Box lifts and conveyors are widespread in material handling locations such as order fulfillment centers and delivery warehouses such as the US postal service. These devices, often rigidly bolted to the floor of a material handling center or suspended from above in a manufacturing plant, have dramatically reduced industrial injuries [9], [10]. In unstructured environments, such as construction sites, these rigidly mounted devices are limited to areas around work vehicles. For most job tasks, often high in the air, remote, or requiring high mobility, these assist devices remain largely impractical.

Exoskeletons have been developed over many years for many applications [11]–[13], including several by our team [14]–[17]. Since Ralph Mosher introduced the Hardiman at General Electric Research in 1968, (and long before that in the entertainment/science fiction domain) there has been considerable interest in exoskeletons to assist humans with various assistance, augmentation, rehabilitation, and evaluation tasks [18], [19]. Exoskeletons have been developed, in both passive (unpowered, relying on pulleys, springs, elastic straps for energy storage) and active (using stored energy such as batteries and motors or compressed gas and pneumatic actuators) forms, by academic groups for research and by the private sector as products. Many EXOs have been developed for medical applications (to evaluate or rehabilitate motion, correct gait, augment those with reduced ability). Another type of EXO, largely funded by the military, aims to reduce the metabolic cost of walking or reduce effort needed to carry heavy backpacks long distances. While members of our team have developed both types of EXOs, here, we do not cover medical or backpack-carrying devices,

*Research supported by the National Science Foundation.

S. T. Bennett, P. G. Adamczyk, M. Wehner, are with the Mechanical Engineering Department, University of Wisconsin, Madison, WI. 53706 USA (e-mails: stbennett2@wisc.edu, peter.adamczyk@wisc.edu, wehner2@wisc.edu respectively).

F. Dai is with the Civil and Environmental Engineering Department, West Virginia University, Morgantown, WV. 26506 USA (e-mail: fei.dai@mail.wvu.edu).

D. Veeramani is with the Industrial and Systems Engineering Department, University of Wisconsin, Madison, WI. 53706 USA (e-mail: raj.veeramani@uwebc.wisc.edu).

Z. Zhu is with the Civil and Environmental Engineering Department, University of Wisconsin, Madison, WI. 53706 USA (corresponding author: (608) 265-3228; zhu286@wisc.edu).

and instead focus on EXOs primarily used to assist able-bodied wearers in occupational tasks.

The construction industry, comprised of highly variable tasks in fast-changing environments, often in temporary/short-term jobsites do not lend themselves well to traditional automation devices such as overhead lift-assist, industrial robots, and conveyor systems. Thus, the construction trades rely largely on the strength and skill of able-bodied workers. It is our hypothesis that EXOs are better suited to assisting workers than traditional industrial automation tools. It is our long-term goal to study the tasks performed by construction tradesmen, and better understand the potential role that EXOs may play, including most appropriate tasks, potential for augmentation and injury reduction, and limitations of EXOs on the worksite.

II. METHOD

A. Defining EXOs

This work describes a task performed in three configurations: First unassisted, then wearing each of two EXOs (EXO 1: Hilti EXO-01, and EXO 2: Ekso Evo). Both EXOs are passive shoulder exoskeletons as shown in Figure 1. For this study, passive EXOs were selected (vs. active EXOs), as they are less complex, require no charging/charge monitoring, and several models are now commercially available [20]. Many EXOs have been developed in laboratory settings. These devices are often faced with user complaints including poor fit, chafing, uncomfortable contact stress from high assistive force, and little perceived assistance [21]–[23]. Further, in the construction trades, any device which limits worker speed or range of motion could be seen as reducing productivity, and may face an insurmountable barrier to acceptance [24], [25]. The two EXOs selected for this work have undergone extensive evaluation and testing for ergonomics, fit, and comfort during the development process from laboratory prototypes to commercial systems, giving them greater promise for user acceptance.

B. Defining the Task

Often, EXO evaluation studies focus on an EXO's ability to reduce muscle activation level (as measured via change in electromyographic data), reduce metabolic cost (as measured

changes are generally evaluated on subjects wearing EXOs while performing tasks in controlled laboratory environments [26], [27]. To perform consistent evaluations, tasks are often reduced and experimentally controlled, such as maintaining specific postures or repeated lifting and lowering of a package in the sagittal plane. Such tasks are generally designed to isolate parameters (e.g., activation level of specific muscles in the back, shoulder, etc.), rather than to emulate real-world construction tasks. While these simulations are valuable for initial explorations of prototype EXO effectiveness, real-world demonstrations of effectiveness are necessary if the broader industry is to adopt EXOs on the worksite. Previous evaluations have found that EXOs are quite effective in reducing activation levels in specific targeted muscles during highly structured predefined tasks. However, when evaluating the effects of an exoskeleton on muscles which it was NOT designed to assist, one study showed an increase of mean and peak muscle activation in most cases [28]. Thus careful analysis of the EXOs in real-world tasks, and the overall effectiveness of the EXOs is critical.

C. Experimental Procedure

We partnered with a prominent local construction contractor to evaluate workers as they performed typical construction tasks. Worker motion data was collected in the unassisted case as well as while wearing each of the two EXOs shown in Figure 1. Workers installed and later removed wooden blocks from a metal support structure. For this experiment, we analyzed the block removal operation to investigate the highly non-neutral postures required to remove screws in various locations in the framework. This task required working at or above shoulder height, supporting a wooden block (50 mm x 150 mm x 400 mm, mass of 910 gram) in one hand and a power screwdriver in the other. After removing four screws holding the block in place, the block is removed from inside the sheet-metal studs and placed on a pile of blocks.

Three workers (male, age 25 to 61 with 4-35 years in their current jobs) participated in the task. Each worker initially performed their task in an unassisted state (no EXO). To reconstruct full-body kinematics, video was recorded through the duration of the experiment. Additionally, subjects



Figure 1. The two passive shoulder exoskeleton systems, and evaluation of the block removal task. A. Hilti EXO-01 (left) and Ekso Evo (right). B Still image from video data of a worker performing the block removal task (left), and a still from motion capture data from the sensor suit (right).

via change in oxygen consumption), and increase overall satisfaction (as measured via survey responses). These

performed all tasks while wearing a suite of movement sensors (XSens MVN Awinda). Each subject removed 18 blocks over

roughly 15 minutes without EXO. Next, the subject donned the first EXO (still wearing the suite of motion sensors) and installed then removed an additional 18 blocks. Finally, the worker switched to the second EXO and installed then removed an additional 18 blocks (still wearing the suite of motion sensors). All subjects completed a survey on comfort, pain, and perceived effectiveness of using EXOs.

III. RESULTS

Results from the block removal tests by three subjects suggested changes in body kinematics from using the EXO versus performing the same task unassisted. The results are summarized with mean \pm SD in Table 1. Shoulder flexion/extension and shoulder abduction/adduction are given as combined results for the three subjects. Flexion/extension data shows little change based on EXO use vs unassisted task performance, but shoulder abduction/adduction showed more difference between the three cases (unassisted, Hilti EXO-01, and Ekso Evo). The Ekso Evo showed the greatest difference in shoulder abduction/adduction of the three cases. In order to explore data for individual subjects, shoulder abduction/adduction data is shown in Figure 2 for left and right arms for each of the three subjects. Because the exo is providing a restoring force (assisting in attaining elevated shoulder postures with reduced muscle activation), we can no longer say that increased shoulder flexion or abduction is necessarily an undesirable result. Note how in several cases

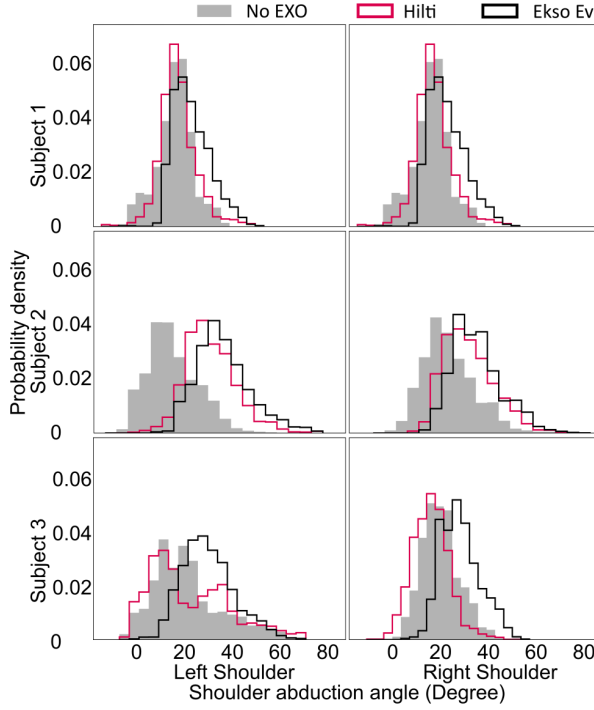


Figure 2. Results for 3 subjects, shoulder abduction (adduction shown as negative) during block removal task. Comparing unassisted vs. two EXOs. Both EXOs (and especially Ekso Evo increased abduction angle through most of task duration. Fraction of task duration recorded as probability density. For all curves, Overall probability (area under curve) equals one.

(especially notable with subject 2), the most common posture (highest probability density) is “shifted” toward non-neutral.

That may simply be the EXO restoring force causing an at-rest shoulder posture to be slightly abducted.

TABLE I. RANGE OF MOTION, FLEXION/EXTENSION

	Condition	Shoulder Flexion/Extension		
		Mean \pm S.D.	IQR (25-75%)	ROM (5-95%)
Left	No EXO	51.1 \pm 1.1	52 \pm 3	92.7 \pm 0.9
	Hilti EXO-01	45 \pm 6	45 \pm 3	91 \pm 8
	Ekso Evo	48 \pm 7	47 \pm 10	90 \pm 25
Right	No EXO	42 \pm 6	61 \pm 13	103 \pm 3
	Hilti EXO-01	37 \pm 4	47 \pm 12	90 \pm 11
	Ekso Evo	41 \pm 15	46 \pm 5	87 \pm 12

TABLE II. RANGE OF MOTION, ABDUCTION/ADDITION

	Condition	Shoulder Abduction/Adduction		
		Mean \pm S.D.	IQR (25-75%)	ROM (5-95%)
Left	No EXO	17 \pm 4	15.5 \pm 1.4	42 \pm 8
	Hilti EXO-01	24 \pm 6	19 \pm 6	44 \pm 11
	Ekso Evo	33 \pm 3	17 \pm 5	39 \pm 3
Right	No EXO	20 \pm 4	11 \pm 3	30 \pm 5
	Hilti EXO-01	22 \pm 9	11 \pm 3	28 \pm 6
	Ekso Evo	29 \pm 6	11.8 \pm 1.2	29 \pm 5

IV. DISCUSSION

The critical overall finding is that results from both exoskeletons suggest systematic changes in body kinematics during the construction tasks tested. Data in Figure 2 demonstrates that not all subjects changed their kinematics equally. This phenomenon of responders and non-responders is common in human-subjects research, including with exoskeletons in laboratory tests; it nevertheless impedes us from drawing consistent conclusions. Issues such as discomfort or imperfect fit could cause certain individuals to reject the available assistance or fight against it. Certain devices may be inappropriate for these individuals, or they might just take more time to adapt [29].

During the block removal task, the major finding was that both the Hilti EXO-01 and Ekso Evo exoskeletons both led to a reduced 5-95% range of motion in shoulder flexion/extension on the right arm. It is interesting to note that the effect appears unilateral. While the EXO is symmetrical in its assisting force, the task itself is not symmetrical, and so certain motions might not happen on both arms. The change in probability density (particularly in abduction/adduction) is more pronounced with the Ekso Evo than for the Hilti EXO-01. This finding offers the opportunity to contrast the two designs. One notable difference is that the support columns along the back of these exoskeletons are attached in very different ways. On the Ekso Evo, they are mounted rigidly to the waist belt at a relatively medial location, whereas on the Hilti EXO-01 they are mounted to a free-moving ball joint on the belt at a relatively lateral location. It could be that the movement or lack of movement in these uprights could impede the motion more in the Ekso Evo. Alternatively, the Ekso Evo has a multi-link folding mechanism concealed inside the textile pouch along the upright; this could restrict movement.

Or, it could be that the shoulder joint itself could produce torque in a way that pushes the arm into different directions, even if it does not actually restrict movement. One observation about the task itself is that overall hand height is largely dictated by shoulder flexion; thus, shoulder flexion/extension may be less affected by the use of an EXO and more affected by task design. Given the various possible reasons for the observed behavioral change in angles and range, further investigation of the mechanisms of the two exoskeletons is needed.

Shoulder abduction/adduction results are also interesting. The main finding is that the Ekso Evo caused an increase in the mean shoulder abduction angle, in this case bilaterally. The users' experience was that the spring force tended to lift the arms away from neutral into abduction even when the user had no specific intention to do so. Perhaps this considerable increase in shoulder abduction is an indication that the compensating force of the EXOs allows subjects to more comfortably sustain non-neutral postures during tasks.

A secondary finding is that the Hilti EXO-01 may reduce the shoulder abduction 5-95% range of motion. These results provide encouraging preliminary data, motivating us to continue our investigations. Future testing can include additional sensors such as electromyography (EMG) sensors to sense muscle activation, instrumented insoles to record gait and stance variations, and perhaps even VO₂ measurements to record metabolic cost of performing the tasks.

ACKNOWLEDGMENT

This research was supported by the National Science Foundation via grants #CNS-2128823 and #CNS-2128716. The authors also acknowledge M.A. Mortenson Company for their collaboration on this research.

REFERENCES

- [1] D. B. Chaffin, G. B. J. Andersson, and B. J. Martin, *Occupational Biomechanics*. John Wiley & Sons, 2006.
- [2] Eastman Kodak Company, *Ergonomic design for people at work: Volume 1.*, 1st ed. Belmont, CA. USA.: Lifetime Learning Publications, 1983.
- [3] Eastman Kodak Company, *Ergonomic design for people at work: Volume 2.*, 1st ed. Belmont, CA. USA.: Van Nostrand Rienhold, 1986.
- [4] P. Jacobs, "Kodak's Ergonomic Design for People at Work," *Prof. Saf.*, vol. 49, no. 3, p. 49, 2004.
- [5] A. Hrdlička, *Anthropometry*. Wistar Institute of Anatomy and Biology, 1920.
- [6] S. Pheasant, *Bodyspace, Anthropometry, Ergonomics and the Design of Work*, 3rd ed. Boca Raton: CRC Press, 2018.
- [7] W. S. Marras *et al.*, "The role of dynamic three-dimensional trunk motion in occupationally-related low back disorders. The effects of workplace factors, trunk position, and trunk motion characteristics on risk of injury," *Spine*, vol. 18, no. 5, pp. 617–628, Apr. 1993, doi: 10.1097/00007632-199304000-00015.
- [8] S. Gallagher and W. S. Marras, "Tolerance of the lumbar spine to shear: A review and recommended exposure limits," *Clin. Biomech.*, vol. 27, no. 10, pp. 973–978, Dec. 2012, doi: 10.1016/j.clinbiomech.2012.08.009.
- [9] S. J. Schwartz, "Minimizing Severe Injury & Fatality Risk in Warehouse Operations," *Prof. Saf.*, vol. 66, no. 7, pp. 15–17, Jul. 2021.
- [10] B. Gutelius and N. Theodore, "The Future of Warehouse Work: Technological Change in the U.S. Logistics Industry," *UC Berkeley Labor Cent.*, p. 8, 2019.
- [11] Z. Zhu, A. Dutta, and F. Dai, "Exoskeletons for manual material handling – A review and implication for construction applications," *Autom. Constr.*, vol. 122, p. 103493, Feb. 2021, doi: 10.1016/j.autcon.2020.103493.
- [12] D. Shi, W. Zhang, W. Zhang, and X. Ding, "A Review on Lower Limb Rehabilitation Exoskeleton Robots," *Chin. J. Mech. Eng.*, vol. 32, no. 1, p. 74, Aug. 2019, doi: 10.1186/s10033-019-0389-8.
- [13] R. A. R. C. Gopura, D. S. V. Bandara, K. Kiguchi, and G. K. I. Mann, "Developments in hardware systems of active upper-limb exoskeleton robots: A review," *Robot. Auton. Syst.*, vol. 75, pp. 203–220, Jan. 2016, doi: 10.1016/j.robot.2015.10.001.
- [14] M. Wehner, "Lower extremity exoskeleton as lift assist device," Ph.D., University of California, Berkeley, United States -- California. Accessed: May 03, 2022. [Online]. Available: <https://www.proquest.com/docview/304836262/abstract/1D02AFBEFB434EE8PQ1>
- [15] M. Wehner, D. Rempel, and H. Kazerooni, "Lower Extremity Exoskeleton Reduces Back Forces in Lifting," Sep. 2010, pp. 49–56. doi: 10.1115/DSCC2009-2644.
- [16] M. Wehner *et al.*, "Experimental characterization of components for active soft orthotics," in *2012 4th IEEE RAS EMBS International Conference on Biomedical Robotics and Biomechatronics (BioRob)*, Jun. 2012, pp. 1586–1592. doi: 10.1109/BioRob.2012.6290903.
- [17] M. Wehner, "Man to machine, applications in electromyography," *EMG Methods Eval. Muscle Nerve Funct.*, vol. 29, pp. 427–454, 2012.
- [18] R. S. Mosher, "Handyman to Hardiman," *SAE Trans.*, vol. 76, pp. 588–597, 1968.
- [19] R. S. Mosher, "Exploring the Potential of a Quadruped," *SAE Trans.*, vol. 78, pp. 836–843, 1969.
- [20] J. P. Pinho *et al.*, "A comparison between three commercially available exoskeletons in the automotive industry: an electromyographic pilot study," in *2020 8th IEEE RAS/EMBS International Conference for Biomedical Robotics and Biomechatronics (BioRob)*, Nov. 2020, pp. 246–251. doi: 10.1109/BioRob49111.2020.9224362.
- [21] L. Xing, M. Wang, J. Zhang, X. Chen, and X. Ye, "A Survey on Flexible Exoskeleton Robot," in *2020 IEEE 4th Information Technology, Networking, Electronic and Automation Control Conference (ITNEC)*, Jun. 2020, vol. 1, pp. 170–174. doi: 10.1109/ITNEC48623.2020.9084920.
- [22] J. Wolff, C. Parker, J. Borisoff, W. B. Mortenson, and J. Mattie, "A survey of stakeholder perspectives on exoskeleton technology," *J. NeuroEngineering Rehabil.*, vol. 11, no. 1, p. 169, Dec. 2014, doi: 10.1186/1743-0003-11-169.
- [23] D. Hill, C. S. Holloway, D. Z. M. Ramirez, P. Smitham, and Y. Pappas, "WHAT ARE USER PERSPECTIVES OF EXOSKELETON TECHNOLOGY? A LITERATURE REVIEW," *Int. J. Technol. Assess. Health Care*, vol. 33, no. 2, pp. 160–167, ed 2017, doi: 10.1017/S0266462317000460.
- [24] S. Kim *et al.*, "Potential of Exoskeleton Technologies to Enhance Safety, Health, and Performance in Construction: Industry Perspectives and Future Research Directions," *IIE Trans. Occup. Ergon. Hum. Factors*, vol. 7, no. 3–4, pp. 185–191, Oct. 2019, doi: 10.1080/24725838.2018.1561557.
- [25] A. S. Koopman, I. Kingma, M. P. de Looze, and J. H. van Dieën, "Effects of a passive back exoskeleton on the mechanical loading of the low-back during symmetric lifting," *J. Biomech.*, vol. 102, p. 109486, Mar. 2020, doi: 10.1016/j.jbiomech.2019.109486.
- [26] N. J. Gonsalves, O. R. Ogunseju, A. A. Akanmu, and C. A. Nnaji, "Assessment of a passive wearable robot for reducing low back disorders during rebar work," *J. Inf. Technol. Constr. ITcon*, vol. 26, no. 50, pp. 936–952, Nov. 2021, doi: 10.36680/j.itcon.2021.050.
- [27] M. F. Antwi-afari *et al.*, "Assessment of a passive exoskeleton system on spinal biomechanics and subjective responses during manual repetitive handling tasks among construction workers," *Saf. Sci.*, vol. 142, Oct. 2021, Accessed: May 03, 2022. [Online]. Available: <https://publications.aston.ac.uk/id/eprint/42772/>
- [28] E. B. Weston, M. Alizadeh, G. G. Knapik, X. Wang, and W. S. Marras, "Biomechanical evaluation of exoskeleton use on loading of the lumbar spine," *Appl. Ergon.*, vol. 68, pp. 101–108, Apr. 2018, doi: 10.1016/j.apergo.2017.11.006.
- [29] K. L. Poggensee and S. H. Collins, "How adaptation, training, and customization contribute to benefits from exoskeleton assistance," *Sci. Robot.*, vol. 6, no. 58, p. eabf1078, Sep. 2021, doi: 10.1126/scirobotics.abf1078.

Sharing Construction Safety Inspection Experiences and Site-Specific Knowledge through XR-Augmented Visual Assistance

Pengkun Liu^{1*}, Jinding Xing^{1*}, Ruoxin Xiong¹ and Pingbo Tang^{1**}

Abstract— Early identification of on-site hazards is crucial for accident prevention in the construction industry. Currently, the construction industry relies on experienced safety advisors (SAs) to identify site hazards and generate mitigation measures to guide field workers. However, more than half of the site hazards remain unrecognized due to the lack of field experience or site-specific knowledge of some SAs. To address these limitations, this study proposed an Extended Reality (XR)-augmented visual assistance framework, including Virtual Reality (VR) and Augmented Reality (AR), that enables capturing and transferring subconscious inspection strategies between workers or workers/machines for a construction safety inspection. The purpose is to enhance SA's training and real-time situational awareness for identifying on-site hazards while reducing their mental workloads.

I. INTRODUCTION

The construction site is one of the most hazardous places. In the U.S., among all the fatalities in the private sector, more than 21% of fatalities occurred in the construction industry in 2020 [1]. Besides the fatal injuries, the non-fatal injury rate in the construction industry is still around 29% higher than in the other industries [1]. The cost of these safety incidents exceeds \$170 billion each year alone in the U.S [2]. Besides the enormous economic loss, these safety incidents can result in project schedule delays and loss of reputation damage for contractors.

In current practice, safety advisors (SA) perform a routine on-site inspection to identify potential safety hazards and generate mitigation measures accordingly. During on-site visits, the SA firstly analyzes the current safety plans, then walks around the job site to check the current safety situation of the workers, materials, and equipment. After the visit, the SA will report the visit and update the safety plans to mitigate unsafe situations and practices [3-5].

However, previous studies revealed that about 57% of the construction hazards remain unrecognized on the job site [6]. The SA's limited experience or lack of familiarity with certain workspaces or certain parts of domain knowledge are possible contributors. The insufficient number of experienced SAs and the dynamic nature of construction sites further increase SAs' misses of on-site hazards [7].

Extended Reality (XR), which is an emerging technology that melds Augmented Reality (AR) and Virtual Reality (VR), shows the potential to help SA identify on-site hazards effectively. In XR, the SA can navigate or control a digital robot to navigate a virtual construction site (VR) and interact with a virtual interface that contains safety-related information in real construction workspaces (AR). Existing XR-related solutions rely on computer simulations and computer vision techniques to infer the on-site hazards [8]. Current studies provide limited information on less salient on-site hazards, such as hazards associated with manual material handling. The less salient on-site hazards are often interdependences with the construction schedule, physical space, and material properties [9]. In some cases, identifying less salient on-site hazards requires the SA has in-depth safety-related knowledge, rich experiences, and site-specific knowledge. Nevertheless, collecting and reusing experts' safety-related knowledge and site inspection experiences to identify less salient on-site hazards has not been fully explored.

This study presents an XR-augmented visual assistance framework that incorporates the benefits of VR, expert knowledge, and AR to enhance the SA's situation awareness in the safety inspection of the construction site. The proposed framework consists of three major components: (1) VR environment for capturing expert's visual trajectories in safety inspection; (2) inspection strategy discovery through process mining of the captured visual trajectories of a digital drone; (3) AR user interface for visualization inspection strategies.

The contribution of this study to the body of knowledge is three folds: (1) review existing studies relevant to XR and point out the research gaps; (2) propose a framework that captures and shares expert site-specific knowledge and inspection experiences through process mining and XR for assisting SA's safety inspection on construction sites; (3) provide a proof-of-concept model for XR-augmented visual assistance to the SA through a case study of fire safety equipment inspection with a digital drone.

II. RELATED WORK

This section reviews recent work that uses new technologies to enhance safety inspection on site.

A. Virtual Reality for Construction

VR is a graphic representation technology that generates a three-dimensional representation of the construction field. Many studies used VR to enhance SAs' safety inspection knowledge by asking the SAs to perform inspection tasks on a virtual construction site [10, 11]. Particularly, the VR model generated from the as-built 3D point cloud provides the SA with a full experience of the real construction site and can offer an effective learning experience for the SA [12]. However, the

*Contributes Equally

** Corresponding Author

Pengkun Liu, Jinding Xing, Ruoxin Xiong and Pingbo Tang is with the Department of Civil and Environmental Engineering, Carnegie Mellon University; e-mail: pengkunl, jindingx, ruoxinx, ptang@andrew.cmu.edu.

VR system does not provide any dynamic highlights to guide SAs in discovering safety-critical objects in given scenes. As a result, the SA needs to interpret the scenarios in the virtual construction site when performing an inspection on a real site, which adds extra cognitive workload to the SA.

B. Augmented Reality for Construction

AR is a promising approach to mitigate the limitations of VR. Some other studies used AR as a 3D viewer that overlays virtual objects and information on the physical site views to help SA identify and recognize hazards [13, 14]. The virtual information generated from building information modeling (BIM) provides rich geometry information about the construction project [15]. Such methods help the SA maintain better situational awareness of the construction site. Yet, the virtual information generated from computer simulations of a construction environment provides a limited reflection of real-world environments, such as time, physical space, and material properties [9]. Often the virtual information helps the

SA infer geometry-related hazards, such as falls, struck by an object [16]. It remains challenging for naive SA to identify less salient hazards, such as the spreading of chemical hazards and fires.

C. Extended Reality for Construction

Some studies used a combination of XR and machine learning techniques to deliver and visualize hazard information to SAs [16]. These studies use an AR interface to visualize information relevant to site hazards detection. The virtual information is generated through computer vision techniques that detect hazardous scenarios. Navigation planning algorithms are also used to generate a safe and efficient path for SAs [17]. The combined solution for improving safety inspection on-site has been provided to be very effective. However, this solution overlooked experts' experiences and site-specific knowledge, which is critical to identifying less salient hazards in dynamic and cluttered environments.

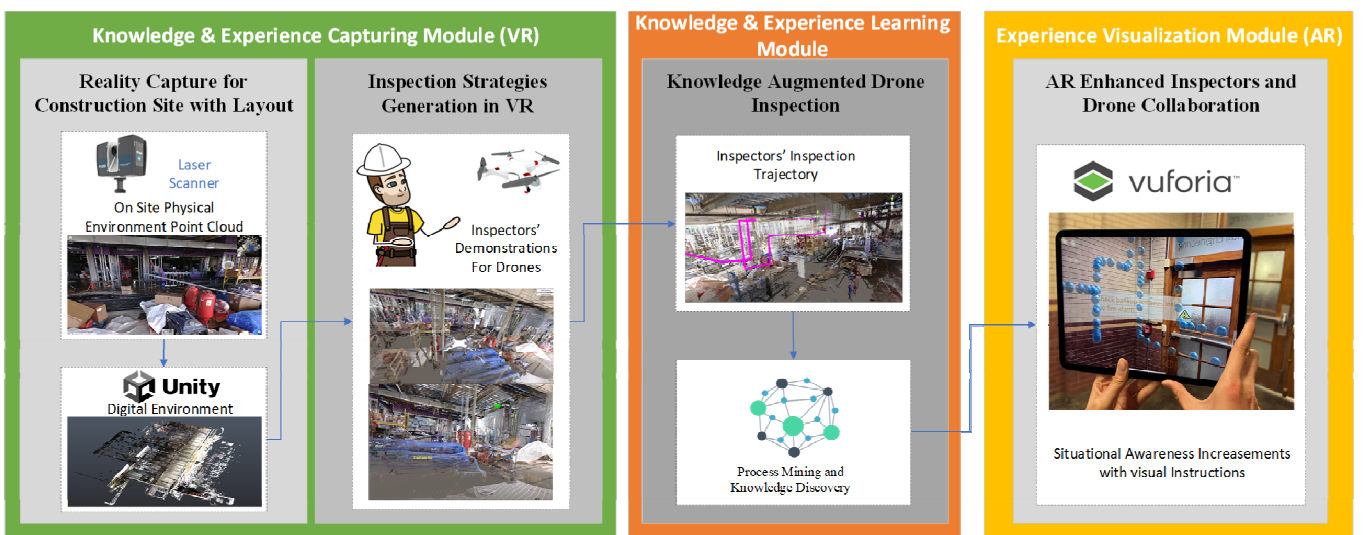


Figure 1. The proposed XR-augmented visual assistance framework for assisting construction safety inspection

III. PROPOSED SOLUTION

This study proposed an XR-augmented visual assistance system aiming to learn and transfer implicit inspection strategies associated with subconscious experiences and site-specific knowledge between SAs or SAs/machines for a construction safety inspection to enhance SA's situational awareness. The proposed system comprises three modules, as shown in Figure 1: (1) inspection visual trajectory capture module (VR module): where a SA's behaviors and inspection strategies are recorded through controlling a digital drone during the interaction with the reconstructed digital environment in the VR environment; (2) inspection knowledge & experience learning module (learning module), where process mining algorithms will be applied to discover knowledge and inspection strategies captured from the VR module; (3) and a visualization interface (AR interface), where AR-enhanced SAs and digital drone collaborate to detect real-hazards or hazardous scenarios with unsafe combinations of objects' states. Figure 1 shows the overall framework of the proposed system.

The VR module aims to capture SA's observation trajectories in identifying on-site construction hazards. The inspection knowledge and experience capturing module includes a virtual construction site generated from a 3D scan of the construction site and a virtual drone. The SA can control a digital drone from the first perspective to observe and interact with the virtual construction site in the VR module, as shown in Figure 2. Meanwhile, the virtual drone will record the SA's observation trajectories in the VR environment.

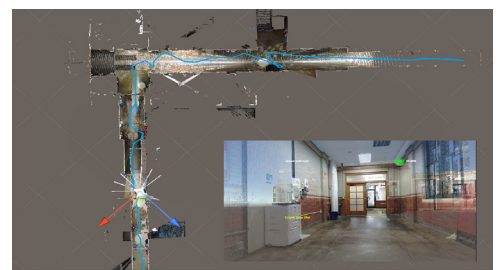


Figure 2. Safety inspectors use a digital drone to explore and search hazards on the virtual construction site

The knowledge and experience learning module is tasked with collecting multiple SAs' inspection strategies, especially the object detection sequences and related contextual information. As shown in Figure 3, the digital drone equipped with laser for fire safety equipment detection, such as the emergency exit lights, fire alarm panels and so on. Furthermore, the point cloud segmentation for scene understanding and semantic mapping with building information modeling is also significant for learning such inspection strategies. Then the knowledge of inspection of SA's observations and related decisions could be stored as a knowledge graph [18-20].

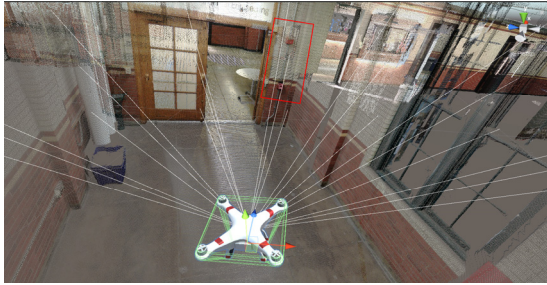


Figure 3. Digital drone equipped with laser for object detection (emergency exit lights and fire alarm panels)

The AR interface is used to visualize and replay the learned inspection strategies and knowledge. This paper developed an iOS app by Vuforia to facilitate the SA's safety inspection process. In the app, augmented information (expert's observation trajectories and relevant safety information) overlay in the real construction site to direct the SAs for identifying on-site hazards and increasing their situational awareness.

IV. CASE STUDY

This study used a campus building to test the proposed system. The participants are asked to perform fire safety inspections inside the building. During the inspection process, SAs should check the status of the fire extinguishers, fire alarms, exit signs, and fire rescue equipment as required by the current building safety regulations. Missed potential safety hazards can lead to devastating consequences in the fire situation. The goal of the inspection task is to ensure that the fire equipment is in functional conditions.



Figure 4. Visualization of SA's inspection histories

This study used iPad pro 11 to capture the 3D layout of the campus building and visualize the generated fire inspection information. The first phase is to create a digital VR model from the physical world in Unity 3D. Given that, the laser scanner is used to capture the high-quality point cloud of a campus building. Once the point cloud of the physical world is

collected, it will be imported into Unity 3D to rebuild the digital environment. Then in the digital environment, the SA can navigate in the environment and carry out fire equipment inspection without any guidance. Then the SA's inspection strategies would be recorded through the first-person perspective with timestamps, as shown in Figure 2. The blue lines demonstrate the SA's inspection strategies and attention division. Especially, inspectors would spend more time checking the fire equipment and switching the camera angle to look around the surrounding environments. Therefore, the blue lines represent the inspection strategies which would be denser and clustered near the fire equipment. Once the strategies are collected, the SA's inspection visual trajectory will be used to guide the digital drone to navigate and search the objects in the digital environment, as shown in Figure 3. In addition, to make the digital drone capable of sensing, the digital drone is equipped with multiple laser sensors to detect the objects in the digital environment, as shown in Figure 4. Therefore, the collected inspection trajectories are mapped with semantic information to understand the mechanics of SAs' observations and decisions.

Finally, with the help of AR, in the physical world, the on-site SA equipped with an iPad could replay the inspection strategies and check the inspection instructions, as shown in Figure 5. The optimal trajectories and instructions representing expert knowledge could be delivered to naive SAs. For example, in the fire extinguisher inspection task, the AR module maps the visual inspection trajectory in the reconstructed VR environment (the trajectory constitutes of blue spheres) to the real world. Such mapping can also show detailed inspection instructions, such as checking the test and maintenance dates. Furthermore, the density of the blue spheres represents the relative attention time, which means the SA spends more time at this place to check the equipment, such as the SA would check the battery conditions of fire alarms and exit signs/lights.

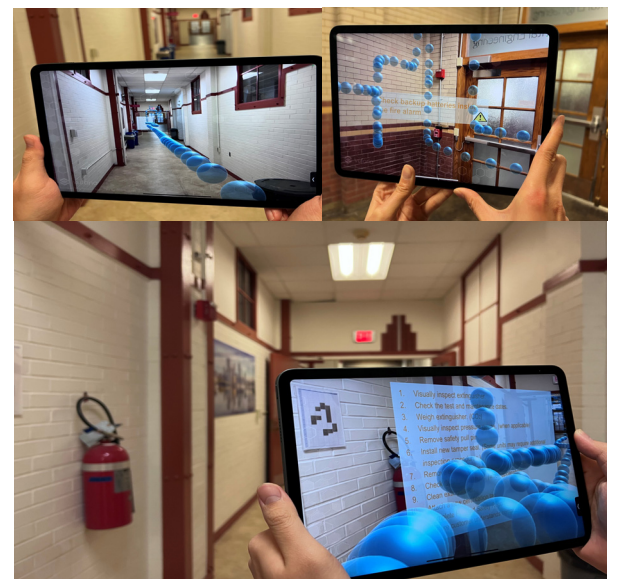


Figure 5. An inspector navigates to target equipment with the XR-augmented visual assistance platform

Therefore, the authors demonstrate the potential of the proposed XR-augmented system for the fire safety equipment inspection tasks in a physical-digital environment where a digital drone collects and learn from the SA's inspection strategies and replays the searching strategies for SAs in the physical environment with detailed instructions.

V. CONCLUSION AND FUTURE WORK

The authors demonstrated the potential for increasing the inspectors' situational awareness in a fire equipment safety inspection task with XR. In the case study, the SA perform inspection tasks by controlling a digital drone to navigate in a VR construction site. The digital drone could learn from the SA's inspection strategies and localizes potential safety hazards to assist safety inspectors to identify field hazards. Furthermore, the AR module could replay the inspection strategies in the physical world to enhance the SAs' situational awareness.

This paper has not fully considered the process mining and knowledge discovery from the multiple inspectors' observation trajectories. For future work, this paper will pattern mining of the SAs' observation trajectories collected in the VR world and explore the relationship between the mined pattern and the BIM model to summarize the knowledge of SAs.

ACKNOWLEDGMENT

This material is based on work supported by the Nuclear Energy University Program (NEUP) of the U.S. Department of Energy (DOE) under Award No. DE-NE0008864, and NASA University Leadership Initiative program (Contract No. NNX17AJ86A, Project Officer: Dr. Anupa Bajwa, Principal Investigator: Dr. Yongming Liu).

REFERENCES

- [1] U. S. Bureau of Labor Statistics. *Fatal occupational injuries by industry and event or exposure, all United States*, <https://www.bls.gov/iif/oshwc/cfoi/cftb0340.htm> (accessed: May. 8, 2020)
- [2] NSC analysis of data from the BLS CFOI surveillance program. 2020 *Occupational Safety Highlights*, <https://injuryfacts.nsc.org/work/work-overview/work-safety-introduction/> (accessed: May. 19, 2020)
- [3] J. Irizarry, M. Gheisari, and B. N. Walker, "Usability assessment of drone technology as safety inspection tools," *Journal of Information Technology in Construction (ITcon)*, vol. 17, no. 12, pp. 194-212, 2012.
- [4] Q. Chen and R. Jin, "A comparison of subgroup construction workers' perceptions of a safety program," *Safety science*, vol. 74, pp. 15-26, 2015.
- [5] P. Liu, R. Xiong, and P. Tang, "Mining Observation and Cognitive Behavior Process Patterns of Bridge Inspector," arXiv preprint arXiv:2205.09257, 2022.
- [6] P.-C. Liao, X. Sun, and D. Zhang, "A multimodal study to measure the cognitive demands of hazard recognition in construction workplaces," *Safety Science*, vol. 133, p. 105010, 2021.
- [7] A. Albert, M. R. Hallowell, and B. M. Kleiner, "Experimental field testing of a real-time construction hazard identification and transmission technique," *Construction Management and Economics*, vol. 32, no. 10, pp. 1000-1016, 2014.
- [8] F. Dai, A. Olorunfemi, W. Peng, D. Cao, and X. Luo, "Can mixed reality enhance safety communication on construction sites? An industry perspective," *Safety Science*, vol. 133, p. 105009, 2021.
- [9] R. E. Pereira, M. Gheisari, and B. Esmaeili, "Using panoramic augmented reality to develop a virtual safety training environment," in *Construction research congress*, 2018, vol. 2018, pp. 29-39.
- [10] S. Bhoir and B. Esmaeili, "State-of-the-art review of virtual reality environment applications in construction safety," *AEI 2015*, pp. 457-468, 2015.
- [11] X. Li, W. Yi, H.-L. Chi, X. Wang, and A. P. Chan, "A critical review of virtual and augmented reality (VR/AR) applications in construction safety," *Automation in Construction*, vol. 86, pp. 150-162, 2018.
- [12] R. Sacks, A. Perlman, and R. Barak, "Construction safety training using immersive virtual reality," *Construction Management and Economics*, vol. 31, no. 9, pp. 1005-1017, 2013.
- [13] C. Nnaji and A. A. Karakhan, "Technologies for safety and health management in construction: Current use, implementation benefits and limitations, and adoption barriers," *Journal of Building Engineering*, vol. 29, p. 101212, 2020.
- [14] J. Ramos-Hurtado, M.-L. Rivera, J. Mora-Serrano, A. Deraemaeker, and I. Valero, "Proposal for the Deployment of an Augmented Reality Tool for Construction Safety Inspection," *Buildings*, vol. 12, no. 4, p. 500, 2022.
- [15] B. Schiavi, V. Havard, K. Beddiar, and D. Baudry, "BIM data flow architecture with AR/VR technologies: Use cases in architecture, engineering and construction," *Automation in Construction*, vol. 134, p. 104054, 2022.
- [16] S. Wu, L. Hou, G. K. Zhang, and H. Chen, "Real-time mixed reality-based visual warning for construction workforce safety," *Automation in Construction*, vol. 139, p. 104252, 2022.
- [17] C. Reardon, K. Lee, and J. Fink, "Come see this! augmented reality to enable human-robot cooperative search," in *2018 IEEE International Symposium on Safety, Security, and Rescue Robotics (SSRR)*, 2018: IEEE, pp. 1-7.
- [18] A. Jalali, "Graph-based process mining," in *International Conference on Process Mining*, 2020: Springer, pp. 273-285.
- [19] G. Hübscher *et al.*, "Graph-based managing and mining of processes and data in the domain of intellectual property," *Information Systems*, vol. 106, p. 101844, 2022.
- [20] C. dos Santos Garcia *et al.*, "Process mining techniques and applications—A systematic mapping study," *Expert Systems with Applications*, vol. 133, pp. 260-295, 2019.

Accurate matching between BIM-rendered and real-world images

Houhao Liang¹ and Justin K.W.Yeoh¹

Abstract—As the digital representation of the built environment, BIM has been used to assist robot localization. Real-world images captured by the robot camera can be compared with BIM-rendered images to estimate the pose. However, there is a perception gap between the BIM environment and reality; image styles are typically too different to be matched. Hence, this study investigates an advanced image feature detection technique, D2-Net, to identify key points and descriptors on BIM-rendered and real-world images. These key features are further matched via K Nearest Neighbor Search and RANSAC. The ability to bridge the perception gap can be evaluated by the image matching performance, which is the Euclidean distance between the projected key points and the number of inliers. SIFT, as the traditional feature detection technique, was compared in this study. Results show that the average projection error of D2-Net is only 16.55 pixels, while the error of SIFT is 187.46 pixels. It demonstrates that the advanced D2-Net can be utilized to detect representative features on BIM-rendered and real-world images. The matched image pairs can be further utilized to estimate the robot pose in BIM. Overall, it aims to enhance the BIM-assisted localization and improve the robot's reliability as a decision-making tool on-site.

I. INTRODUCTION

In recent decades, Building Information Modeling (BIM) has been widely used to enable digital transformation in Architecture, Engineering, and Construction(AEC) sector. It is able to store infrastructure information digitally and has the potential to reshape the management in an automated way. For example, as-built status collected in a format of images [1] or point cloud [2] can be automatically compared against as-designed BIM to analyze the progress deviation. Instead of sending inspectors on-site to collect data, the feasibility of leveraging robot has been studied in [3]–[5] to replace human work. Light Detection and Ranging (LiDAR) and camera can be mounted and programmed on robot to automate the data acquisition task. It can be further developed as a decision-making tool by analyzing the acquired as-built data.

In order to deploy the robot on-site, waypoints are usually designed based on reference models such as BIM, and corresponding tasks are automatically conducted at these waypoints. Localization is an essential module to ensure the robot reaches its designated waypoints, as it determines the robot position within the environment. However, accurate indoor localization is still challenging to be achieved due to the inaccuracy and incompleteness of the robot's sensors and effectors [7]. Consequently, the robot might not be able to reach the position exactly. The perspective retrieved in BIM

at the designated waypoint is prone to be misaligned with the robot perspective. Analysis such as progress inference and productivity calculation tends to be falsely made when referring to incorrect BIM elements. Hence, it is necessary to enhance the pose estimation in BIM and improve the perspective alignment to strengthen the reliability of the decisions made by the robot.

Since BIM can represent the built environment digitally, recent studies have sought to use it to assist localization. BIM-rendered and real-world images are compared to estimate the pose. However, there is a perception gap between the two domains. Considering this, BIM-PoseNet [8] was developed as a regression model to roughly estimate the pose using BIM-rendered images as the training dataset. Improvement was proposed in [9] by using an advanced recurrent CNN model. Also, the style of BIM-rendered images were transferred into a realistic one by Generative Neural Network (GNN) model, and these generated images were then further compared against real-world images to estimate the pose [10], [11]. Nevertheless, deep learning-based methods still need a massive amount of data to develop the model, and the generalization abilities need to be further studied.

To address the aforementioned limitations, this study investigates an advanced image feature detection technique to bridge the cross-domain perception gap. Detected key features on BIM-rendered and real-world images are further matched via a neighboring search. The Euclidean distance error between projected key points, and the number of matched pixel pairs are reported to demonstrate the matching performance. These matched pixel pairs can be further developed to estimate the robot pose.

II. METHOD

The appearances of BIM-rendered images are significantly different from real-world images due to changes in depiction style, texture, and illumination difference, making cross-domain image matching challenging [10], [12], [13]. Traditional key points detection methods such as SIFT, SURF, ORB, and DoG perform poorly as they only consider small image regions at a low level [14]. The detection results are significantly affected by changes in pixel intensities. Therefore, images with significant appearance differences are difficult to be matched based on these key features.

Considering the style difference, this study exploits a pre-trained D2-Net model [14] to detect key features on BIM-rendered and real-world images. Instead of detecting key points and then describing features given the image patches extracted around the key points, D2-Net detects and describes

¹Authors are with Department of Civil and Environmental Engineering, College of Design and Engineering, National University of Singapore, 117576, Singapore, {houhaol@u.nus.edu, justinyeoh@nus.edu.sg}

TABLE I
THE IMAGE MATCHING EVALUATION USING SIFT AND D2-NET ON BIM-RENDERED AND REAL-WORLD IMAGES

Methods	Image pair 1		Image pair 2		Image pair 3		Overall	
	Projection error	Inliers	Projection error	Inliers	Projection error	Inliers	Mean projection error	Mean inliers
SIFT	196.76	21	124.17	5	241.46	7	187.46	11
D2-Net	14.56	63	19.19	62	15.89	40	16.55	55

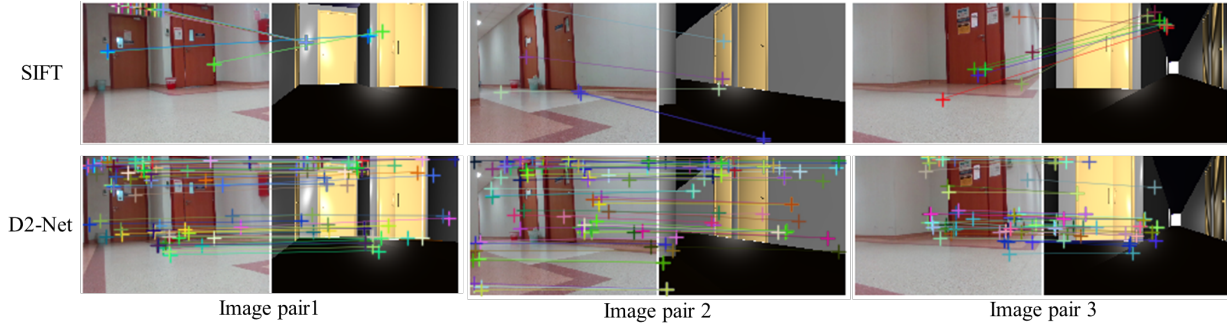


Fig. 1. Matched key features on three image pairs

them simultaneously. It uses VGG16 architecture, pre-trained on ImageNet, to extract the feature maps on images. At a high dimensional space, the key point is the local maxima of VGG derived feature maps by applying Non-Maximum Suppression (NMS). At the same time, the descriptor is computed by chunking VGG derived feature maps for each key point. Finally, upon obtaining the detected key features, K Nearest Neighbour (KNN) search and a ratio test are applied to select the good matches [15]. Random sample consensus (RANSAC) is further adopted to remove outliers.

III. RESULTS AND DISCUSSIONS

To demonstrate the matching performance, a traditional and well-known image feature extraction technique, SIFT, was used as a comparison in this study. Key points and descriptors were detected by SIFT and D2-Net, followed by a KNN search and RANSAC to match the descriptors. The “good” matched pairs are named as inliers. A homography matrix was manually computed by selecting corresponding key points on each set of BIM and real-world images. The matching performance can be measured as the projection error of key points. Specifically, key points detected on BIM-rendered images were projected to the position on real-world images using the homography matrix. The Euclidean distance between projected BIM key points and matched real-world key points was measured in pixels. In this study, three pairs of BIM-rendered and real-world images were used to demonstrate the matching performance of using D2-Net against using SIFT.

Table I reported the average projection error and the number of inliers. It can be seen the overall projection error of SIFT reaches 187.46 pixels, implying that the SIFT failed to find correctly matched key points between both BIM-rendered and real-world images. However, the D2-Net is robust to the cross-domain perception issue as the projection error is only 16.55 pixels. In terms of the amount of inliers,

D2-Net outperformed the traditional SIFT, by 55 to 11. Fig.1 shows matched key points pairs on BIM-rendered and real-world images. Overall, the quantitative and qualitative results show that D2-Net is able to find the point pairs despite there being differences in appearances within the images. Besides, it is necessary to mention that BIM in this study have not been rendered to produce more detailed and realistic images. With these better-rendered images, it may be posited that the detection and matching could be significantly improved by using a pre-trained D2-net model. However this implies greater computational effort to obtain these rendered images.

IV. CONCLUSIONS

This study investigates the performance of finding matched key features on BIM-rendered and real-world images using a pre-trained D2-Net model. Without the efforts to prepare a large building-oriented dataset to train new deep learning model, this study shows a pre-trained D2-Net model is potentially able to associate BIM environment and reality to a certain extent. One potential research work that can be conducted in the future is to estimate the robot pose by using the matched 2D key features. It also can be developed to rectify the robot pose to have a better-aligned perspective between BIM and the real-world.

REFERENCES

- [1] Kevin K. Han and Mani Golparvar-Fard. Appearance-based material classification for monitoring of operation-level construction progress using 4d bim and site photologs. *Automation in Construction*, 53:44–57, 2015.
- [2] Frédéric Bosché, Mahmoud Ahmed, Yelda Turkan, Carl T Haas, and Ralph Haas. The value of integrating scan-to-bim and scan-vs-bim techniques for construction monitoring using laser scanning and bim: The case of cylindrical mep components. *Automation in Construction*, 49:201–213, 2015.
- [3] Pileum Kim, Jingdao Chen, and Yong K Cho. Slam-driven robotic mapping and registration of 3d point clouds. *Automation in Construction*, 89:38–48, 2018.

- [4] Khashayar Asadi, Hariharan Ramshankar, Harish Pullagurla, Aishwarya Bhandare, Suraj Shambhag, Pooja Mehta, Spondon Kundu, Kevin Han, Edgar Lobaton, and Tianfu Wu. Vision-based integrated mobile robotic system for real-time applications in construction. *Automation in Construction*, 96:470–482, 2018.
- [5] A Adán, B Quintana, SA Prieto, and F Bosché. An autonomous robotic platform for automatic extraction of detailed semantic models of buildings. *Automation in Construction*, 109:102963, 2020.
- [6] Amir Ibrahim, Ali Sabet, and M. Golparvar-Fard. Bim-driven mission planning and navigation for automatic indoor construction progress detection using robotic ground platform.
- [7] Prabin Kumar Panigrahi and Sukant Kishoro Bisoy. Localization strategies for autonomous mobile robots: A review. *Journal of King Saud University - Computer and Information Sciences*, 2021.
- [8] Debaditya Acharya, Kourosh Khoshelham, and Stephan Winter. Bim-posesnet: Indoor camera localisation using a 3d indoor model and deep learning from synthetic images. *ISPRS Journal of Photogrammetry and Remote Sensing*, 150:245–258, 2019.
- [9] Debaditya Acharya, Sesa Singha Roy, Kourosh Khoshelham, and Stephan Winter. A recurrent deep network for estimating the pose of real indoor images from synthetic image sequences. *Sensors*, 20(19), 2020.
- [10] Junjie Chen, Shuai Li, Donghai Liu, and Weisheng Lu. Indoor camera pose estimation via style-transfer 3d models. *Computer-Aided Civil and Infrastructure Engineering*, 37(3):335–353, 2022.
- [11] Junjie Chen, Shuai Li, and Weisheng Lu. Align to locate: Registering photogrammetric point clouds to bim for robust indoor localization. *Building and Environment*, 209:108675, 2022.
- [12] Hao Zhou, Torsten Sattler, and David W. Jacobs. Evaluating local features for day-night matching. In *ECCV Workshops*.
- [13] Torsten Sattler, William P. Maddern, Carl Toft, Akihiko Torii, Lars Hammarstrand, Erik Stenborg, Daniel Safari, M. Okutomi, Marc Pollefeys, Josef Sivic, Fredrik Kahl, and Tomás Pajdla. Benchmarking 6dof outdoor visual localization in changing conditions. *2018 IEEE/CVF Conference on Computer Vision and Pattern Recognition*, pages 8601–8610, 2018.
- [14] Mihai Dusmanu, Ignacio Rocco, Tomás Pajdla, Marc Pollefeys, Josef Sivic, Akihiko Torii, and Torsten Sattler. D2-net: A trainable cnn for joint detection and description of local features. *ArXiv*, abs/1905.03561, 2019.
- [15] David G. Lowe. Distinctive image features from scale-invariant keypoints. *International Journal of Computer Vision*, 60(2):91–110, 2004.

Low-cost Thermal Mapping for Concrete Heat Monitoring

Alex Junho Lee¹, Younggun Cho² and Hyun Myung^{3*}, *Senior Member, IEEE*

Abstract—Robotics has been widely applied in smart construction for generating the digital twin or for autonomous inspection of construction sites. For example, for thermal inspection during concrete curing, continual monitoring of the concrete temperature is required to ensure concrete strength and to avoid cracks. However, buildings are typically too large to be monitored by installing fixed thermal cameras, and post-processing is required to compute the accumulated heat of each measurement point. Thus, by using an autonomous monitoring system with the capability of long-term thermal mapping at a large construction site, both cost-effectiveness and a precise safety margin of the curing period estimation can be acquired. Therefore, this study proposes a low-cost thermal mapping system consisting of a 2D range scanner attached to a consumer-level inertial measurement unit and a thermal camera for automated heat monitoring in construction using mobile robots.

I. PRELIMINARIES

In the construction industry, heavy equipment and human-robot interaction interfaces have been widely used to enhance efficiency and ensure the safety of construction sites. These technologies primarily focus on assisting and scaling up human manipulations, enabling faster and safer labor during construction procedures [1].

The concept of smart construction has been introduced to provide greater autonomy as compared with assistive robots based on human manipulations. Smart construction topics cover the overall management of construction resources and elements (e.g., materials, equipment, and devices) for autonomy and interactivity [2, 3]. To achieve this goal, information from the construction site should be gathered and managed for delivery to the right person or system in proper format and provide a basis for precise decision-making [4].

However, smart construction has been only partially applied in the field due to application difficulties. For instance, a versatile perception algorithm and control mechanism are required to establish spatial interaction between a robot and the construction environment. A construction site continuously changes over time and on a large scale, and AI must be cognizant of up-to-date spatial information. Recently, simultaneous localization and mapping (SLAM) based on cameras [5–7] or light detection and ranging (LiDAR) systems [8, 9] have been introduced to help robots localize themselves and recognize spaces even in unseen or unknown environments. When these localization and mapping

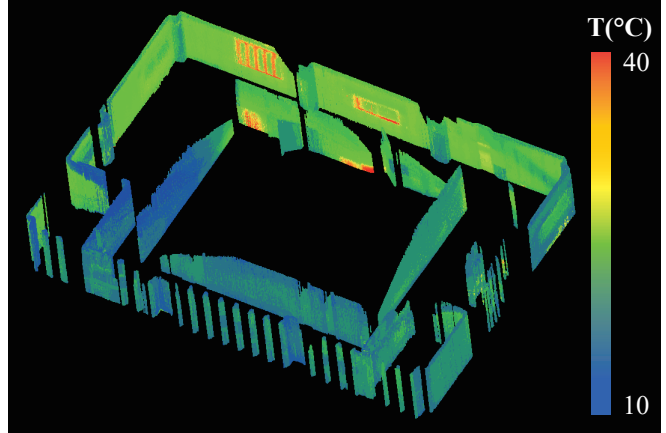


Fig. 1. Sample of a thermal map reconstructed from our experiment. We used a low-cost mapping system with a range scanner, IMU, and thermal camera. We obtained the thermal point cloud map from SLAM using pose-graph optimization (PGO) by assuming a ground robot at a known height.

capabilities are combined with path planning and automated inspection technologies, the structural information of a site can be periodically updated, and a construction project can be monitored in real time.

The information updated by an autonomous system could include 3D structures, tracking results of dynamic objects, geodetic surveying, etc. In our study, we concentrated on the thermal behavior of a construction site with respect to both the safety and energy efficiency of buildings. When concrete is cured, the accumulated heat over time [10] is a critical variable for calculating the required curing period, and the temperature change rate should remain within a certain range [11]. Thus, at construction sites, adjustments to the curing period or maintenance of the temperature of the concrete based on the atmosphere is necessary. However, criteria based on air temperature provide an indirect estimation of the accumulated heat and make it possible for defects or accidents to occur. As an alternative approach, we propose that the concrete's surface temperature be used to calculate the accumulated heat by providing a SLAM-generated thermal point cloud from a low-cost system of sensors mounted on a ground robot as in Fig. 1. Assuming concrete walls of known height in a curing period, we show that a thermal point cloud of the walls can be acquired using only a 2D range scanner combined with a consumer-level IMU and a thermal camera. Throughout this study, we introduce a method for building thermal point clouds of walls using the proposed sensor system and compare the mapping results derived from experiments.

¹Alex Junho Lee is with the Department of Civil and Environmental Engineering, KAIST, Daejeon, S. Korea alex_jhlee@kaist.ac.kr

²Y. Cho is with the Department of Electrical Engineering, Inha University, Incheon, S. Korea yg.cho@inha.ac.kr

³Hyun Myung is with the School of Electrical Engineering, KAIST, Daejeon, S. Korea hmyung@kaist.ac.kr

*Corresponding author: Prof. Hyun Myung

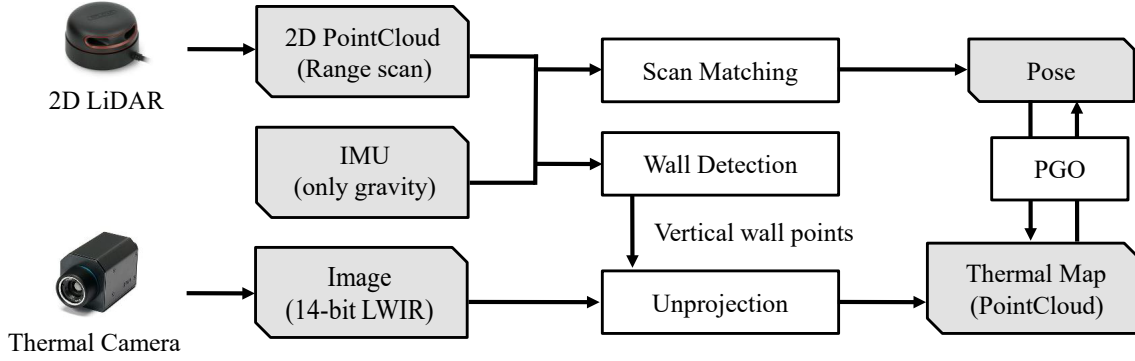


Fig. 2. Outline of our algorithm. We used a sensor system consisting of a 2D LiDAR combined with a consumer-level IMU and a thermal camera. We used only the gravity direction from an IMU to compensate for the range scans and used the compensated range scans for scan matching and wall detection. After the vertical walls were detected, the points were projected onto thermal images to obtain temperature information and then unprojected to a point cloud. Then, with the constructed point cloud map and pose information from scan matching, we refined the final pose with the map by PGO.

II. THERMAL-LIDAR SLAM

A robot pose can be described in 6 variables (x , y , z , roll θ_x , pitch θ_y , and yaw θ_z). However, because we rely on a 2D range scanner to estimate the depth of a scene, we constrained the robot motion in 2D space (x , y , θ_z) for initial pose estimation. To obtain the pose and map simultaneously, we used SLAM based on 2D range scans, as shown in the pipeline in Fig. 2. We projected the range scans into a horizontal plane using the gravity direction detected from the IMU and used scan matching to estimate the relative transformation between scans. Then, assuming that a mobile robot is operating at a fixed elevation in a building layout with a known floor height, we generated vertical wall points and assigned the corresponding thermal values. Then, through unprojection, we obtained the thermal map as a point cloud, and the relative transformations between its poses were refined by pose-graph optimization (PGO) based on both the geometry and thermal values of the wall point cloud.

A. Scan Matching and Pose Estimation

To identify the initial poses, we first projected the range scans from a 2D LiDAR into the xy plane using the gravity vector g obtained from the IMU. Because the update rate of the IMU (~ 100 Hz) was higher than that of the range scanner (~ 10 Hz), we searched for the IMU message with the closest timestamp to each scan message and assigned the gravity vector to points x_S in each scan S . Assuming that a robot seldom experience a large slope ($\theta_x, \theta_y \simeq 0$), the laser scans mostly fall on the wall surface. Using the scanned wall points, we next calculated the projection of the scan points toward an imaginary plane at the level of the mobile robot and gravity vector g as a plane vector:

$x_{xy} = x_S - \frac{x_S \cdot g}{g \cdot g} g$. Using the projected scan points in 2D, x_{xy} , we then calculated the relative transformation $T_{ij}(x, y, \theta_z)$ between scans of nodes i and j , l_i and l_j to minimize the reprojection error e :

$$\underset{T_{ij}}{\operatorname{argmin}} e = \|l_i - T_{ij}(l_j)\|. \quad (1)$$

B. Thermal Map Generation

After acquiring the relative transformations between the scans, we generated the thermal point clouds. From the 2D-projected laser scans at the level of the mobile robot, we expanded the scan points at the elevation of a robot x_{xy} vertically by repeating points in the gravity direction g and opposite the gravity direction $-g$. Because we assumed that the floor height and sensor elevation were known, we could easily calculate the wall points p_{wall} around the robot.

Then, the vertical wall points p_{wall} are projected onto the thermal image I with known intrinsic matrix K and extrinsic transformation T . By transforming the wall points into thermal image coordinates $u = (u, v)$ using $u = K \cdot (T \cdot p_{wall})$, we obtained the image coordinates of each wall point. In this procedure, points outside the thermal camera's field of view were filtered out. Then, with the thermal values in the image $I(u)$ assigned to each corresponding point, the temperature \mathcal{T} from the thermal image was saved in the intensity field of the thermal point cloud x .

While we obtained the whole poses and thermal point clouds assigned to each node, we ran PGO based on the geometry of points and intensity. We used the Ceres solver [12] in this procedure, setting up the loss to optimize both the geometry and temperature difference. Between selected point pairs x_i and x_j of nodes i and j , we calculated the optimal transformations T between nodes to minimize the error e :

$$\underset{T}{\operatorname{argmin}} e = \sum_{(i,j)} (\|\mathcal{T}(x_i) - \mathcal{T}(x_j)\| + \|x_i - T_{ij} \cdot x_j\|). \quad (2)$$

We calculated the optimal relative transformation between nodes by applying this error function for every selected point pair between the selected nodes. We then obtained the optimized poses and their corresponding thermal point clouds x . We accumulated the thermal point clouds of every node given the poses of the nodes and obtained the final thermal point cloud.

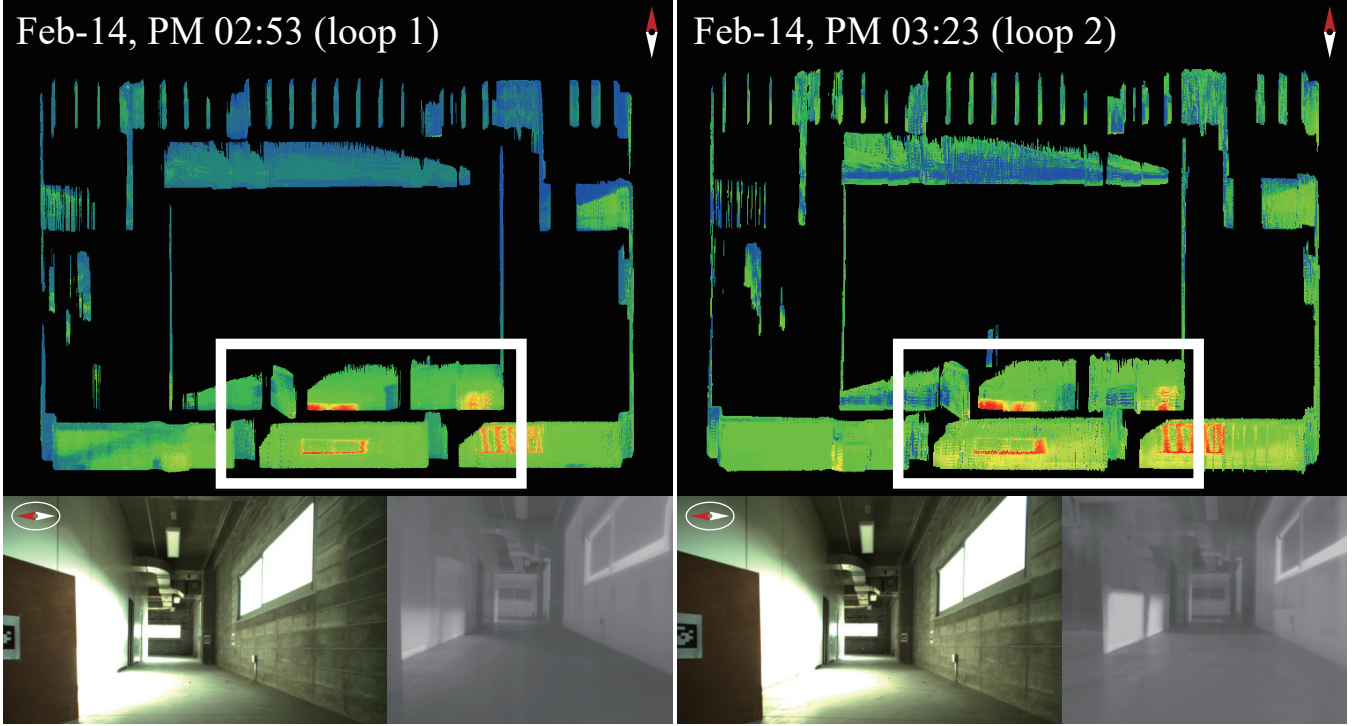


Fig. 3. Examples of constructed thermal maps with RGB and thermal images obtained at each space. In both runs, walls facing sunlight showed higher temperature (green) than opposing walls (blue). In addition, due to the direct sunlight, window frames exhibited higher temperatures. This can also be seen in the thermal image displayed at the lower right.

III. EXPERIMENTS AND RESULTS

We run our experiments on a construction site at Heunghae-eup, Pohang, South Korea, in Feb. 2020, in which a concrete building was part of the actual construction. We used a sensor system that was mounted on a mobile robot, and we recorded the data in a rosbag file. To test the sensor reliability under the environmental variances of different construction sites, we executed multiple repetitions at different times and based on different noise sources such as haze. We plan to release the data used in the experiment in the near future.

A. SLAM

During optimization, we used a levenberg-marquardt (LM) [13] based solver combined with the huber loss [14]. To ensure robust optimization, the translation and rotation weights were set to 5.0 and 400.0. In Fig. 3, we present the results of our method using our dataset. The obtained thermal maps and sample images from each run were plotted. Although our algorithm assumes that no other type of structure exists other than plain walls in the environment, the results of SLAM succeeded in estimating the pose and in constructing an aligned point-cloud map. In Fig. 4, we compare the thermal map and results of 2D SLAM based on Google Cartographer [15] before temperature-based PGO using LM solver in Ceres, from different runs, respectively. As the figure shows, consistent layouts were reconstructed and our SLAM pipeline did not diverge or become lost during the two experiments.

B. Thermal Mapping

Using the algorithm suggested in the previous section, we built a thermal point cloud of the environment through two iterations as derived from PGO. As shown in the upper parts of Fig. 3, clear wall point clouds were extracted, where the temperature of each wall is shown in a rainbow color scale from 10°C to 40°C. In Fig. 3, the point clouds are rotated to face north. As the experimental site was in the northern hemisphere of the Earth, heat dissipation from the Sun was more concentrated on the southern (lower) walls of the structure during the daytime. As a result, a smaller blue area (lower temperature) on the walls facing south could be observed. In addition, we observed that the

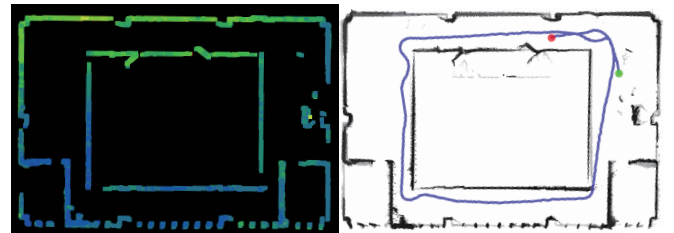


Fig. 4. Generated maps from thermal point clouds at loop 1 (left) and 2D SLAM at loop 2 (right). The green and red dots on the right are the start and end points of the estimated SLAM trajectory. With the wall layouts obtained from the generated map, we could monitor how precisely the walls were located during construction.

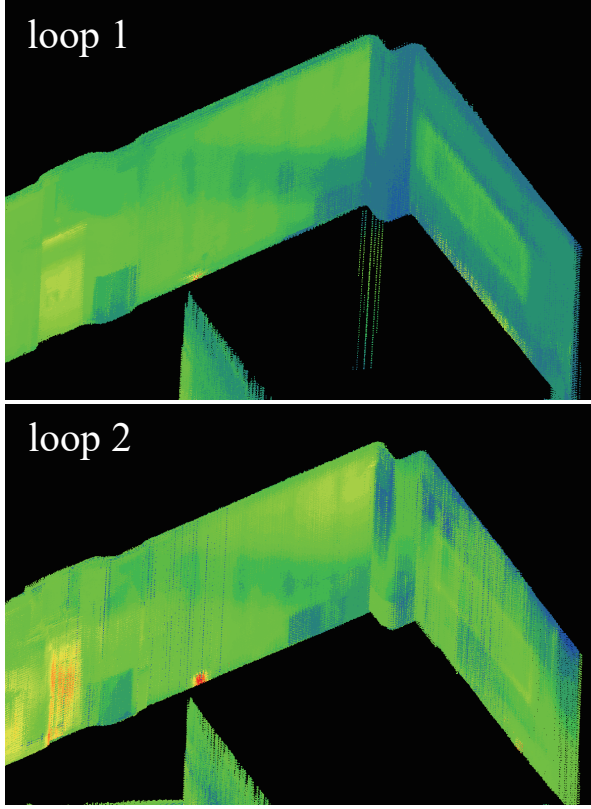


Fig. 5. Measured temperature of the same corner wall at different times after alignment. Through ICP alignment, thermal point clouds were easily registered, and measurement points are successfully monitored over time.

overall temperature of the construction site increased as time passed based on temperature visualization. The temperature difference could be easily monitored by running a simple registration algorithm such as the iterative closest point (ICP) [16] between thermal point clouds from experiments, as shown in Fig. 5.

IV. CONCLUSION AND FUTURE WORKS

In this study, we proposed a low-cost thermal mapping system for automated thermal monitoring during concrete curing. We also proposed a 2D range scanner system combined with an IMU and thermal camera to estimate the thermal point clouds of concrete walls. For more precision, we also suggested thermal-based PGO to optimize the obtained pose and point cloud. We hope our study can be used as a reference in ensuring that the temperature constraint in concrete curing is maintained and in helping to prevent accidents in construction due to inappropriate estimation of the accumulated heat in concrete.

Our method does have limitations. Specifically, it uses only vertically compensated 2D scans for vertical wall detection and cannot distinguish between walls and non-walls such as handrails or obstacles. Thus, in future studies, non-wall objects should be filtered by combining them with the

additional constraints from thermal images. This will enable our work to be expanded from 2.5D (only vertical planes) to 3D.

REFERENCES

- [1] K. S. Saidi, T. Bock, and C. Georgoulas, “Robotics in construction,” in *Springer Handbook of Robotics*, 2016, pp. 1493–1520.
- [2] Y. Niu, W. Lu, K. Chen, G. G. Huang, and C. Anumba, “Smart construction objects,” *Journal of Computing in Civil Engineering*, vol. 30, no. 4, p. 04015070, 2016.
- [3] H. Myung and Y. Wang, “Robotic sensing and systems for smart cities,” *Sensors*, vol. 21, no. 9, p. 2963, Apr. 2021.
- [4] K. Chen, W. Lu, Y. Peng, S. Rowlinson, and G. Q. Huang, “Bridging BIM and building: From a literature review to an integrated conceptual framework,” *International Journal of Project Management*, vol. 33, no. 6, pp. 1405–1416, 2015.
- [5] H. Lim, J. Lim, and H. J. Kim, “Real-time 6-DOF monocular visual SLAM in a large-scale environment,” in *Proc. IEEE International Conference on Robotics and Automation (ICRA)*, 2014, pp. 1532–1539.
- [6] H. Lim, J. Jeon, and H. Myung, “UV-SLAM: Unconstrained line-based SLAM using vanishing points for structural mapping,” *IEEE Robotics and Automation Letters*, 2022.
- [7] S. Song, H. Lim, S. Jung, and H. Myung, “G2P-SLAM: Generalized RGB-D SLAM framework for mobile robots in low-dynamic environments,” *IEEE Access*, vol. 10, pp. 21 370–21 383, 2022.
- [8] T. Shan, B. Englot, D. Meyers, W. Wang, C. Ratti, and D. Rus, “LIO-SAM: Tightly-coupled LiDAR inertial odometry via smoothing and mapping,” in *Proc. IEEE/RSJ International Conference on Intelligent Robots and Systems (IROS)*, 2020.
- [9] H. Lim, S. Yeon, S. Ryu, Y. Lee, Y. Kim, J. Yun, D. Lee, and H. Myung, “A single correspondence is enough: Robust global registration to avoid degeneracy in urban environments,” in *Proc. IEEE International Conference on Robotics and Automation (ICRA)*, 2022.
- [10] S. G. Bergström, “Curing temperature, age and strength of concrete,” *Magazine of Concrete Research*, vol. 5, no. 14, pp. 61–66, 1953.
- [11] J.-K. Kim, Y.-H. Moon, and S.-H. Eo, “Compressive strength development of concrete with different curing time and temperature,” *Cement and Concrete Research*, vol. 28, no. 12, pp. 1761–1773, 1998.
- [12] S. Agarwal, K. Mierle, and T. C. S. Team, “Ceres Solver,” March 2022. [Online]. Available: <https://github.com/ceres-solver/ceres-solver>
- [13] D. W. Marquardt, “An algorithm for least-squares estimation of nonlinear parameters,” *Journal of the society for Industrial and Applied Mathematics*, vol. 11, no. 2, pp. 431–441, 1963.
- [14] P. J. Huber, “Robust estimation of a location parameter,” *Breakthroughs in Statistics*, pp. 492–518, 1992.
- [15] W. Hess, D. Kohler, H. Rapp, and D. Andor, “Real-time loop closure in 2D LiDAR SLAM,” in *Proc. IEEE International Conference on Robotics and Automation (ICRA)*, 2016, pp. 1271–1278.
- [16] P. J. Besl and N. D. McKay, “Method for registration of 3D shapes,” in *Sensor Fusion IV: Control Paradigms and Data Structures*, vol. 1611, 1992, pp. 586–606.

A Computational Framework For Robotic Quality Assessment and Management In Construction

Jingyang Liu, Yumeng Zhuang, and Joshua Bard

Abstract—As an integrated process in construction projects, quality assessment and management (QA&M) can be important to prevent failures during construction. The existing QA&M practice such as the evaluation of the geometric tolerance and surface qualities is mostly performed manually which can be labor-intensive and tedious. This study proposes a computational framework for a robot to perform automatic QA&M in unknown environments. The framework is composed of three parts: (1) motion planning; (2) defect detection; and (3) defect registration. The motion planning component generates efficient robotic path for autonomous exploration and surface inspection. The defect detection component quantifies surface anomalies within a user-defined area of interests through multiple sensor measurements. The defect registration component localizes the detected defects and registers the defects to a site model. To demonstrate the feasibility of the proposed framework, we present a user case for assessing geometric tolerance and surface quality of a 1500 mm (L) x 745 mm (W) x 1980 mm interior wall mockup. The result of the case study shows that the proposed framework has the potential to provide reliable geometric measurement and defect detection for gypsum wall panels in a lab environment.

I. INTRODUCTION

Surface quality assessment and management play a key role in construction operations such as infrastructure safety monitoring, prefab component inspection, and architectural finish quality assurance. Currently, most quality assessment and management (QA&M) tasks are conducted manually by a certified inspector using a visual inspection approach or contact-type measurement devices such as measuring tapes, levels, and calipers. Manual inspection methods can be tedious, costly, and dangerous, especially when the work environment is hazardous and inaccessible. To overcome these limits, the main goal of this paper is to provide a computational framework for robots to assist humans in QA&M by (1) traversing and inspecting the area of interest on a job site where the environment may not be known a priori (2) performing remote non-contact defect detection and registration at different levels of details (LoD). The framework is composed of three components (Figure 1):

- **Motion Planning** — The motion planning component generates near-optimal paths for robots to explore the surrounding environment and scan the target area. The component integrates frontier-based and information-based methods to maximize coverage in three stage. At the first stage, the environment is unknown, the component

returns the exploration path by searching and identifying the frontier points between free and unknown parts of the map. At the second stage, a user can define a target volume within the partially known environment for detailed reconstruction, the component plans a next-best view based on the information gain of each sampled view candidate. At the third stage, a user can define an area of interest within the known environment for surface inspection. The component generates an efficient and collision-free path by minimizing the cost defined by the total traveling distance.

- **Defect Detection** — The defect detection component extracts surface anomalies and quantifies geometric tolerance based on multi-sensor measurements. The component integrates a learning-based method for recognizing components such as screws on a panel. Processing techniques including edge detection are used to detect common surface defects such as discoloration and cracks. Considering the lighting variation on construction sites, we fuse 2D images with 3D laser scanning data at decision-making level for more accurate surface anomaly detection.
- **Defect Registration** — The defect registration component registers and localizes defects in a scene model. We combine a classical ICP [1] framework and its variant Cluster ICP [2] for dense-to-dense and dense-to-sparse data registration.

This study contributes to the domain of QA&M for construction by (1) a framework for robots to explore, detect and document surface defects for construction practices. (2) expanding the surface inspection framework from a factory setting to complex unknown construction environments by introducing a three-stage autonomous exploration and reconstruction method (3) combining multi-resolution 3D reconstructions to address the discrepancies in scanning resolution and range - for instance, in construction QA&M, we need to identify surface defects at millimeter scale within a wide area at meter scale. To demonstrate the framework, we performed a surface inspection on a interior wall mockup with a 6 DoF industrial robot (Figure 2).

II. METHOD

The framework is composed of three components: a motion planning component for generating coverage paths, a surface defect detection component for identifying and classifying surface defects at mm scale, and a defect localization component for registering and localizing defects in a scene model.

Jingyang Liu, Yumeng Zhuang, Joshua Bard are with Carnegie Mellon University, Pittsburgh, 15206, PA, United States, e-mail: jingyanl@andrew.cmu.edu, e-mail: yumengzh@andrew.cmu.edu , e-mail: jdbard@cmu.edu

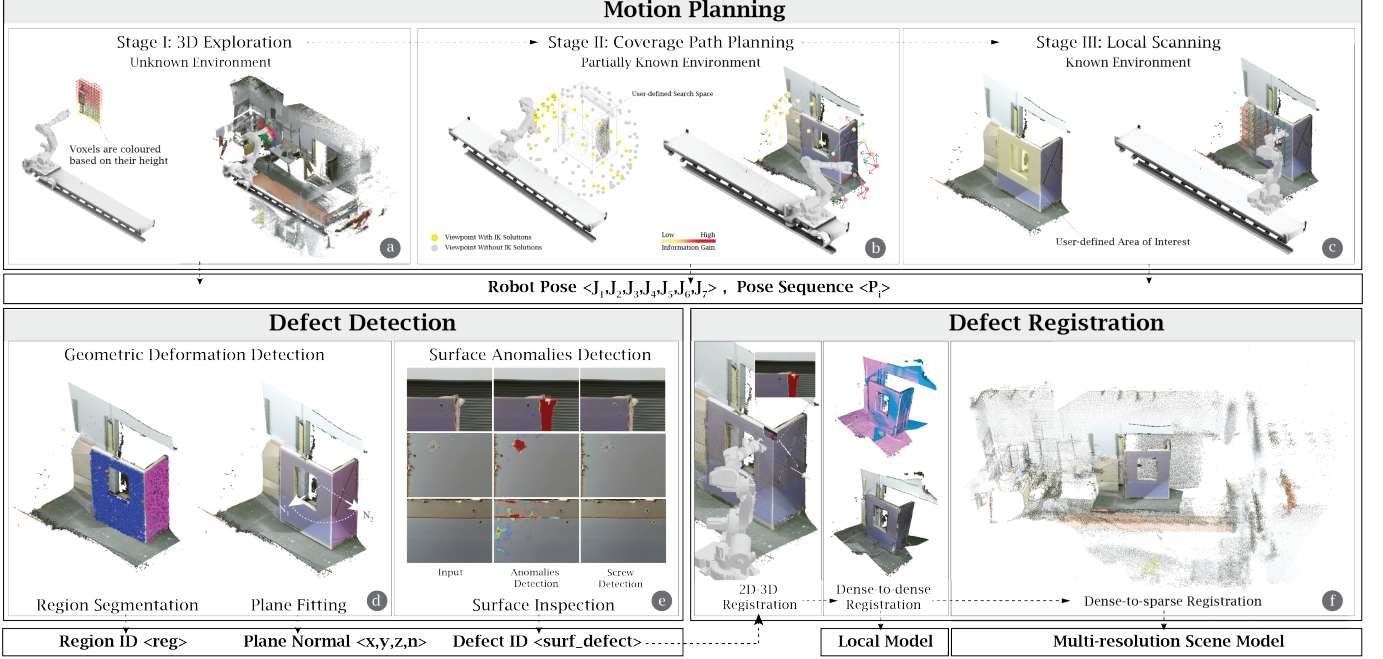


Fig. 1. The computational framework of the robotic QA&M system: (a) Frontier-based autonomous exploration in an unknown environment (b) Viewpoint generation and path planning based on information gain for covering a user-defined search space in a partially known environment (c) Local scanning path planning for covering a user-defined surface in a known environment (d) Geometric deformation detection (e) Surface anomalies detection (f) Defect registration — 2D images are registered to the target 3D surface based on known extrinsic and intrinsic parameters. local dense point clouds obtained from the same source are registered through ICP [1]. Local dense point clouds are registered to a sparse scene model through the cluster ICP framework [2].

A. Motion Planning

The motion planning component automatically generates a collision-free path for a robot to reconstruct the site scene and inspect the user-defined areas of interest. The problem can be formulated as a coverage path planning (CPP) problem or a variant of the well-known traveling salesman problem (TSP) — an agent needs to pass over a set of target points with minimum cost (usually time or path length). However, in contrast to the traditional TSP where the environment is stationary and known a priori, in site surface inspection operations, full prior knowledge of the environment might be unrealistic. In this work, we use a three-phase approach including 3D exploration, coverage path planning, and local scanning for reconstructing a multi-resolution scene model of an unknown environment.

In the initial exploration phase, the robot explores the space by finding a set of poses along the frontier of the unknown environment and creates the occupied space map (a volumetric representation of space in a hierarchical structure). The robot first looks for a frontier located on the boundary between the explored and the unknown part of the environment, and then chooses the one with the maximum information gain weighted by its cost to reach [3] [4], which can be defined as:

$$I_f = \frac{N_0}{N} \cdot \frac{1}{|P_f - P_0|},$$

where I_f is the information gain of a candidate frontier cell. P_f and P_0 represent the coordinates of the candidate frontier cell and the current pose respectively. N_0 represents the unknown

voxels within a sphere of radius R around the candidate frontier that contains N voxels.

After the goal frontier is selected, the planner generates a path to move the robot 30 mm towards the frontier and look towards the direction of the frontier through an Inverse Kinematic (IK) solver unless the planner can not find a valid IK solution. The exploration procedure terminates when the void voxels within the bounded space are classified as either free or occupied.

The 3D exploration phase reconstructs a partially known scene model of the site (93.67% coverage rate) at a relatively low resolution (50 points per m^3). Based on this model, the remote inspector can define a smaller search space for the second phase of coverage path planning. The coverage path planning aims at automatically generating collision-free robotic paths covering the required surface area within the target volume. We first combine the voxels in the volume into a binary status — “occupied” and “unoccupied” [5] [6]. The system then uniformly samples a set of viewpoint candidates on a sphere to capture the most variations of perspectives that can cover the target volume [7]. The quality of each viewpoint candidate is defined by measuring the mean entropy $e_{(x)}$ over all voxels within the sensor frustum of a potential next pose, which can be defined as [8] :

$$e_{(x)} = -\frac{1}{k} \sum_{i=1}^k p_i(x) \log p_i(x) + p_i(x^c) \log p_i(x^c),$$

where $p_i(x)$ is the probability of voxel x being occupied, and $p_i(x^c)$ $p_i(x)$ denotes the complement probability of $p_i(x)$,



Fig. 2. Experiment setup (a) a 6 DoF industrial robot on a 5800 mm linear track and a interior wall mockup of 1500 mm (L) x 745 mm (W) x 1980 mm (H) (b) an end-effector sensor kit including RGB-D cameras (Kinect V2, Intel Realsense D415), laser range finders and a laser module (c) the robot highlights a detected surface defect with a laser cross-line.

i.e. $p_i(x^c) = 1 - p_i(x)$. Based on this volumetric function, we select 10 candidates with the highest visible uncertainties for coverage path planning.

After the exploration phase, we use a region-growing approach based on smoothness constraints to cluster point clouds into surface patches. The remote inspector can then choose a target surface or an area of interest on a surface for local scanning. To generate the local scanning path, we take an offline path planning algorithm formulated as an optimization process of minimizing the cost function by adjusting decision variables such as candidate viewpoints and their traversing sequence. The function is defined by the total length of robot trajectories covering the target area. An online path planning process is then integrated to address real-time adaptive motion planning to avoid collisions caused by tolerances in reconstruction.

B. Defect Detection

Defect detection of interior wall surfaces (gypsum board) aims at identifying two types of defects — geometric deformation and surface anomalies — before finishing and painting and after the gypsum board installation. Geometric deformation can be caused by irregularities in the underlying substructure and the failure of screwing onsite. The warping of the board due to poor storage can also affect the drywall surface evenness [9]. Failures in screwing such as loosing and recession can cause surface discontinuities and result in bulges on the wall after surface finishing. Surface anomalies such as discoloration, cracks, and the detachment of the board covering can affect the aesthetics of interior wall surfaces and cause the degradation of the structure which needs to be repaired before the application of surface finishing materials.

To detect geometric deformation, we first use a principal component analysis-based approach to fit a plane within the selected point cloud. Then we can calculate the orthogonal distance between each point and the plane to evaluate surface flatness errors and calculate the connecting angle between two adjacent surfaces by computing the angle between their normal vectors.

Screwing failures need to be detected in two steps. First, screws are located based on 2D images. Their conditions are then measured using a laser range finder. To locate screws in

an image, we first detect circles with Hough circles as potential screw regions. The minimum radius and maximum radius for Hough circles are set based on the image size. We find that a minimum radius of image height divided by 150, and a maximum radius of 15 times the minimum radius work well with the Intel Realsense D415 sensor. We crop these circles as regions of interest. The regions are then classified as screw or non-screw with a fine-tuned Xception model [10]. We built our own dataset with screw pictures taken on interior wall surfaces under different lighting conditions.

Surface anomalies on gypsum boards can be visually detected by changes in color on the surface. Discoloration and cracks often have clear boundaries and/or rougher texture than the normal areas. We apply Contrast Limited Adaptive Histogram Equalization (CLAHE) to blurred images to reduce the effect of lighting changes. Then we extract edges with a Canny edge detector, and use morphological operations to cover the regions with dense edges, which correspond to the rougher texture of surface anomalies. We also use the depth information to discard the pixels with depth greater than 50 cm, since they are not on the wall. With the remaining regions, we filter out the regions with contour areas greater than one standard deviation above average and classify them as surface anomalies. We also notice that surface anomaly detection and screw detection work optimally at different distances from the gypsum board.

As construction sites can be affected by complex and unpredictable lighting environments, to compensate for illumination variations and shadows, we combine both 2D and 3D data for defect detection. 2D image processing can extract the potential defects in images. 3D geometric information is used for detecting volumetric defects defined by sharp changes in a depth reading. Depth reading is acquired by a fusion of a stereo camera and laser range finder to compensate for each individual sensor's deficiencies — stereo vision can produce dense output but performs poorly on textureless surfaces or regions with repetitive patterns, and the data collected from the laser range finder is accurate but relatively sparse in nature [11]. The extracted defects from 2D and 3D data are fused at the decision-making level based on evidence theory — a general framework for modeling epistemic uncertainty for multi-sensor fusion.

C. Defect Registration

The detected surface defects need to be registered to a site scene model, an inspector can thus localize the surface defects and authorize surface repair tasks. The registration process is completed in two phases - common source registration and cross-source registration. During common source registration, we first register the detected defects to a point cloud paired with the current robot pose and then fuse the point cloud acquired between different robot poses into a local model. The detected defects are registered to a point cloud by applying the transform matrix that is known after sensor calibration. We then use the Iterative Closest Point (ICP) algorithm for point cloud registration between frames. Since the local model and site scene model are of large discrepancies in densities, the registration method based on classical ICP may yield inaccurate pose estimation. To address the cross-source registration issue, we used the clustering iterative closest point (CICP) approach [2]. CICP integrates a novel correspondence point selection process based on voxelization and clustering before the matching. Each selected point can represent a local surface in a voxel of the source and target point clouds. Based on the selected correspondence points, the matching process is invariant to the point cloud density and scanning pattern. After the two-phase registration, defects and robots can share a common world-locked coordinate system for the user to reference.

III. RESULT

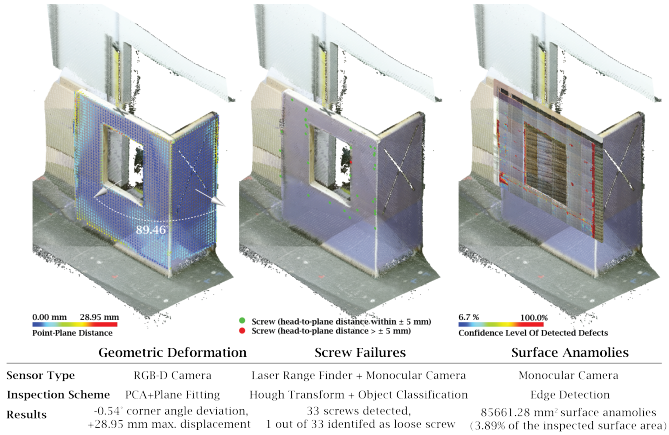


Fig. 3. The robotic quality assessment result of the interior wall mockup

To validate the proposed framework, we conducted a lab experiment using a 6 DoF industrial robot mounted on a linear track for surface inspection of an L-shaped mock-up wall in the dimension of $1500\text{mm}(L) \times 745\text{mm}(W) \times 1980\text{mm}$. We used a Kinect V2 sensor for 3D exploration and a combination of Intel RealSense D415 Sensor and laser range finders for the detection of surface anomalies. According to the surface inspection results (Figure 3), the mockup wall has 8.18% area identified as not flat (deviation from the fitted plane > 10 mm). The maximum displacement on the drywall is 28.95 mm. The angle between the two surfaces is -0.54 degrees deviating from the expected angle (90 degrees). The total

area of surface anomalies is 85661.28 mm^2 , accounting for 3.86% of the total surface area. 1 out of 33 of screws detected is identified as loose. To further optimize the framework, the potential focus could be on (1) a more efficient 3D exploration process: the existing framework examines every cell in the robot's map to trace the frontier for a next move. With the increase of searching space, the frontier evaluation process can be computationally inefficient. A faster frontier detection algorithm such as [12] or an active sub-map with bounded space can potentially improve the performance of 3D exploration. (2) a more robust view planning algorithm: job sites can be cluttered and dynamic which may result in occlusion. The compensation of occlusion adaptive to dynamic scenes can be integrated into the view planning process to avoid failures in coverage requirements. (3) a more accurate registration process: the discrepancies between the scale of the site and the scale of defects in construction practices can be large. A multi-resolution 3D reconstruction is efficient for capturing high resolution details of selected areas within a wide range space. As the density difference, scale variation, and noises from different types of sensors can pose challenges to the accuracy of point cloud fusion, optimization in transformation estimation between cross-source 3D data can be further explored in future work.

REFERENCES

- [1] P. J. Besl and N. D. McKay, "Method for registration of 3-D shapes," in *Sensor fusion IV: control paradigms and data structures*, vol. 1611, 1992, pp. 586–606.
- [2] M. L. Tazir, T. Gokhool, P. Checchin, L. Malaterre, and L. Trassoudaine, "CICP: Cluster Iterative Closest Point for sparse-dense point cloud registration," *Robotics and Autonomous Systems*, vol. 108, pp. 66–86, 2018.
- [3] C. Zhu, R. Ding, M. Lin, and Y. Wu, "A 3d frontier-based exploration tool for mavs," in *2015 IEEE 27th International Conference on Tools with Artificial Intelligence (ICTAI)*, 2015, pp. 348–352.
- [4] L. Lu, C. Redondo, and P. Campoy, "Optimal frontier-based autonomous exploration in unconstructed environment using RGB-D sensor," *Sensors*, vol. 20, no. 22, p. 6507, 2020.
- [5] J. I. Vasquez-Gomez, L. E. Sucar, R. Murrieta-Cid, and E. Lopez-Damian, "Volumetric next-best-view planning for 3D object reconstruction with positioning error," *International Journal of Advanced Robotic Systems*, vol. 11, no. 10, p. 159, 2014.
- [6] P. S. Blaer and P. K. Allen, "Data acquisition and view planning for 3-D modeling tasks," in *2007 IEEE/RSJ International Conference on Intelligent Robots and Systems*, 2007, pp. 417–422.
- [7] S. Isler, R. Sabzevari, J. Delmerico, and D. Scaramuzza, "An information gain formulation for active volumetric 3D reconstruction," in *2016 IEEE International Conference on Robotics and Automation (ICRA)*, 2016, pp. 3477–3484.
- [8] J. Daudelin and M. Campbell, "An adaptable, probabilistic, next-best view algorithm for reconstruction of unknown 3-d objects," *IEEE Robotics and Automation Letters*, vol. 2, no. 3, pp. 1540–1547, 2017.
- [9] C. Gaião, J. de de Brito, and J. Silvestre, "Inspection and diagnosis of gypsum plasterboard walls," *Journal of Performance of Constructed Facilities*, vol. 25, no. 3, pp. 172–180, 2011.
- [10] E. Yildiz and F. Wörgötter, "Dcnn-based screw detection for automated disassembly processes," in *2019 15th International Conference on Signal-Image Technology & Internet-Based Systems (SITIS)*, 2019, pp. 187–192.
- [11] D. Huber and T. Kanade, "Integrating lidar into stereo for fast and improved disparity computation," in *2011 International Conference on 3D Imaging, Modeling, Processing, Visualization and Transmission*, 2011, pp. 405–412.
- [12] M. Keidar and G. A. Kaminka, "Efficient frontier detection for robot exploration," *The International Journal of Robotics Research*, vol. 33, no. 2, pp. 215–236, 2014.

EASEEbot: A Robotic Envelope Assessment for Energy Efficiency

Guanbo Chen¹, Beyza Kiper¹, Xuchu Xu², Bilal Sher², Semiha Ergan[†], Chen Feng[†]

Abstract—Building envelope inspections are necessary to maintain buildings’ energy efficiency, but current solutions are expensive, time-consuming, and destructive. Furthermore, inspectors often face safety and accessibility issues. To mitigate these issues, we propose a holistic system, EASEEbot, consisting of robots to capture data and help retrofit and employ artificial intelligence to assist in data analysis. The robots including an unmanned aerial system (UAS) and ground-penetrating radar (GPR) accommodate data collection while the Robo-dog offers guidance to inspectors in retrofitting phase. The machine learning algorithm helps to analyze the captured data, identifies envelope issues, and generates a building’s digital twin to map identified defects spatially to buildings’ façades. The retrofit Robo-Dog uses the generated digital twin to project previously recorded defect imagery onto corresponding areas of the building’s envelope. It further guides workers to ensure the identified defective areas are addressed. EASEEbot offers non-destructive sensing, risk mitigation, and high-quality building envelope inspections.

Index Terms—Unmanned Aerial System, Wall-climber, Building envelope

I. INTRODUCTION

Reductions in energy usage and carbon emissions became mandatory with stringent regulations enacted by municipalities nationwide. Now, building owners are required to reduce their emissions to avoid fees and they already have reached maximum efficiency in their mechanical and electrical systems, so their focus has shifted to diagnosing building envelope issues and retrofitting. Identifying building envelope issues and proposing solutions are possible only with high-quality building envelope inspections and energy audits. Current methods mostly depend on ground-based or handheld infrared thermography (IRT) to detect building envelope defects [1]. However, for a large-scale inspection, inspectors often face safety hazards, extra instrument cost and accessibility issues which highlights that solutions must be non-destructive, act as a productivity multiplier, mitigate risk, and produce high quality results.

In this paper, we propose a system of a Robotic Envelope Assessment for Energy Efficiency (EASEEbot). EASEEbot consists of robots and AI for building envelope inspections and analysis to assist inspectors at every stage of the building retrofit process. At a high level, there are three stages of EASEEbot, namely data capturing, data analysis, and retrofitting. During the data capturing stage, EASEEbot utilizes an UAS and a GPR; later, the captured data is analyzed during the data analysis stage, and finally, EASEEbot Retrofit Robo-Dog aids workers and inspectors during the retrofitting phase. The EASEEbot UAS safely flies around a building and non-destructively captures color and infrared imagery in a fraction of the time of a conventional inspection. This data is processed by the EASEEbot’s thermal

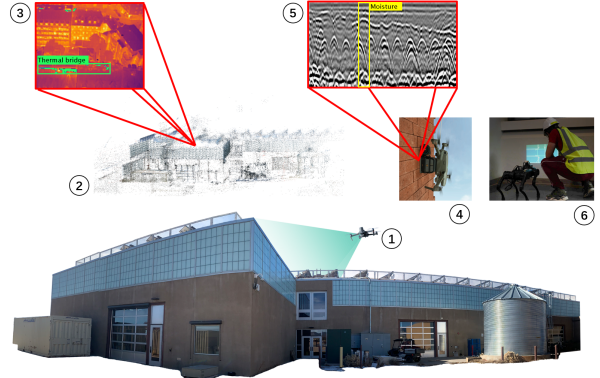


Fig. 1: Illustration of the EASEEbot system: 1. RGBT data capture; 2. 3D RGBT point cloud; 3. Thermal bridge detection; 4. GPR scanning by UAS wall climber mode; 5. Moisture detection; 6. Robo-dog retrofitting assistant

AI to detect envelope issues such as trapped moisture, air leaks, and thermal bridges. Attaching the EASEEbot radar module converts the UAS into a wall climber and allows users to find previously undetectable envelope issues (i.e., deep moisture penetration and corroded wall ties) in a non-destructive fashion. The dataset is further processed and then fed to the EASEEbot’s 3D reconstruction algorithm to generate a digital twin of the inspected scene and map it out as a 3D point cloud of the exterior façade - scanned imagery data is organized by its 3D pose. These analyses enables inspectors to make informed decisions easily on where and how to retrofit and repair building envelopes. During retrofitting phase, the EASEEbot Retrofit Robo-Dog uses building information models procured from previous 3D point cloud scans to visualize the previously recorded and detected defects onto corresponding surface areas of the building’s envelope through a projector-based augmented reality system on the Robo-Dog. In the process, it guides construction inspectors and retrofit workers to ensure those defects are properly addressed. The Retrofit Robo-dog makes it easy for workers to understand where issues are and conveys context-specific retrofitting information related to those issues.

II. RELATED WORK

Drones & Thermography: Research is being conducted on infrared scans of building envelopes conducted by drones [2]. A literature review reveals that authors have explored automated ways of detecting thermal anomalies. These initial attempts make use of the superpixel method of clustering neighbouring image pixels with similarities [3]. Other attempts at creating an automatic anomaly detection algorithm for building envelope issues incorporate segmentation neural networks [4]. However, these approaches do not differentiate between different types of building envelope failures and

New York University, Brooklyn, NY 11201, USA
{gc2720,bk2569,xuchuxu,bas9876,semiha,cfeng}@nyu.edu

¹ Equal contributions.

² Equal contributions.

[†] Corresponding authors.

such as failed insulative double paned windows, acceptable thermal bridges on rooftops due to the presence of mechanical units, or open windows that show a hot spot. Another unexplored area is training a neural network to understand the difference between positive and negative scans of a building. Positively pressurizing a building (turning the HVAC on such that there is more pressure inside the building than outside) allows a thermal scan to detect air leaking out of a building. Negatively pressurizing it prevents a thermal scan from detecting air leaking out of the building. A subtraction of the two images should isolate for thermal bridges, and a subtraction of this image with the positively pressurized building scan should isolate for areas of air leakage. This is currently done manually by industry engineers, without the widespread use of computer-based image processing aids.

GPR: In the building space, microwaves have been extensively used for detection and analysis. GPR and through wall imaging radar use microwaves to detect covered and buried objects. Microwave-based radar has been used extensively to find buried pipes and rebar embedded in concrete [5]. Pipe and rebar detection works by establishing a baseline microwave reflectance signal and searching for differences from that baseline. Based on this principle, microwave-based radar has also been used for detecting moisture in building components [6]. Through more complex signal analysis, it has been extended to tracking people behind walls and extracting the internal structure of a wall assembly itself [7]. Researchers have applied supervised deep learning algorithms to automatically extract relevant hyperbola information from GPR scans, but their models are geared towards detecting buried pipes and utility lines [8]. Using GPR to detect moisture and exploring how well machine learning algorithms can capture this information would expand the current body of knowledge.

III. METHODS

The experiment platform includes UAS flight mode, UAS wall climber mode and retrofit Robo-Dog as the hardware, Thermal AI, GPR AI and 3D Reconstruction Algorithm as the software.

A. Hardware

1) *UAS flight mode:* As the primary mobile platform for data collection, UAS flies with sensors and follows preset flight trajectories. The EASEEBot UAS is designed to be foldable. Bounding box dimensions are $8.43 \times 3.58 \times 3.31$ inches ($L \times W \times H$) for folded and $12.68 \times 9.53 \times 3.31$ inches ($L \times W \times H$) for unfolded. An integrated dual-lens sensor module, which has a 640×512 resolution uncooled VOx microbolometer and a 4K RGB color camera, is attached to the UAS with a gimbal. The UAS also has a micro-USB port on the top of the fuselage to transmit additional sensor data or provide power to the beacon for night flight. There are six cameras and two linear LIDAR sensors installed on the fuselage, which are used as the sensor input for the automatic omnidirectional obstacle avoiding system.

2) *UAS wall climber mode:* When switching to the wall climber mode, the UAS needs to be connected to a tether system and the GPR sensor. The tether is attached to the wall out of safety concern. The GPR sensor is to be installed under the center gravity of the UAS, fixed with 3D printed holder. Meanwhile, the gimbal on the UAS can remain attached, due to the infrared camera sensor module's compact size. The UAS needs to take off from an orientation parallel to the building façade. Prior to take off, the UAS's onboard inertial measurement unit (IMU) and the automatic omnidirectional obstacle-avoiding system will need to be disabled. One LIDAR sensors attached on the bottom of the fuselage will detect the distance between the fuselage and wall and control the motor's throttle to ensure the GPR touches firmly on the building façade.

3) *Retrofit Robo-Dog:* The EASEEBot Retrofit Robo-Dog's flexible legs can navigate around these obstacles better than crawling and wheeled robots. Our robot dog has four high torque motors to control each leg and body pose individually. Meanwhile, we installed a ball-shaped force sensor on the "feet" of each leg, which provides a feedback signal to estimate the pose of the robot dog and the level of the ground. At the front of the robot dog, we installed a distance perception module, including a Lidar and a dual-lens 3D camera. This module assists the Retrofit Robo-dog in mapping, localization, and navigation. We set three main control components inside the robot body: a battery pack, an Nvidia Jetson Xavier NX single-board computer, and Intel NUC mini PC. The Nvidia Jetson is responsible for the sensor data collection, feedback processing, attitude estimation and simple visual obstacle avoidance. The Intel NUC handles more complex program computation, such as map generation, path planning, robot-environment interaction and communication. In order to project the defect points on the construction wall, a projector-based augmented reality (PAR) module [9] is installed on the back of the robot dog. The PAR module consists of a compact projector and Intel Realsense T265 camera. We use a T265 camera as visual input for high-precision visual odometry and a projector as image output from Intel NUC. In addition, the robot dog also has a remote controller and a simple control app for manually remote control.

B. Software

1) *Thermal Camera Calibration:* There have been a number of different attempts at performing geometric camera calibration of a thermal camera. Most solutions use a checkerboard as a camera calibration rig. Some solutions exploit different material emissivity properties to produce a contrast [10]. This is appropriate in some settings, but others find that they need to further increase the contrast between the black and white squares of the checkerboard in order to obtain good results. Their solution was to use computer vision techniques to increase the detectability of the squares and their corners so that a more robust camera calibration could be achieved [citesshibata2017](#) accurate. We tested multiple methods involving active and passive heating

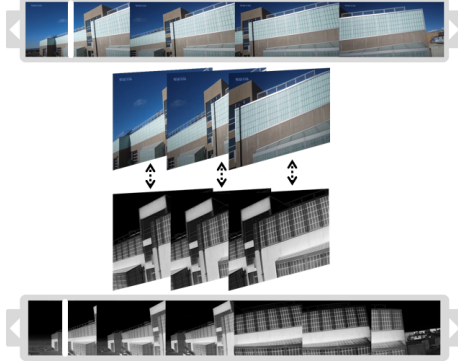


Fig. 2: RGBT image precessed into RGB image and Thermal image

on various materials. We used a lasercut acrylic checkers with a carboard backing, lasercut wood checkerboard with a vinyl backing, and machine cut vinyl with a metal backing. We tested each with and without active heating.

2) *Thermal AI*: EASEEbot's thermal AI algorithm is a modified UNet [11] algorithm created using PyTorch. An image is input as a 4 channel tensor composed of RGB and Thermal channels. Prior to image analysis, thermal and RGB scans taken during UAS inspections are registered with the shooting location and concatenated into a 4 channel RGBT scan video. The scan videos are then sectioned into individual frames, which form a video-specific dataset. The video-specific dataset is fed into our pretrained neural network model to create segmentation masks for detected thermal and moisture anomalies. The segmentation mask is a binary channel picture of the same size as the input RGBT image where every pixel corresponds to the pixel in the image; the top right hand pixel in the RGBT image corresponds to the top right hand pixel in the segmentation mask. Where the AI algorithm has detected a thermal anomaly, the value of the pixel is 1 and the rest is 0. The RGBT image is then processed back into separate RGB and T data streams. The segmentation masks are applied as an outline to both RGB and T data streams and reviewed to ensure that all masks are accurate. The RGB image stream is further processed - segmentation masks are filled in as bright yellow. The processed RGB images are then sent to the 3D reconstruction algorithm.

3) *GPR AI*: GPR is a non-destructive sensing and inspection tool that has traditionally been used to find buried utility pipelines in the ground and metal embedments within concrete. the GPR unit emits radio-frequency waves and records the time and intensity of reflection. We attach the Proceq GP8800 unit to EASEEbot and connect it to their iPad. GPR readings are taken along a wall surface and automatically tracked by Proceq's data capture system on the iPad. Once the wall climber has completed its scan, the scan data is exported from the iPad to our server. Scans are then sent through our GPR-specific AI to label anomalous areas which indicates whether moisture is present within the envelope's assembly. The GPR scans are put through a binary convolutional network. A convolutional neural network (CNN) convolves through the scans to label an approximately

1 ft section as either anomalous or normal. The network is a modified UNet model. The output layer has a sigmoid activation function that makes the final anomalous/non-anomalous determination of a scanned section.

4) *3D Reconstruction Algorithm*: EASEEbot's 3D reconstruction algorithm is based on the structure-from-motion (SfM) algorithm. While the UAS is in flight, images are captured every 15 to 25 frames in RGB color and infrared videos, while onboard GPS records the location of the UAS cameras and their viewpoint direction for when each image is captured. The capture interval depends on the complexity of the building envelope. Once all the images are captured, feature points are extracted from each image through a pre-trained machine learning neural network. By identifying common feature points shared between pairs of video frame images, and knowing the difference between the two images' respective camera 3D locations and viewpoint directions, the 3D location of those feature points can be inferred. The GPS data associated with each image, as well the timing of each image in videos can be used to initially group the images by rough general locations in 3D space. An additional graph neural network and attention mechanism are used for matching feature points among locally grouped images. A global list of feature point matches is then compiled by tabulating common feature points over all localized groups of images. Using this global list of common image-feature points and calculating all matched images' respective differences in camera translation and rotation, the algorithm estimates the 3D location of each feature point, and a sparse 3D point cloud is generated. Noise in 3D point cloud estimations are reduced by bundle adjustment, which tries to make the point estimations more consistent over the entire scan.

IV. EXPERIMENT

With our experiment platform, we validate our software by performing following experiments

A. Thermal AI experiment

Thermal AI is a UNet model trained over the Mayer dataset [12]. Trained the model for 250 epochs. The learning rate was halved every 15 epochs. Once 15 epochs with the latter learning rate were reached, the learning rate was reset to 0.001 and the loop was continued. We also tried FCN-8s and Mobilenet V3, so far UNet was the best. The accuracy is about 65%. Figure 3 shows the results of our thermal AI, the AI reveals the potential thermal bridges on the building and the images with RGB data are further used in 3D reconstruction algorithm.

B. GPR AI experiment

The AI training dataset is generated by scanning a plywood glued with six pieces of paper towel of varying moisture content which can simulate a wall with non-normal moisture condition. Over the plywood was various construction materials like batt insulation, rigid foam insulation, metal and wood stud, more plywood, brick, concrete, and combinations of these. As the figure 3 shows, the GPR AI has the ability to distinguish areas with moisture when

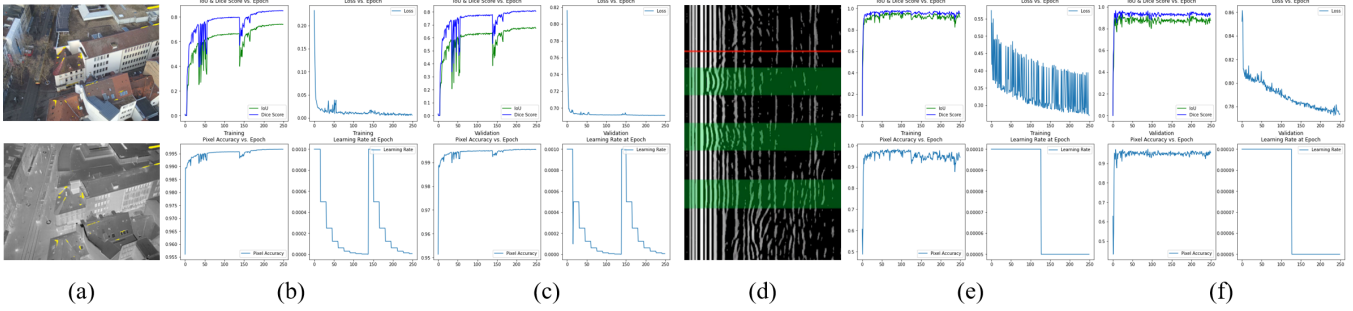


Fig. 3: Thermal AI and GPR AI results: (a) Thermal AI Demonstration; (b) Thermal AI Training results; (c) Thermal AI Validation results; (d) GPR AI Demonstration; (e) GPR AI Training results; (f) GPR AI Validation results



Fig. 4: Comparision between the (a) color image point cloud and (b) Google map

radar module is assembled on the UAS. The output of the modified GPR AI is a $H \times W$ image of size $1 \times$ length of the scan. Areas that are non-dry have a value of 1 and 0 otherwise. Based on this, the AI has an accuracy of 95% and only fails at the edges of generated moisture.

C. 3D Reconstruction Algorithm experiment

We evaluate our 3D reconstruction algorithm by collecting data from Trades and Advanced Technology Center, Santa Fe Community College. The foot print of the building is about $31,000 \text{ ft}^2$ and the height is 36 ft . The total surface scanned is about $8,900 \text{ ft}^2$ and the total flight time is 37 minutes. We planned a zig-zag flight path around the outer wall of the building with a offset of 5m. Figure 4 shows the comparison between color image point cloud and google map where the red blocks are the camera frames. On each corner, the UAS rotates by yaw axis to collect the feature points on both sides of the corner of building. The algorithm has successfully generated the 3D point cloud and the estimations are reduced by bundle adjustment, making it more consistent.

V. CONCLUSION

In this paper, we proposed a system of robots and AI for building envelope inspections called EASEEbot. In current practice, inspections are costly, destructive and inspectors have to deal with safety and accessibility issues. EASEEbot addresses these issues by utilizing a UAS, a GPR, a retrofit Robo-dog, and AI algorithms which can significantly reduce the inspection costs, risks of working at heights, and inaccessibility issues. During the non-destructive data collection and analysis phase, EASEEbot uses the UAS in flight mode to collect the thermal & RGB images and wall climber mode to collect GPR scans. Further, the thermal AI identifies thermal defects while the GPR AI finds hidden moisture content

on building envelopes. To eliminate safety risks, EASEEbot employs an omnidirectional obstacle avoiding system on UAS flight mode and a tether system on UAS wall climber mode. Moreover, EASEEbot offers a retrofit Robo-dog to help with the building defect point visualization to increase the productivity of the retrofit process. In the future, we plan to showcase an autonomous robot with a GPR unit to scan horizontal and slightly inclined surfaces such as a roof, train the GPR AI to detect and predict the corrosion condition of masonry ties in masonry walls, and improve the UAS wall climber motion on rough building façades.

REFERENCES

- [1] M. H. Shariq and B. R. Hughes, "Revolutionising building inspection techniques to meet large-scale energy demands: A review of the state-of-the-art," *Renewable and Sustainable Energy Reviews*, vol. 130, p. 109979, 2020.
- [2] T. Rakha and A. Gorodetsky, "Review of unmanned aerial system (uas) applications in the built environment: Towards automated building inspection procedures using drones," *Automation in Construction*, vol. 93, pp. 252–264, 2018.
- [3] T. Rakha, A. Liberty, A. Gorodetsky, B. Kakillioglu, and S. Velipasalar, "Heat mapping drones: an autonomous computer-vision-based procedure for building envelope inspection using unmanned aerial systems (uas)," *Technology Architecture+ Design*, vol. 2, no. 1, pp. 30–44, 2018.
- [4] Y. Arjoune, S. Peri, N. Sugunarat, A. Biswas, D. Sadhukhan, and P. Ranganathan, "An instance segmentation and clustering model for energy audit assessments in built environments: A multi-stage approach," *Sensors*, vol. 21, no. 13, p. 4375, 2021.
- [5] Y. El Masri and T. Rakha, "A scoping review of non-destructive testing (ndt) techniques in building performance diagnostic inspections," *Construction Building Materials*, vol. 265, p. 120542, 2020.
- [6] A. Horsley and D. S. Thaler, "Microwave detection and quantification of water hidden in and on building materials: implications for healthy buildings and microbiome studies," *BMC Infectious Diseases*, vol. 19, no. 1, p. 67, 2019. [Online]. Available: <https://doi.org/10.1186/s12879-019-3720-1>
- [7] P. Sévigny and J. Fournier, "Automated front wall feature extraction and material assessment using fused lidar and through-wall radar imagery," *Defence Research and Development Canada (DRDC)*, 2014.
- [8] Y. Li, Z. Zhao, Y. Luo, and Z. Qiu, "Real-time pattern-recognition of gpr images with yolo v3 implemented by tensorflow," *Sensors (Basel, Switzerland)*, vol. 20, no. 22, p. 6476, 2020. [Online]. Available: <https://pubmed.ncbi.nlm.nih.gov/33198420/>
- [9] S. Xiang, R. Wang, and C. Feng, "Mobile projective augmented reality for collaborative robots in construction," *Automation in Construction*, vol. 127, p. 103704, 2021.
- [10] W. Ursine, F. Calado, G. Teixeira, H. Diniz, S. Silvino, and R. De Andrade, "Thermal/visible autonomous stereo visio system calibration methodology for non-controlled environments," in *11th International Conference on Quantitative Infrared Thermography*, 2012, pp. 1–10.
- [11] O. Ronneberger, P. Fischer, and T. Brox, "U-net: Convolutional networks for biomedical image segmentation," in *International Conference on Medical image computing and computer-assisted intervention*. Springer, 2015, pp. 234–241.
- [12] Z. Mayer, Y. Hou, J. Kahn, T. Beiersdörfer, and R. Volk, "Thermal Bridges on Building Rooftops - Hyperspectral (RGB + Thermal + Height) drone images of Karlsruhe, Germany, with thermal bridge annotations," May 2021. [Online]. Available: <https://doi.org/10.5281/zenodo.4767772>

AGPNet - Autonomous Grading Policy Network

Chana Ross¹, Yakov Miron^{1,2}, Yuval Goldfracht¹, Dotan Di Castro¹

{Chana.Ross, Yakov.Miron, Yuval.Goldfracht, Dotan.DiCastro}@bosch.com,

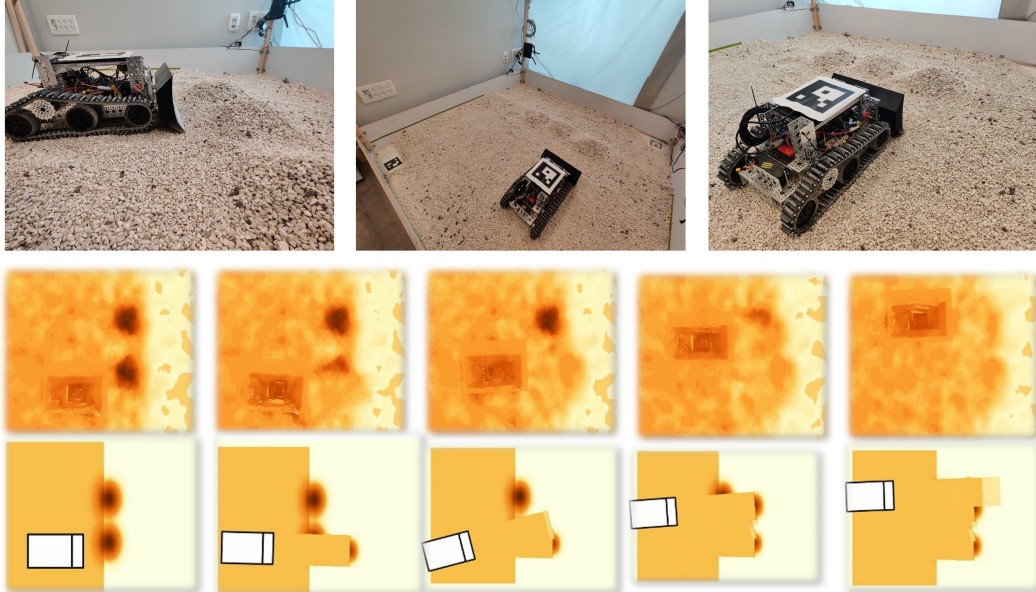


Fig. 1. A comparison of a trained agent executing autonomous grading on a **simulated environment** and a **real-world scaled environment**. **Top Row:** RGB images of our experimental setup (see Section III) showing the scaled dozer prototype facing the sand piles. **Middle and Bottom Rows:** A selection of heatmaps that depict actual states extracted from our real-world scaled environment and simulated environment respectively. Dark blobs indicate the sand piles while the left column represents the initial state of both environments.

Abstract—In this work, we establish heuristics and learning strategies for autonomous control of a dozer grading an uneven area studded with sand piles. We formalize the problem as a Markov Decision Process, design a simulation which mimics dozer-soil interactions and finally, compare our simulator to a real-world scaled environment. We use methods from reinforcement learning, behavior cloning and contrastive learning to train a hybrid policy. Our trained agent, AGPNet, reaches human-level performance and outperforms current state-of-the-art machine learning methods for the autonomous grading task. In addition, we show that our agent is capable of generalizing from random scenarios to unseen real world problems.

I. INTRODUCTION

The off-road autonomous driving industry has attracted increasing interest in the past two decades due to shortage in experienced drivers as well as rising demand in the construction industry. Previous work in the field has mainly focused on obstacle avoidance [4], [11], optimal trajectory planning [12], [6], [11] and traversability [13]. The autonomous grading task was first tackled from a path-planning perspective by [2]. This pioneering study was the first to directly address the autonomous grading problem. In their work, [2] implemented a rule-based approach, where, given a large sand pile, the system

selects the goal points the agent needs to reach and the grading leg it needs to perform. After the agent aggregates several of these legs, the pile is graded and the task is considered done. While this approach relies on rule-based heuristics, recent successes with machine learning methods have demonstrated the possibility of automating and optimizing such complex problems.

In this work, We focus on autonomous path planning for construction site vehicles. Specifically, we discuss the task of grading a given area with a number of sand piles. In this task, the dozer is confronted with an uneven terrain (Fig. 1) and is required to level the ground, in a minimal amount of time, to a predefined target height. We solve this problem using a hybrid approach which combines Reinforcement Learning (RL), a sub-field of machine learning, Behavior Cloning (BC) and Contrastive Learning (CL). In addition, We simplified the learning process by utilizing domain knowledge regarding the action space and added a prior on the initial action distribution.

As we demonstrate herein, our model is capable of training on a random scene, and then generalize to a more complex realistic problem. To validate our method, we created a simulation for training and evaluating our models, which includes all the important interactions between the dozer and the soil. In addition, we've built an scaled prototype environment in order to validate our methods on real-world data (see III).

¹Bosch Center for Artificial Intelligence, Haifa, Israel

²ANFSL, The Hatter Department of Marine Technologies, University of Haifa, Israel

Our main contributions are: (1) We provide an end-to-end pipeline for training autonomous dozers that combines **BC** and **RL** for improved robustness, enhanced performance and reduced sample complexity. Here, we implement a hierarchical architecture in which high-level trajectory planning is learnt and low-level action control is performed. (2) We establish a **RL** environment simulator for the earth-moving dynamics and the interaction between the dozer and the soil. Using this simulator, we train a **RL** agent for the autonomous-grading task. (3) We validate the simulator using a scaled prototype environment and compare heightmaps generated by our simulator to those taken using a real depth camera.

II. PROBLEM FORMULATION AND PRELIMINARIES

Our goal is to create an optimal policy for a bulldozer performing a grading task, where given an initial grading area which contains a number of sand piles, the dozer must find an optimal trajectory to flatten the sand piles to a predetermined target height. We solve the problem using a combination of Behavioral Cloning (**BC**), Contrastive Learning (**CL**) and model-free Reinforcement Learning (**RL**) techniques. In our suggested method, we split the autonomous grading task into three independent sub-tasks: the initialization task, the continuous task, and the edge task (see Fig. 2). In addition, we formulate all tasks as a POMDP [10] where both the initial and target heightmaps are given.

A. Partially Observable Markov Decision Processes

A Partially-Observable Markov Decision Process (POMDP; [10]) is comprised of the tuple $(\mathcal{S}, \mathcal{O}, \mathcal{A}, \mathcal{P}, \mathcal{R})$. While a state $s \in \mathcal{S}$ contains all the required information, in practice, agents are presented with partial information regarding the environment i.e observation $o \in \mathcal{O}$. After the agent selects an action $a \in \mathcal{A}$, the system transitions to the next state s' based on the transition kernel $P(s'|s, a)$ and the agent is provided with a reward $r(s, a)$.

The goal of an agent is to learn a behavior policy π^* (stochastic or deterministic) that maximizes the cumulative reward to go according to $\pi^* = \arg \max_{\pi \in \Pi} \mathbb{E}[\sum_{t=0}^T (\gamma^t r_t)]$.

B. Problem Formulation

In this section, we will describe all of the POMDP components as they are reflected in the suggested solution.

State: The state s_t includes the target area size, dozer's location within this area, the full dozer trajectory up until the current time point, and the relative heightmap of the target area (denoted as $\delta_{H_t} = H_t - H_{des}$ where H_t is the current heightmap and H_{des} is the target heightmap).

Observation: The observation o_t is comprised of an *EGO view* heightmap i.e a bounding box view around the current location of the dozer (derived from the full state's heightmap). While the state's heightmap dimensions can vary we keep the ego view's size fixed to make training simpler.

Action: While control over the dozer can be executed at a low level resolution, i.e speed and rotation, we chose to formulate our action space at a higher level selecting way-points to which the dozer should move. Each action a_t is parametrized as a way-point tuple $a_t = (p_t, s_t)$ where p_t

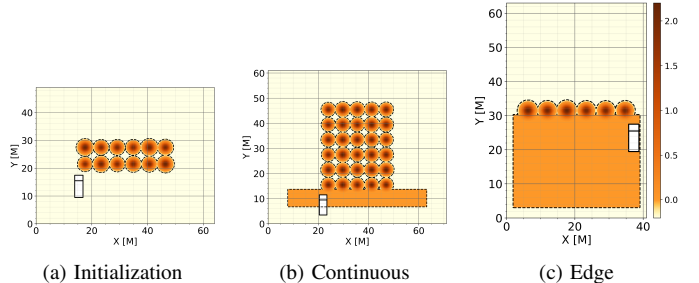


Fig. 2. The first state for each sub problem. In the **initial** scenarios, there is no graded area and a few rows of sand are dumped. The dozer is required to create an incline and reach the target height, H_{des} , if possible. Meanwhile, the dumper will add more sand piles for grading in front of the initial ones, creating more rows of sand. In the **continuous** scenarios, the agent is located at H_{des} , i.e., on top of the previously graded area, and sand piles are continuously being added in the vicinity of the graded area. The task is to constantly grade them to H_{des} . The main difference from the previous problem is that the piles are dumped on top of H_{des} and the dozer needs to push it forward, thus enlarging the area in which $H = H_{des}$. Finally, in the **edge** scenarios, the final row of sand piles is dumped, most of the area is already graded, and the sand leftovers need to be cleared. The dozer must create a decline to flatten the sand and then smooth the graded area.

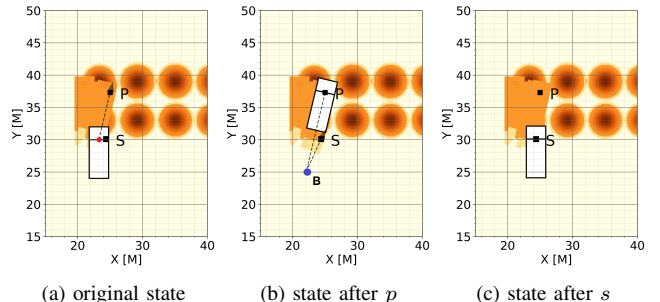


Fig. 3. Example of MDP actions (p, s) and the trajectory between these actions. In 3a, the initial position is the red dot. The action's order is as follows: (i) From origin rotate to face p . (ii) Drive forward to p . This action has the greatest value w.r.t. the received reward, as it is the only one that grades sand. (iii) Reverse back to B (blue dot in 3b). (iv) Rotate to face next s . (v) Drive forward to next s . (vi) Rotate to face the sand piles (3c).

is the first way-point reached by a forward movement and s_t is the starting point of the next action. Each action a_t is sampled from the two policy distributions over the FOV pixel map of the agent ($\pi \in R^{2 \times \hat{m} \times \hat{n}}$, $\hat{m} = \frac{m}{2^N}$, $\hat{n} = \frac{n}{2^N}$), where $N = 3$ is the down-sampling factor, for reduced state and action space dimensions. Once these points are selected, we can continue and generate the low-level actions that form the entire trajectory of the vehicle as seen in figure 3 and similarly to [2]. Since a dozer typically drives in straight lines to avoid slippage, we chose to define these actions as a continuous movement in the dozer's body axis: δ_x for translation and δ_ψ for rotation.

Reward: The grading task involves many objectives, which need to be reflected in the reward function. In our environment, the reward is multi-modal. One mode takes *time* as an objective, so only discounting over the horizon might collapse to the trivial solution (minimal time while not completing the task or not touching the sand at all in the fatal case). In the general case, the optimal agent will *complete the task*, i.e., reach the target surface, H_{des} , not leave sand

piles/bumps in the area i.e., will remove the *maximum volume*, and grade sand in every leg, i.e., will minimize the legs in which reverse/rotation actions are selected. Moreover, upon *task completion*, the agent gets a large reward, and if not accomplished, the agent receives a large negative reward. See section III-B. The multi-objective reward function is:

$$R_t = \lambda_v * f_v - \lambda_t * f_t + \lambda_h * f_h + \lambda_d * \mathbb{1}_{is_done} - \lambda_f * \mathbb{1}_{is_failed}$$

where the current volume removed f_v (calculated as the sum over $H_T - H_{init}$, current height removed f_h and time spent f_t on executing the action. All the f_i functions and λ_i coefficients of the specific rewards were tuned during the hyper-parameter search.

III. METHOD

In order to tackle the problem of autonomous grading we focus our efforts on several fronts: (1) implementing a realistic simulation environment (2) creating a rule-based heuristic policy for autonomous grading (3) exploring machine learning methods that can succeed in solving this challenging task. (4) Validating our simulation and policy on a scaled prototype environment

A. Simulation

The movement of the soil due to a dozer's action is not trivial and can be *simulated* using different techniques, each one capturing different aspects of the full interaction [7], [9], [5]. We aim to create a computationally inexpensive simulation, while taking into account key aspects of the environment which are needed to estimate an optimal policy. These aspects include the interaction between the dozer and the soil as well as the dozer's behaviour such as velocity change due to torque.. In our simulation, each sand pile is modeled as a Multivariate Gaussian Distribution with two variables (x, y). These variables are the cartesian coordinates of the height map, both taken from an i.i.d normal distribution,

$$f(x, y) = \frac{V}{2\pi\sigma_x\sigma_y} * \exp\left(-\frac{1}{2}\left[\left(\frac{x - \mu_x}{\sigma_x}\right)^2 + \left(\frac{y - \mu_y}{\sigma_y}\right)^2\right]\right),$$

where $f(x, y)$ is the height of the soil at each point, $V[cm^3]$ is the volume, and $\sigma_x[cm], \sigma_y[cm]$ define the footprint of the sand pile. For example, given a volume V , as σ_x and σ_y grow, the piles height is reduced and footprint grows.

B. Heuristic Policy

Throughout our work, we used the rule-based heuristic policy, denoted as **SnP** (“start point” and “push point”), inspired by [2] as an experienced agent and a good baseline comparison. This policy is based on a human expert and mimics the expert's behaviour. As done in the trained policies, we used two levels of action here: The way-point planner chooses the destination point and then the origin (p_t, s_t) and the path planner creates 6 low-level actions, as shown in Figure 3. Unlike our learnt algorithms, the high-level actions are chosen using a combination of classical detection algorithms for sand-pile detection and search heuristics.

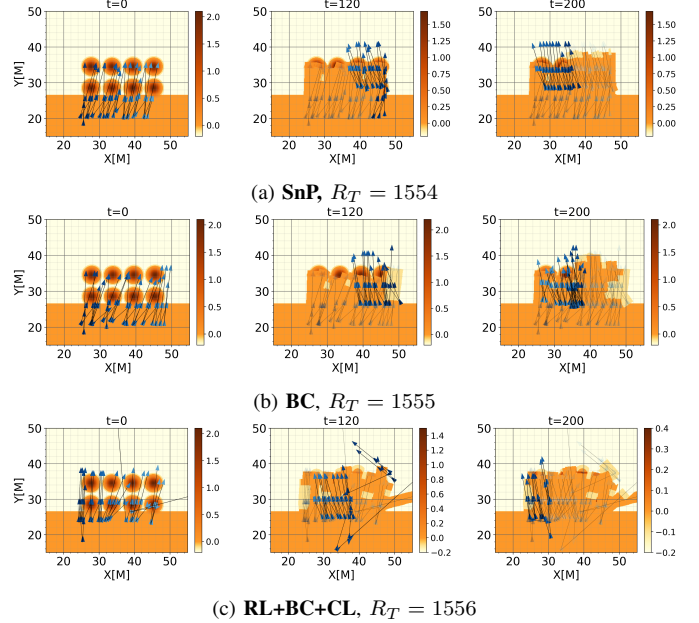


Fig. 4. Comparison between trajectories from different policies for the continuous problem. Each triangle is another action and the lines indicate the paths between these actions. Each row shows a different policy (**SnP**, **BC**, **RL+BC+CL**) and each column a different stage of the episode. R_T is the total reward.

C. Scaled Prototype Environment

To validate our simulation, we created a **scaled prototype environment** at a 1 : 9 scale compared to a real dozer. We built a sand box with an RGBD sensor that provides both heightmaps and agent locations within a global coordinate system. The prototype dozer interacts with the sand, and the height-maps can be recorded throughout the episode and be post-processed with the simulation of the same scenario. Figure 1 (center image) shows the experimental setup with (i) a sand box filled with sand prior to grading, (ii) the prototype dozer, and (iii) the localization system. ArUco [8] markers are used to localize the dozer and calibrate the camera w.r.t world coordinates. The dozer is controlled by 3 motors: two control the tracks and the third controls the blade. The second row in Fig. 1 shows the output of the experimental setup.

D. Policy Model

For all the methods, we utilized a deep neural network for estimating the policy for each state. Our models have an embedding layer followed by a number of convolution layers and a fully connected layer at the end. We used Yolo lite [3] or Resnet [1] architectures as a baseline and assumed a discrete action space. To ease the learning process, and improved robustness, we added a prior that the agent will initially prefer to move within its near vicinity, by adding a spatial Gaussian layer. Finally, a softmax layer for each sub-action was calculated to produce a distribution over the pixels.

IV. EXPERIMENTS

To demonstrate our method and the robustness of our algorithms, we compared them on three types of problems,

scenario type	metric	BC	BC+CL	RL	RL+BC	RL+BC+CL	RL+CL	SnP
Init	volume ↓	0.63	21.97	1.03	0.57	0.25	0.07	0.36
	height ↓	2.06E-04	7.20E-03	2.71E-04	1.76E-04	7.12E-05	2.19E-05	1.15E-04
	time ↓	5024	6566	14464	14326	12975	11140	3278
	reward ↑	1478	930	1714	1916	2687	3132	1934
Continuous	volume ↓	15.04	46.53	0.70	0.36	0.29	0.16	0.12
	height ↓	4.10E-03	1.28E-02	1.87E-04	9.92E-05	8.63E-05	4.98E-05	3.74E-05
	time ↓	6232	7282	11455	15775	12857	8864	3451
	reward ↑	1584	712	1681	2910	2271	3123	2585
Edge	volume ↓	0.25	4.65	1.22	0.42	0.30	0.10	0.05
	height ↓	7.74E-05	1.81E-03	3.49E-04	1.20E-04	8.89E-05	3.39E-05	1.42E-05
	time ↓	4657	5670	10981	12065	5993	8468	3094
	reward ↑	939	475	1624	2447	3690	3512	2791

TABLE I. All the results for our algorithms, including the **SnP** heuristic, **BC**, **RL** and hybrid methods. Our hybrid methods achieve better results on the main metric (height) and the overall reward. Results are mean over 50 i.i.d. runs.

as outlined in Figure 2 and explained in Section II. We used 3 different algorithms: **BC**, **CL**, **RL** as building blocks for 8 different hybrid models and focused our comparison on 4 metrics. The dataset used to train the **BC** policies included 150 episodes, each with a range of states drawn from our simulator. For the purpose of evaluation, we ran 50 runs for each scenario type generated from the same distribution and compared the mean result for each metric. Each initial state had a different number of sand piles, set up in a lattice format, and the dozer was positioned facing the piles. All the algorithms were calculated on the same scenarios to ensure a fair comparison. Autonomous off-road planning is complex and, specifically, the grading assignment does not have classic solvers for comparison. We, therefore, compared our results to the **SnP** heuristic that is based on [2], who used experienced expert drivers and mimicked their behaviour.

We show our results on all the metrics in Table I. The results of the majority of our approaches are on par with the baseline heuristic. We found that our combined algorithms approach (**RL+BC+CL**) outperforms the heuristic in terms of important metrics and overall reward. In our approaches, the agent learns from experienced rule-based algorithms similar to other **BC** models but also trains on online policies allowing for exploration. In addition, we enhanced the policies' ability to detect important features in the state space by adding a **CL** loss (**CL**), and the final Gaussian masking layer in the policy ensures our agent does not explore irrelevant areas. In Figure 4, we show a comparison between the trajectories of 3 agents (**SnP**, **BC** and **RL+BC+CL**). As the **BC** agent is able to generalize to episodes it never saw, it successfully follow the pattern of the **SnP** heuristic. The **RL+BC+CL** trajectory has less actions and manages to grade more soil at an earlier step (see left column). Moreover, this policy reaches an overall higher reward and lower final height (better agent).

V. DISCUSSION

We here present AGPNet, an end-to-end pipeline for autonomous grading using a dozer. First, we formulate the problem as an *MDP* and use **RL** and **BC** algorithms to solve the problem. Second, we create a light yet detailed simulation for training algorithms and suggest a new and innovative approach for simulating earth-moving vehicles and

their interaction with the soil. We prove the validity of our simulation with a real prototype dozer and show how height-maps from the real dozer are comparable to the ones from our simulation. Last, we train multiple policies and show that combining different **RL** and **BC** approaches with a high level of detection training such as **CL** achieves on par results with the heuristic and generalizes in more complex scenarios. Our method is ideal for tasks where a vehicle has an interaction with the soil that effects the environment and changes the optimal sequence of actions. It can also be used in other construction vehicles where the way-point planning is complex but the low-level actions can be defined using simple rule-based methods.

REFERENCES

- [1] Kaiming He, Xiangyu Zhang, Shaoqing Ren, and Jian Sun. Deep residual learning for image recognition. *CVPR*, 2016. 3
- [2] Masami Hirayama, Jose Guivant, Jayantha Katupitiya, and Mark Whitty. Path planning for autonomous bulldozers. *Mechatronics*, 2019. 1, 2, 3, 4
- [3] Rachel Huang, Jonathan Pedoeem, and Cuixian Chen. Yolo-lite: A real-time object detection algorithm optimized for non-gpu computers. *2018 IEEE International Conference on Big Data*, 2018. 3
- [4] A. Kelly, A. Stentz, O. Amidi, M. Bode, D. Bradley, A. Diaz-Calderon, M. Happold, H. Herman, R. Mandelbaum, T. Pilarski, P. Rander, S. Thayer, N. Vallidis, and R. Warner. Toward reliable off road av operating in challenging environments. *I. J. Robotic Res.*, 2006. 1
- [5] Wooshik Kim, Catherine Pavlov, and Aaron M Johnson. Developing a simple model for sand-tool interaction and autonomously shaping sand. *arXiv:1908.02745*, 2019. 3
- [6] H. Jayakody M. Swift and M. Whitty. Path planning for multi-object push problems in continuous domain. *IFAC-PapersOnLine*, 2019. 1
- [7] M. Pla-Castells, I. Garcia-Fernández, and R. J. Martinez. Interactive terrain simulation and force distribution models in sand piles. 3
- [8] Francisco J Romero-Ramirez, Rafael Muñoz-Salinas, and Rafael Medina-Carnicer. Speeded up detection of squared fiducial markers. *Image and vision Computing*, 76:38–47, 2018. 3
- [9] A. Sauret, N. Balmforth, C. Caulfield, and J. McElwaine. Bulldozing of granular material. *Journal of Fluid Mechanics*, 748:143 – 174, 2014. 3
- [10] Richard S Sutton and Andrew G Barto. *Reinforcement learning: An introduction*. MIT press, 2018. 2
- [11] Yusheng Xiang, Kailun Liu, Tianqing Su, Jun Li, Shirui Ouyang, Samuel S Mao, and Marcus Geimer. Extension of bim using ai: a multi working-machines pathfinding solution. *arXiv:2105.06635*, 2021. 1
- [12] Yanfu Zhang, Wenshan Wang, Rogerio Bonatti, Daniel Maturana, and Sebastian Scherer. Integrating kinematics and environment context into deep inverse reinforcement learning for predicting off-road vehicle trajectories. *arXiv preprint 1810.07225*, 2018. 1
- [13] Zeyu Zhu, Nan Li, Ruoyu Sun, Donghao Xu, and Huijing Zhao. Off-road autonomous vehicles traversability analysis and trajectory planning based on deep inverse rl. *Intelligent Vehicles Symposium (IV)*, 2020. 1

A Reinforcement Learning Based Approach for Conducting Multiple Tasks using Robots in Virtual Construction Environments

Weijia Cai¹ and Zhengbo Zou¹

Abstract—Construction robots are considered a promising solution for reducing onsite injuries and increasing productivity. One of the bottlenecks in deploying construction robots is solving the problem of robotic motion planning, considering the dynamic nature of construction sites. Specifically, current works in robotic motion planning for construction lack the generalization capacity for different tasks (i.e., a robot is generally optimized for a highly specialized task and fails to generalize when the task deviates slightly from its original form). In this paper, we proposed a reinforcement learning based approach for robotic motion planning using curriculum learning, which enables robots to conduct multiple construction tasks using a single trained agent. We tested our approach on three common construction tasks (ceiling installation, window installation, and flooring), resulting in an average success rate of around 80%.

I. INTRODUCTION

Robotization of construction tasks has been deemed a promising path to reduce the risks of occupational injuries and increase the productivity of the onsite operations [1], [2]. This is because fundamental tasks onsite, such as reaching, carrying, and placing of construction materials and building objects (e.g., ceiling panel) are physically-demanding and repetitive operations which have the potential to obtain significant improvement through automation [1]. One of the main challenges of robotizing these tasks is the problem of robotic motion planning [3], which refers to producing an optimal trajectory to move onsite objects safely from a starting location to a goal placement.

Construction sites are considered dynamic environments, with constant movements of labor, equipment, and materials, which requires adaptive motion planning for construction robots [4]. In achieving this, two main types of solutions were proposed in previous works. The first type is to preprogram the motions of robots [5], [6]. Preprogrammed robots achieved a limited level of automation, especially when the robot itself [6] or parts of the tooling [5] are designed specifically for a task. These robots are designed to work in isolated and structured environments such as modular construction factories, where the movements and locations of the robots and operated objects are known at all times. However, these designed robots can only be used for the tasks they were designed for; hence lacking the capacity to generalize to other tasks even when they are

similar. Another type is to implement and improve on classic motion planning methods such as sampling based motion planning (SMP) [7], [8], which attempt to obtain collision free trajectories by searching for an optimal series of sampled robot configurations given the geometric information of the robots and obstacles. However, the sampling process is computationally expensive if the geometries of the robot or obstacles are complex [9].

Reinforcement Learning (RL) has gained attention for improving the efficiency and generalization performance for robotic motion planning in dynamic environments [10]. In general, RL attempts to train an agent that produces an optimal policy, mapping the observed states (e.g., a robot arm's joint positions) to actions (e.g., forces applied to the joints). RL allows for generalization of multiple similar tasks through Transfer Learning (TL) [11]. TL techniques utilize the transferability of Deep Neural Network (DNN) to learn similarities among different tasks. For instance, many construction tasks can be seen as a special case of the fundamental pick-and-place task; therefore, it is feasible to train a single general agent for pick-and-place with embedded uncertainties such as starting and final placements, and then use the general agent to conduct multiple different but similar tasks such as ceiling installation and window installation.

In this study, an RL based motion planning approach is proposed to conduct three different construction tasks using a 6 Degree of Freedom (DoF) robotic arm in a Virtual Construction Environment (VCE). We first built a realistic VCE using a game engine (i.e., Unity3D) as the training and testing environment for the RL agent. We then trained the agent, named the general agent, for the fundamental pick-and-place task. Training of the general agent followed a designed training plan based on Curriculum Learning (CL) [12], which schedules the training by ascending difficulty. Lastly, we tested the generalization performance of the general agent on three common construction tasks, namely, flooring, window installation, and ceiling installation. To further prove the effectiveness of our approach, we trained three additional agents without CL as control group agents. The results were evaluated by the final cumulative reward and the success rate of each task.

II. METHODOLOGY AND EXPERIMENT DESIGN

In this section, training and testing of the general agent will be introduced (see Figure 1). We first provide details regarding the development of the VCE in Unity3D. Next, we introduce details about training of the general agents based on CL. Finally, we provide details regarding the

*We acknowledge the support of the Natural Sciences and Engineering Research Council of Canada (NSERC), [funding reference number: ALLRP 570442-2021]

¹Weijia Cai and Zhengbo Zou are with the Department of Civil Engineering, The University of British Columbia, V6T 1Z1 BC, Canada. andycai@student.ubc.ca, zhengbo@civil.ubc.ca

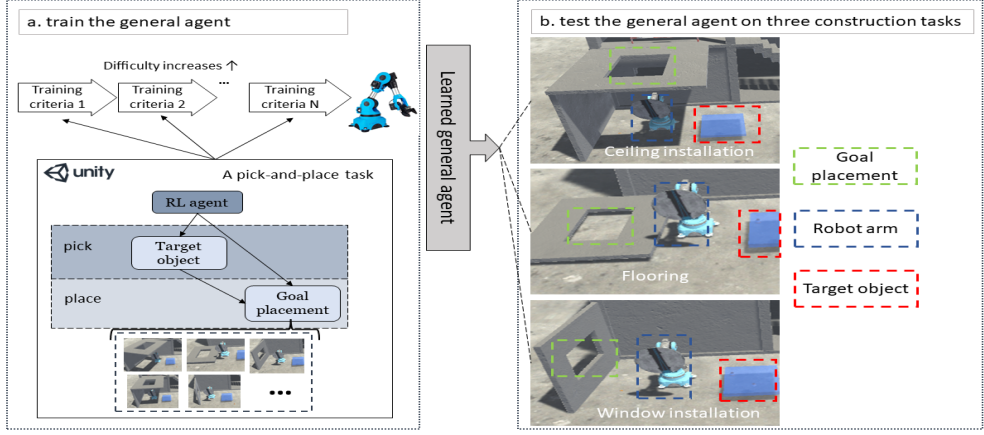


Fig. 1: Overview of the proposed method

experiments designed to test the learned general agent on three construction tasks.

A. Virtual Construction Environment Development

The development of the VCE has three main steps, as: 1) set up the physical characteristics (e.g., dimensions, weight) of objects in the VCE; 2) deploy virtual sensors for task completion detection; 3) establish a link between the RL agent and the VCE. For the first step, our VCE was designed as a construction site for a two-story building that includes a 6 DoF robot arm, a target object (i.e., ceiling panel, window, and flooring panel), three types of openings as the goal placement (i.e., goal position and orientation for the target object), and several barriers that make sure the target objects do not exceed the reachable area of the robot. We set the force limit of the robot to be 400 N, which is sufficient for lifting the target object weighted 15 kilograms. Examples of the three types of opening are shown in Fig. 1b.

Then, we set up the virtual sensors to detect whether the robot has completed the following sub-tasks: 1) picking up the target object and 2) placing the target object at a predefined goal placement. For the first sub-task, we used a ray-cast sensor in Unity3D, analogous to an ultra sonic sensor in real-world. The detection range of the sensor is used as the distance tolerance in our training plan. For the second sub-task, a ray-cast sensor with a angle detector is deployed to determine whether the target object is placed at the predefined placement. The angle detector measures the angular tolerance in the training plan.

Lastly, we linked the RL agent to the VCE to provide action control for the robot. In this study, we utilized the ML-Agents toolkits[13], a package that provides a "brain" module for decision making and an "agent" module for receiving observation and rewards from the environment. We randomized the starting location of the target objects and the goal placements during training, forcing the robot to gain the ability to adapt to different scenarios onsite.

B. Training the General Agent

1) *Problem Formulation:* An RL agent learns to obtain an optimal policy π^* that maximized the return G_t (i.e., the summation of the discounted future reward) overtime by interacting with the environment, as shown in the equation (1) [14]:

$$\pi^*(A|S) = \arg \max_{\pi} G_t = \arg \max_{\pi} \sum_{k=t+1}^T \delta^{k-t-1} R_k \quad (1)$$

In (1), A refers to actions. S refers to the observed state of the robot. The common approach to obtain π^* is to maximize a q value function $q(s, a) = E_{\pi}(\delta G_{t+1} + R_{t+1}|S_t = s, A_t = a)$ that refers to the expected reward given the current policy (see equation (2)).

$$q^*(s, a) = \sum_{\bar{s}, r} \pi^*(a|s) T(\bar{s}|s, a) (r + \max_{\bar{a}} q^*(s, \bar{a})) \quad (2)$$

In (2), T is a transition function that maps the current state s and action a to the next state \bar{s} ; r is the reward from the environment at state s . Due to the complexity of updating the q value, modern RL algorithms such as Policy gradient (PG) methods [15] tend to use neural network to approximate the policy function and q value function. In this study, we used Proximal Policy Optimization (PPO) [16] for its stable performance.

2) *General Agent Reward Design:* The general agent aims to learn a fundamental pick-and-place task that normally has two sub-tasks: picking up the target object and placing the target object at a predefined goal placement. For picking, the agent aims to reach the target object within the distance tolerance. After picking up, the target object is attached to the gripper panel by adding a constant force from the target object to the panel. For placing, the agent attempts to place the target object at a predefined goal placement within the distance and angle tolerance.

The reward function design is based on the goals of completing the above sub-tasks. Designing a successful reward function is one of the most important parts in RL [17] as it decides the success of the task completion. In this study, the

reward function R is composed of two parts, including an extrinsic reward R^E and a curiosity-based intrinsic reward R^I [18], shown in Fig. 2.

Algorithm 1: Reward function

```

1 for episode  $e = 1$  to  $N$  do
2   for training step  $t = 1$  to  $MaxStep$  do
      # get intrinsic reward from the agent's exploration#
       $R_{e,t}^I$  = the distance between the next state's predicted feature
      and the ground truth
      # get extrinsic reward from the environment#
       $R_{e,t}^E = -\frac{1}{MaxStep}$ 
      if Grasped then
         $R_{e,t}^E = 1$  (only assigned for the first time)
        if Placed then
           $R_{e,t}^E = 2$ 
          # get total reward#
           $R_{e,t} = R_{e,t}^I + R_{e,t}^E$ 
          End current episode
      else
        continue
    
```

Fig. 2: The reward function design

3) *Curriculum Learning based Training Plan*: To make stable improvements during training, we designed a CL-based training plan for the general agent (see Table I). Table I contains three training criteria: 1) the distance tolerance for reaching the target object τ_{pick} ; 2) the distance tolerance for reaching the goal placement τ_{place} ; 3) the angle tolerance for placing the target object τ_{angle} . Every row in Table I represents a curriculum plan of the agent. The model parameters (i.e., policy function, q value function, and the intrinsic reward function) of the general agent starting from cp2 inherits model parameters resulted from the former curriculum plan.

TABLE I: Curriculum Plan (cp) for the general agent

Training criteria	τ_{pick} (m)	τ_{place} (m)	τ_{angle} (degree)
cp1	0.40	0.50	80.00
cp2	0.30	0.25	60.00
cp3	0.30	0.13	40.00
cp4	0.30	0.10	20.00

C. Testing Generalization of the General Agent on Three Construction Tasks

We tested generalization performance of the general agent on three construction tasks, namely window installation, ceiling installation, and flooring. These three tasks can be seen as a pick-and-place task but are different in the operations of placing the target object. More specifically, for window installation, the window should be placed vertically at the goal placement; for ceiling installation, the ceiling panel should be placed horizontally above the robot; for flooring, the flooring panel should be placed horizontally on the ground. To further test the effectiveness of our training plan, we trained three additional agents for the three tasks without the curriculum plan, as a control group. The control group agents (i.e., controlGroup4.1, controlGroup4.2, and

controlGroup4.3) used the same training criteria as cp4 shown in Table I. We used the cumulative reward and the success rates of picking $\frac{N_{pick}}{N_{episode}}$ and placing $\frac{N_{place}}{N_{episode}}$ as evaluation metrics.

III. RESULTS AND DISCUSSION

In this section, we show the training results of the general agent and the comparison between the general agent and the control group agents.

A. Training Results of the General Agent

The training results of the general agent are shown in Fig. 3. Each line of the same color base refers to the cumulative extrinsic reward over two million action steps. The transparent line around the solid line represents the raw data while the solid line refers to the moving average of the raw data. From Fig. 3, we can see that cp1 and cp2 converged to a reward around 2.5 while the cp3 and cp4 converged to a slightly lower reward of around 2.1. This is because the acceptable placing of the target object for each type of goal placement was similar in cp1 and cp2. However, the acceptable placing became distinct for different goal placement in cp3 and cp4 with smaller angle tolerance. Overall, cp1 to cp4 all approached the upper bounds of the cumulative reward of 3 (i.e., 1 for picking and 2 for placing).

B. Comparison between the General Agent and the Control Group Agents

The cumulative reward results of cp4 and the control group agents are shown in Fig. 4. It can be observed that the final cumulative rewards of all control group agents were lower than that of cp4. This indicates that the training criteria of cp4 might be too difficult for the agents to learn without prior knowledge.

We tested the generalization performance of the general agent by executing the inference of the learned general agent for an additional 50K action steps for each construction task. The success rates of the testing (i.e., cp4) and the control group agents are shown in Table II. It can be seen that the general agent achieved higher success rates in all three tasks. To elaborate, the control group agents have an average picking success rate of around 63%, much lower than the average testing result (89%) of the general agent. For placing, the control group agents have an average success rate of around 1.7%, indicating that the curriculum plan is effective for stable improvement of the training. It can also be observed that the placing success rate (68.04%) for ceiling installation is lower than the other two tasks (84.82% and 85.17%). An important reason is that the motion planning for ceiling installation is more difficult than the other tasks. For instance, the agent is supposed to flip the robot's gripper to place the ceiling panel because the goal placement is above the robot. On the other hand, the agent can simply rotate the base joint to place the floor panel since the initial orientation of the panel remains the same as its goal placement.

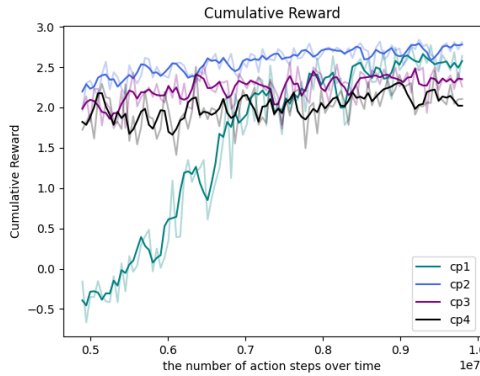


Fig. 3: Cumulative reward over the number of action steps for the general agent

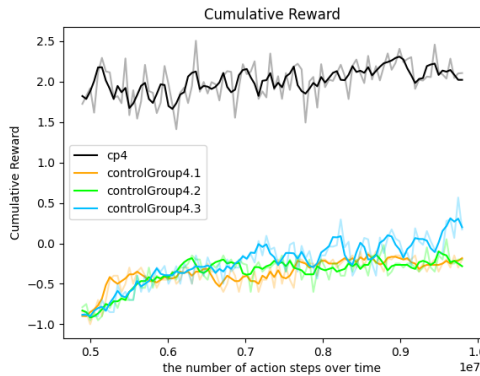


Fig. 4: Cumulative reward over the number of action steps for the cp4 and the control group agents

IV. CONCLUSION

In this study, we explored the generalization performance of the proposed RL based robotic motion planning approach in a virtual construction environment. We first built a realistic virtual construction environment. Then we trained the general agent following a designed curriculum learning based training plan. We showed the generalization performance of the general agent by testing it on three common construction tasks, namely ceiling installation, window installation, and flooring. Finally, we showed the effectiveness of the designed curriculum plan by comparing the results of the control group agents and the general agent. Only three common construction tasks were tested using the approach, but our approach can be easily extended to other construction tasks such as paneling and framing. We also noticed that the generalization performance of the general agent differs among the tested tasks due to the difference of the task difficulties, which is the main limitation of this study. In the future, we intend to design a more flexible algorithm to better distinguish the difference among tasks, since the current RL agent design only captures the similarity among the tasks.

TABLE II: The success rates of cp4 testing and the control group agents

Construction task	Training criteria	$\frac{N_{pick}}{N_{episode}}(\%)$	$\frac{N_{place}}{N_{episode}}(\%)$
Ceiling installation	controlGroup4.1/cp4	63.00/84.55	0.21/68.04
Window installation	controlGroup4.2/cp4	62.89/ 95.32	0.30/84.82
Flooring	controlGroup4.3/cp4	64.72/88.43	4.45/ 85.17

REFERENCES

- [1] J. G. Everett and A. H. Slocum, “Automation and robotics opportunities: construction versus manufacturing,” *Journal of construction engineering and management*, vol. 120, no. 2, pp. 443–452, 1994.
- [2] T. Bock, “The future of construction automation: Technological disruption and the upcoming ubiquity of robotics,” *Automation in construction*, vol. 59, pp. 113–121, 2015.
- [3] K. M. Lundein, V. R. Kamat, C. C. Menassa, and W. McGee, “Autonomous motion planning and task execution in geometrically adaptive robotized construction work,” *Automation in Construction*, vol. 100, pp. 24–45, 2019.
- [4] C. Feng, Y. Xiao, A. Willette, W. McGee, and V. Kamat, “Towards autonomous robotic in-situ assembly on unstructured construction sites using monocular vision,” in *Proceedings of the 31th International Symposium on Automation and Robotics in Construction*, 2014, pp. 163–170.
- [5] N. Kumar, N. Hack, K. Doerfler, A. N. Walzer, G. J. Rey, F. Gramazio, M. D. Kohler, and J. Buchli, “Design, development and experimental assessment of a robotic end-effector for non-standard concrete applications,” in *2017 IEEE International Conference on Robotics and Automation (ICRA)*. IEEE, 2017, pp. 1707–1713.
- [6] K. Iturralde, M. Feucht, R. Hu, W. Pan, M. Schlandt, T. Linner, T. Bock, J. Izard, I. Eskudero, M. Rodriguez, et al., “A cable driven parallel robot with a modular end effector for the installation of curtain wall modules,” in *ISARC. Proceedings of the International Symposium on Automation and Robotics in Construction*, vol. 37. IAARC Publications, 2020, pp. 1472–1479.
- [7] L. E. Kavraki, P. Svestka, J.-C. Latombe, and M. H. Overmars, “Probabilistic roadmaps for path planning in high-dimensional configuration spaces,” *IEEE transactions on Robotics and Automation*, vol. 12, no. 4, pp. 566–580, 1996.
- [8] S. M. LaValle et al., “Rapidly-exploring random trees: A new tool for path planning,” 1998.
- [9] C. Yu and S. Gao, “Reducing collision checking for sampling-based motion planning using graph neural networks,” *Advances in Neural Information Processing Systems*, vol. 34, 2021.
- [10] S. Gu, T. Lillicrap, I. Sutskever, and S. Levine, “Continuous deep q-learning with model-based acceleration,” in *International conference on machine learning*. PMLR, 2016, pp. 2829–2838.
- [11] J. Yosinski, J. Clune, Y. Bengio, and H. Lipson, “How transferable are features in deep neural networks?” *Advances in neural information processing systems*, vol. 27, 2014.
- [12] Y. Bengio, J. Louradour, R. Collobert, and J. Weston, “Curriculum learning,” in *Proceedings of the 26th annual international conference on machine learning*, 2009, pp. 41–48.
- [13] A. Juliani, V.-P. Berges, E. Teng, A. Cohen, J. Harper, C. Elion, C. Goy, Y. Gao, H. Henry, M. Mattar, et al., “Unity: A general platform for intelligent agents,” *arXiv preprint arXiv:1809.02627*, 2018.
- [14] R. S. Sutton and A. G. Barto, *Reinforcement learning: An introduction*. MIT press, 2018.
- [15] R. S. Sutton, D. McAllester, S. Singh, and Y. Mansour, “Policy gradient methods for reinforcement learning with function approximation,” *Advances in neural information processing systems*, vol. 12, 1999.
- [16] J. Schulman, F. Wolski, P. Dhariwal, A. Radford, and O. Klimov, “Proximal policy optimization algorithms,” *arXiv preprint arXiv:1707.06347*, 2017.
- [17] P. Abbeel and A. Y. Ng, “Apprenticeship learning via inverse reinforcement learning,” in *Proceedings of the twenty-first international conference on Machine learning*, 2004, p. 1.
- [18] D. Pathak, P. Agrawal, A. A. Efros, and T. Darrell, “Curiosity-driven exploration by self-supervised prediction,” in *International conference on machine learning*. PMLR, 2017, pp. 2778–2787.

Deep Reinforcement Learning-based Construction Robots Collaboration for Sequential Tasks

Lei Huang¹ and Zhengbo Zou¹

Abstract—The integration of robots into the construction industry shows promise in addressing challenges such as stagnant productivity and low efficiency. Recently, an increasing amount of research develops construction robots based on reinforcement learning (RL). However, most existing RL-based construction robots are trained to conduct specific tasks individually without cooperation. This paper proposes an approach that utilizes two RL-based construction robots (an unmanned ground vehicle and a robot arm) to collaboratively finish the task of window panel transport and installation in sequence without human intervention. Our experiment results show that the two construction robots can successfully collaborate to finish all tasks in an end-to-end manner after they are trained separately with a success rate of 79.6%.

I. INTRODUCTION

The construction industry has reached an output of over \$10 trillion dollars worldwide by the end of 2020 and is expected to continue flourishing [1]. However, the construction industry is prone to poor productivity and low efficiency due to skilled labor shortages and labor-intensive tasks [2]. Moreover, the construction industry has been struggling to provide workers with safe working conditions, as it has the highest rate of fatal accidents accounting for nearly 20% of occupational deaths in the U.S. [3]. The solution of utilizing construction robots to tackle these challenges was first proposed as early as the 1980s [4]. By having robots conduct treacherous and arduous construction tasks, the workers' responsibility shifts from operation to supervision [5], which also reduces the possibility of workers being exposed to dangerous situations.

With the rapid development of reinforcement learning (RL) for generating optimal control policies without hand-crafted designs [6], RL-based construction robots have recently drawn researchers' attention [5]. Existing works focus on training a single construction robot to conduct each task individually, such as installing a ceiling panel [7], assembling a lap joint [8], and placing a wood building block [9]. However, similar to multiple workers are responsible for different tasks as a team on-site, construction robots should also have the capability of working collaboratively. For example, before having a robot arm install a window panel, we could first have an unmanned ground vehicle (UGV)

*We acknowledge the support of the Natural Sciences and Engineering Research Council of Canada (NSERC), [funding reference number: ALLRP 570442-2021]

¹Lei Huang and Zhengbo Zou are with the Department of Civil Engineering, Faculty of Applied Science, University of British Columbia, 6250 Applied Science Lane, Vancouver, BC V6T 1Z4, CANADA
lei.huang@ubc.ca, zhengbo@civil.ubc.ca

transport the window panel to a location within the robot arm's working reach.

As a first attempt to explore multiple construction robots conducting tasks collaboratively, we propose an approach that utilizes a UGV and a robot arm to conduct the task of window panel transportation and installation in collaboration after they are separately trained using RL. During the entire inference process, the UGV and the robot arm deliver the tasks in an end-to-end manner without any human intervention such as handcrafted adjustment or manipulation.

II. RELATED WORK

We can roughly divide construction robots into pre-programmed robots and RL-based robots according to how the control policies are produced [5].

Pre-programmed construction robots conduct tasks following a pre-designed control policy. Specialists design the control policy in detail outlining step-by-step instructions for construction robots. Pre-programmed construction robots are mature enough for practical deployment and have achieved success on-site [10]. For example, [11] used pre-programmed construction robots to bolt steel structures; [12] provided trajectories for robot arms to assemble timber frames. However, the control policies of pre-programmed robots are usually deterministic; hence only adaptable to specific working scenarios that were considered during policy design. Consequently, pre-programmed robots cannot generalize to dynamic environments, and tend to fail once the working condition is changed.

To equip construction robots with adaptability and flexibility, researchers recently start to develop control policies using RL methods [13]. RL-based construction robots actively learn control policies by interacting with environments [14]. During repeated interactions, robots receive different rewards while taking actions under various scenarios (e.g., positions, poses, and surrounding elements). Their objective is to learn control policies such that they maximize the expected total reward. For example, if picking up a window panel will give a robot arm the maximum reward, a properly trained RL-based robot arm should be able to complete the task regardless of the location of the panel, as long as the environment is capable of communicating the current states and the rewards for a specific action. Researchers have trained RL-based construction robots to conduct various tasks. [7] trained a robot arm using an RL method that imitated behaviors from video demonstrations [15] to install ceiling panels. [8] trained a robot arm using a variant of the Deep Deterministic Policy Gradient algorithm (DDPG)

[16] to assemble lap joints for timber frames in simulation and then migrated the control policy to a real robot arm. [9] trained a robot arm using Twin Delayed DDPG [17] to place a building block for assembly. However, these RL-based construction robots [7]–[9] were trained to conduct tasks alone without collaborating or communicating with other robots, which can be problematic when we incorporate multiple robots to achieve a higher level of automation.

To enable construction robots to work collaboratively, we propose a novel RL-based approach that allows a UGV and a robot arm to conduct a sequence of tasks consisting of window panel transportation (by UGV) and installation (by robot arm) in an end-to-end manner without external instructions. Due to the extensive time and resource requirements when training using real robots, we train our robots in simulation following the norm of the existing RL-based construction robots [7]–[9].

III. METHODOLOGY

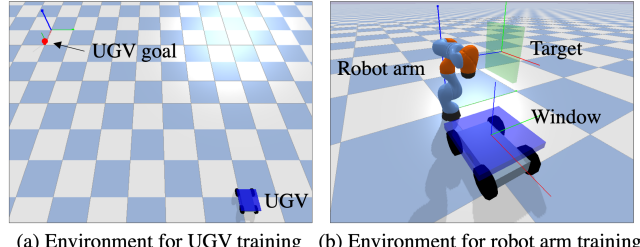
Our approach trains a UGV agent for window panel transportation and a robot arm agent for window installation in two separate RL environments using the proximal policy optimization (PPO) algorithm [18]. We then test these two robots to conduct tasks sequentially in collaboration using control policy inference in a joint environment that contains both the UGV and the robot arm.

A. Building Virtual Environments

The first step is to build two different environments for the UGV and the robot arm in Pybullet [19], which is a physics simulation engine widely used in RL community. As shown in Fig.1(a), the UGV’s environment contains a simplified UGV, a blue transparent window panel on the UGV, and a goal for UGV. The starting point of the UGV is randomly and uniformly distributed in an area away from the goal point, while the goal point is fixed. The observation space has eight dimensions including the position, orientation, and velocity of the UGV, and the position of the goal, all of which are in the X-Y plane. The control policy generates two-dimensional continuous actions to control the steering angle of the front wheels and the driving speed of the four wheels. The objective is for the UGV to navigate towards the goal point such that the mass center of the window panel is as close to the goal point’s coordinates as possible. For the navigation task, we are only concerned about if it arrives within the robot arm’s reach. Thus, we make the environment setting and the reward function concise and straightforward. The reward function for training the UGV agent is as follows:

$$R_t^{UGV} = \begin{cases} 2, & \text{reaching goal} \\ \frac{\Delta d}{C}, & \Delta d > 0 \\ 0, & \text{otherwise,} \end{cases} \quad (1)$$

where R_{UGV} represents the immediate reward, Δd represents the change of distances from the window panel to the goal point between the current timestep and the previous timestep, and C is a scaling factor. Essentially, in the transportation process, a scaled positive reward would be



(a) Environment for UGV training (b) Environment for robot arm training

Fig. 1. Environments for training construction robots

returned only if the window panel was getting closer to the goal; otherwise, no reward (zero) would be returned.

As shown in Fig.1(b), the robot arm’s environment contains a robot arm, a window panel on the UGV, and a green transparent cuboid marking the target where the window is expected to be installed. We use the seven-axis KUKA LBR iiwa robot as the robot arm due to its wide application for RL tasks such as object pick and place and human-robot collaboration [20]. Following general poses on real robot arms, the robot arm is initialized such that the rotations of the fourth joint and the sixth joint are 1.57 radians and -1.57 radians, respectively, and the rest of the joint rotations are all zeros. To ensure the robot arm can conduct the tasks of pickup and installation, the window panel and the target should be both within the range of the robot arm. Considering that the UGV trained in Fig.1(a) might reach the destination with small offsets, we randomize the initial location of the window panel so that the robot arm learns to pick up window panels considering uncertainties of the initial location distributed in an area. The observation space for the RL agent has 21 dimensions, including seven-dimensional joint rotations of the robot arm, seven-dimensional position and orientation of the window, and seven-dimensional position and orientation of the target. The control policy generates seven-dimensional continuous actions to control the rotation increments of the seven joints. The objective of this task is for the robot arm to first pick up the window panel and then move it towards the target opening. We use the distance between the mass center of the window panel and the target for measuring successful installations. The reward function for training the robot arm is as follows:

$$R_t^{Arm} = \begin{cases} 1, & \text{pick} \\ 2, & \text{install} \\ -1, & \text{collision} \\ -\frac{1}{3000}, & \text{otherwise,} \end{cases} \quad (2)$$

where R_{arm} represents the immediate reward. The reward function is designed this way so that the cumulative reward in each trial (a maximum of 3000 timesteps) is always bounded between -2 and 3.

B. Training Construction Robots

After building the virtual environments, we train the UGV for navigation and the robot arm for window panel pickup and installation using policy gradient algorithms, which are

Algorithm 1 Vanilla Policy Gradient Algorithm

- 1: Initialize policy and value function parameters θ_0, ϕ_0 .
 - 2: **for** $k = 0, 1, 2, \dots$ **do**
 - 3: Collect $\mathcal{D}_k = \{\tau_i\}$ by running $\pi_k = \pi(\theta_k)$.
 - 4: Compute rewards-to-go \hat{R}_t .
 - 5: Compute advantage estimates \hat{A}_t based on V_{ϕ_k} .
 - 6: Estimate policy gradient as
$$\hat{g}_k = \frac{1}{|\mathcal{D}_k|} \sum_{\tau \in \mathcal{D}_k} \sum_{t=0}^T \nabla_{\theta} \log \pi_{\theta}(a_t | s_t) |_{\theta_k} \hat{A}_t.$$
 - 7: Compute policy update, $\theta_{k+1} = \theta_k + \alpha_k \hat{g}_k$.
$$\theta_{k+1} = \theta_k + \alpha_k \hat{g}_k.$$
 - 8: Fit value function:
$$\phi_{k+1} = \arg \min_{\phi} \frac{1}{|\mathcal{D}_k| T} \sum_{\tau \in \mathcal{D}_k} \sum_{t=0}^T (V_{\phi}(s_t) - \hat{R}_t)^2.$$
-
- 9: **end for**
-

suitable for continuous control of RL agents deployed on robots [14]. Policy gradient methods use parameterized functions such as neural networks to model control policies π . The policy functions are optimized using gradient ascent so as to generate actions (a) that maximize cumulative rewards for agents.

Algorithm 1 shows the process of how a general policy gradient algorithm works in detail. First, we collect a set of trajectories \mathcal{D}_k by having the agent interact with the environment using the current control policy π_k . For each trajectory, we compute the rewards-to-go. We then compute the advantage estimations based on the current value function V_{ϕ_k} . After calculating the policy gradients based on the objective function, we update the control policy using gradient ascent methods such as Adam [21]. Lastly, we fit the value function by regression on mean-squared error via gradient descent. This process is repeated until convergence.

The vanilla policy gradient algorithm's performance is susceptible to collapse since it does not constrain how much the new control policy deviates from the previous policy. To avoid this limitation, we specifically adopt PPO-Clip [18], which constrains the gradients. Meanwhile, compared to other policy gradient algorithms that tackle the gradient issue such as trust region policy optimization (TRPO) [22], PPO is more widely used for its easier implementation and tuning. PPO is similar to the vanilla policy gradient algorithm except for the objective function. PPO's objective function [18] is as follows:

$$L = \min \left(\frac{\pi_{\theta}(a|s)}{\pi_{\theta_k}(a|s)} A^{\pi_{\theta_k}}(s, a), g(\epsilon, A^{\pi_{\theta_k}}(s, a)) \right), \quad (3)$$

where

$$g(\epsilon, A) = \begin{cases} (1 + \epsilon)A & A \geq 0 \\ (1 - \epsilon)A & A < 0 \end{cases}.$$

Instead of using KL-divergence or other constraint terms,

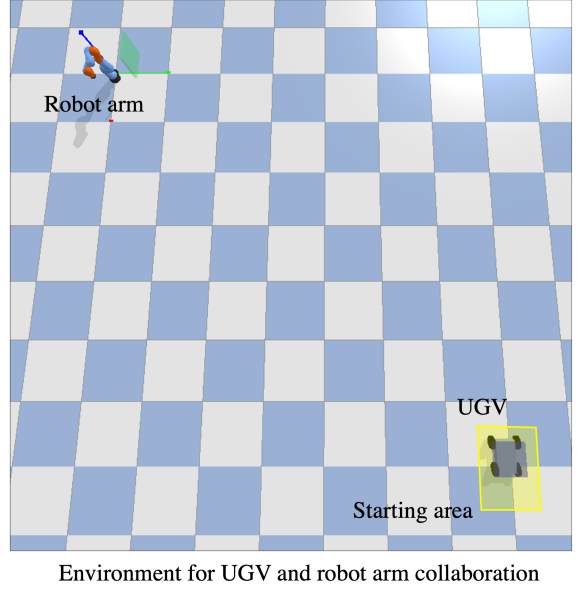


Fig. 2. The environment for testing robot collaboration

PPO-Clip achieves the constraint by clipping in the objective function.

C. Collaborating Using Inference

After training the UGV and the robot arm in their respective environments using PPO-Clip, we build a third environment (the collaboration environment, as shown in Fig.2) for robot collaboration as testing. The collaboration environment accommodates the trained UGV and robot arm, the window panel, and the non collidable marker used as the robot arm's target. Without any human intervention, a successful collaboration between the two robots would require that the UGV has to navigate to the area around the goal point first; only then will the robot arm start operating for window panel pickup and installation.

IV. EXPERIMENTS AND RESULTS

To validate our approach, we tested the trained UGV and the robot arm in the collaboration environment by inference from their learned control policies. In the experiment, we randomized the starting point of the UGV in the yellow area as shown in Fig.2. We conducted experiments repeatedly for 10 times, each of which we ran 100 trials and counted the number of successful attempts to arrive, pick, and install.

TABLE I presents the experiment result. Out of 1000 trials, the success rate of the UGV arriving in the designated area is 97.5%; the success rate of the robot arm picking up the window panel is 94.8%, and the success rate of the robot arm installing the window panel is 79.6%. Given that the UGV has arrived in the area, the success rate of the robot arm picking up the window panel is 97.2%; and the success rate of the robot arm installing the window panel is 81.6%. Given that the UGV has arrived, and the robot arm has picked up the window panel, the success rate of the robot arm installing the window panel is 84.0%.

TABLE I

NUMBERS OF SUCCESSFUL ARRIVALS, PICKUPS, AND INSTALLATIONS.

Group Index	Trial	Arrive	Pick	Install
1	100	98	93	78
2	100	97	95	79
3	100	98	95	79
4	100	96	92	80
5	100	97	95	82
6	100	97	94	75
7	100	100	97	79
8	100	98	96	85
9	100	97	95	80
10	100	97	96	79
Total	1000	975	948	796

V. CONCLUSIONS AND DISCUSSIONS

In this paper, we proposed an approach aiming to have a UGV and a robot arm conduct a sequence of tasks (i.e., window transportation and installation) in collaboration after training two RL agents separately in two different environment settings. Results showed that the trained robots could successfully finish the sequence of tasks with considerable success rates. In the construction industry, most tasks are carried out in sequence and are usually connected to each other. Studying how construction robots can partition the tasks and work collaboratively is crucial to achieving a higher level of automation in construction. Our approach makes a first attempt to have multiple robots trained using RL to carry out construction tasks in collaboration. For future work, we will explore simultaneously training multiple construction robots for working in collaboration and migrate the control policies to real construction robots.

REFERENCES

- [1] G. Robinson, J. Leonard, and T. Whittington, “Oxford economics: Future of construction a global forecast for construction to 2030,” sep 2021.
- [2] H. Karimi, T. R. Taylor, G. B. Dadi, P. M. Goodrum, and C. Srinivasan, “Impact of skilled labor availability on construction project cost performance,” *Journal of Construction Engineering and Management*, vol. 144, no. 7, p. 04018057, 2018.
- [3] OSHA, “Occupational safety and health administration, united states department of labor: Commonly used statistics,” 2019.
- [4] C. Haas, M. Skibniewski, and E. Budny, “Robotics in civil engineering,” *Computer-Aided Civil and Infrastructure Engineering*, vol. 10, no. 5, pp. 371–381, 1995.
- [5] C.-J. Liang, X. Wang, V. R. Kamat, and C. C. Menassa, “Human-robot collaboration in construction: Classification and research trends,” *Journal of Construction Engineering and Management*, vol. 147, no. 10, p. 03121006, 2021.
- [6] B. Eysenbach, R. R. Salakhutdinov, and S. Levine, “Robust predictable control,” in *Advances in Neural Information Processing Systems*, 2021.
- [7] C.-J. Liang, V. R. Kamat, and C. C. Menassa, “Teaching robots to perform quasi-repetitive construction tasks through human demonstration,” *Automation in Construction*, vol. 120, p. 103370, 2020.
- [8] A. A. Apolinarska, M. Pacher, H. Li, N. Cote, R. Pastrana, F. Gramazio, and M. Kohler, “Robotic assembly of timber joints using reinforcement learning,” *Automation in Construction*, vol. 125, p. 103569, 2021.
- [9] B. Belousov, B. Wibranek, J. Schneider, T. Schneider, G. Chalvatzaki, J. Peters, and O. Tessmann, “Robotic architectural assembly with tactile skills: Simulation and optimization,” *Automation in Construction*, vol. 133, p. 104006, 2022.
- [10] T. Salmi, J. M. Ahola, T. Heikkilä, P. Kilpeläinen, and T. Malm, “Human-robot collaboration and sensor-based robots in industrial applications and construction,” in *Robotic building*. Springer, 2018, pp. 25–52.
- [11] B. Chu, K. Jung, M.-T. Lim, and D. Hong, “Robot-based construction automation: An application to steel beam assembly (part i),” *Automation in construction*, vol. 32, pp. 46–61, 2013.
- [12] K. Iturralde and T. Bock, “Integrated, automated and robotic process for building upgrading with prefabricated modules,” in *ISARC. Proceedings of the International Symposium on Automation and Robotics in Construction*, vol. 35. IAARC Publications, 2018, pp. 1–8.
- [13] X. Xu and G. B. De Soto, “On-site autonomous construction robots: A review of research areas, technologies, and suggestions for advancement,” in *37th International Symposium on Automation and Robotics in Construction: From Demonstration to Practical Use-To New Stage of Construction Robot, ISARC 2020*. International Association on Automation and Robotics in Construction (IAARC), 2020, pp. 385–392.
- [14] R. S. Sutton and A. G. Barto, *Reinforcement learning: An introduction*, 2nd ed. MIT press, 2018.
- [15] Y. Liu, A. Gupta, P. Abbeel, and S. Levine, “Imitation from observation: Learning to imitate behaviors from raw video via context translation,” in *2018 IEEE International Conference on Robotics and Automation (ICRA)*. IEEE, 2018, pp. 1118–1125.
- [16] D. Horgan, J. Quan, D. Budden, G. Barth-Maron, M. Hessel, H. van Hasselt, and D. Silver, “Distributed prioritized experience replay,” in *International Conference on Learning Representations*, 2018. [Online]. Available: <https://openreview.net/forum?id=H1Dy—0Z>
- [17] S. Fujimoto, H. Hoof, and D. Meger, “Addressing function approximation error in actor-critic methods,” in *International conference on machine learning*. PMLR, 2018, pp. 1587–1596.
- [18] J. Schulman, F. Wolski, P. Dhariwal, A. Radford, and O. Klimov, “Proximal policy optimization algorithms,” *arXiv preprint arXiv:1707.06347*, 2017.
- [19] E. Coumans and Y. Bai, “Pybullet, a python module for physics simulation for games, robotics and machine learning,” <http://pybullet.org>, 2016–2021.
- [20] O. Kyjanek, B. Al Bahar, L. Vasey, B. Wannemacher, and A. Menges, “Implementation of an augmented reality ar workflow for human robot collaboration in timber prefabrication,” in *Proceedings of the 36th international symposium on automation and robotics in construction (ISARC)*. International Association for Automation and Robotics in Construction (IAARC), 2019, pp. 1223–1230.
- [21] D. P. Kingma and J. Ba, “Adam: A method for stochastic optimization,” in *International Conference on Learning Representations*, 2015. [Online]. Available: <https://arxiv.org/abs/1412.6980>
- [22] J. Schulman, S. Levine, P. Abbeel, M. Jordan, and P. Moritz, “Trust region policy optimization,” in *Proceedings of the 32nd International Conference on Machine Learning*, ser. Proceedings of Machine Learning Research, F. Bach and D. Blei, Eds., vol. 37. Lille, France: PMLR, 07–09 Jul 2015, pp. 1889–1897. [Online]. Available: <https://proceedings.mlr.press/v37/schulman15.html>

Towards a Collaborative Future in Construction Robotics: A Human-centered Study in a Multi-user Immersive Operation and Communication System for Excavation

Di Liu, Youngjib Ham, Jeonghee Kim, Hangue Park

Abstract — When operating a construction robot, i.e., an excavator, the excavator operator's unsafe behavior directly affects the underground utility damage occurrence during excavation process. Operator's behavior is greatly affected by the environment and further the communication with other coworkers, i.e., spotter. In this paper, we propose a multi-user immersive operation and communication system for excavation. Further, we investigate how the different types of environments and operator-spotter communication channels affect operator's attention demand and performance during excavation.

I. INTRODUCTION

The damage to utility lines in excavation is one of the most significant crises for contractors and creates great economic and societal loss especially in dense urban areas having the congested underground utility lines [1, 2, 3-5]. Unfortunately, current practices and damage prevention systems are insufficient to prevent these accidents [2,4-5,8-10, 11], and excavator operators heavily rely on their own judgement to avoid utility line damages [6,7]. In fact, in the safety guidelines recommended by CGA Best Practice and some state code [11, 12], once the excavation starts, working with a spotter is a key step to prevent damages and enhance the safety of excavation, and excavation tasks are performed as a teamwork most of the time. When an operator controls an excavator and interacts with a spotter at the same time, the operator often experiences cognitive overload, and unsafe behaviors and accidents are more likely to occur. In this regard, studying the operator-spotter interaction is crucial to ensure the safe human-excavator collaboration in construction tasks, especially with utility lines buried in a challenging environment (e.g., urban jobsite).

To better train operators for preventing the accidents in the real jobsite, excavation simulators are commonly used for task practicing and studying the human factors. The typical excavation simulator in the current market is composed by joysticks and pedals, monitor-based display, and available for a single user to practice the basic excavator operation. Despite the advanced development of technologies, majority of excavation simulator provide an acceptable but less immersive simulation environment. Furthermore, collaborative excavation which has multiple users involved has not been included in the simulator design.

In this study, we develop and evaluate an immersive multi-user simulation system for excavator operation and investigate the operator-spotter communication under different environments. Specifically, we focus on how the types of environments and the operator-spotter communication formats affect operator's attention demand and performance during excavation. The main contributions of the proposed multi-user immersive system are:

- to allow more than one construction workers, i.e., operator and spotter, collaborate with construction robot(s), i.e., excavator, in a high level of immersion
- to assess the human performance in a collaborative human-robot-interaction workplace as needed.

II. SYSTEM DESIGN

A multi-user immersive operation and communication system is composed of two parts, a virtual human excavator interaction platform (Fig. 1), and an immersive multi-user communication system (Fig. 2), which are supported by a set of hardware and software.

A. Virtual Human-Robot Interaction Platform

- Hardware system

The primary goal of the hardware design is to serve as the physical excavator simulator. As the main part of this VR-based platform, HTC Vive Pro Eye is the VR headset being functional as the user display with a resolution of 1440 x 1600 per eye. The embedded eye tracking feature enables eye data collection during the experiment. The realistic excavator joysticks that had a USB connection that could be plugged directly into the PC were selected for this simulator. Due to compatibility issues with the external controller and the Unity software, a software called JoyToKey is selected to emulate the joystick movements as keystrokes. By doing so, we were able to tie the joystick movements to key presses and set these key press inputs as the inputs in Unity model. One of the most common control patterns, ISO control pattern, is utilized in this system. The realistic excavator pedals interfaced with a fabricated printed circuit board (PCB) and Arduino UNO. The analog signals provided by the pedal were sent to two analog pins located on the Arduino UNO. These signals were able to be read by Unity by using a Unity Asset called Uduino. Uduino

*Research supported by the National Science Foundation.

Di Liu is the Ph.D. student, Department of Construction Science, Texas A&M University, College Station, TX 77840 USA (e-mail: catsquito@tamu.edu).

Youngjib Ham, Associate Professor, Department of Construction Science, Texas A&M University, College Station, TX 77840 USA (corresponding author to provide phone: 979-458-0184; e-mail: yham@tamu.edu).

Jeonghee Kim, Assistant Professor, Department of Engineering Technology & Industrial Distribution and Electrical & Computer Engineering, Texas A&M University, College Station, TX 77840 USA (e-mail: jeonghee.kim@tamu.edu).

Hangue Park, Assistant Professor, Department of Electrical & Computer Engineering, Texas A&M University, College Station, TX 77840 USA (e-mail: hpark@ece.tamu.edu).

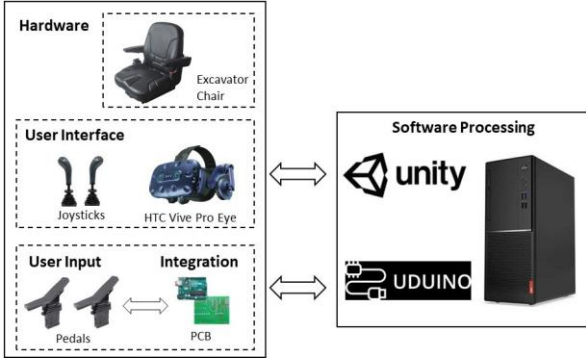


Figure 1. Virtual Human Robot Interaction Platform.

is an asset that helps simplify the communication between the Arduino UNO and Unity software. Uduino can read and write analog and digital signals through C# scripts written in Unity, rather than through the Arduino IDE. Besides the above components, a set of mechanical assembly made by plywood enclosure is built to place the excavator chair, joysticks, and pedals.

- Software system

The excavator simulation is created completely on the Unity3D Game Engine. In addition, to properly stream the simulation to the VR headset with Unity and other external controller inputs, SteamVR is used. A Lenovo ThinkStationP620 is the computer environment of the software system and connected to the VR headset, joysticks, and PCB.

B. Immersive Multi-User Communication Environment

The immersive multi-user communication environment allows a real-person operator (a participant), a real-person spotter, and the excavator simulator to work together. The real-person operator wearing an HTC Vive Pro Eye headset which has an eye tracker and a headphone embedded performs a set of excavation tasks. The real-person spotter wore a Logitech H390 microphone to communicate with the operator and held two Vive controllers to track hand gestures in real time. When the operator was performing the task, the spotter kept monitoring the virtual excavation process and virtual environment from multiple view directions displayed by two 24 inches monitors. The VR headset, microphone, and excavator simulator are connected to a Lenovo ThinkStationP620.

In terms of excavation task, Unity3D is the main platform for modeling and visualization. A roadwork scenario was simulated as the baseline environment, and a downtown scenario is simulated as the challenging environment. Both scenarios include visual and auditory urban elements. An excavation job site area were modeled and a virtual excavator was placed in the center. Underground utility lines were placed in front of the excavator and hidden from the operator's view direction which provides a close-to-real excavation experience. A Collision Detection script recorded the excavator-utility collision automatically. Moreover, a virtual operator and a virtual spotter were simulated in the same scenarios. The virtual operator was represented by a virtual camera located inside of the virtual excavator cabinet. The real-person operator could constantly see the scenario from a

First-Person Point-of-View through VR headset display which showed the view of virtual camera. A virtual avatar representing the spotter stand in front of the virtual camera and can be seen by the operator. To mimic the real-life work, the avatar was model with a construction worker's appearance. The avatar's arm gestures were controlled by the real-person spotter's arm movements via two controllers. Two audio converting scripts were used to enable the real-time verbal communication between operator and spotter. The buried utility lines were set to be visible to the real-person spotter so that the spotter could guide the operator to avoid hitting the utility lines.

Multiple experiments were conducted. Excavation tasks with multiple view perspectives and different sound were recorded by OBS screen recording software. Operator's gaze information was collected through Vive eye tracking SDK and iMotions software. A log file recorded collision numbers and other system information.

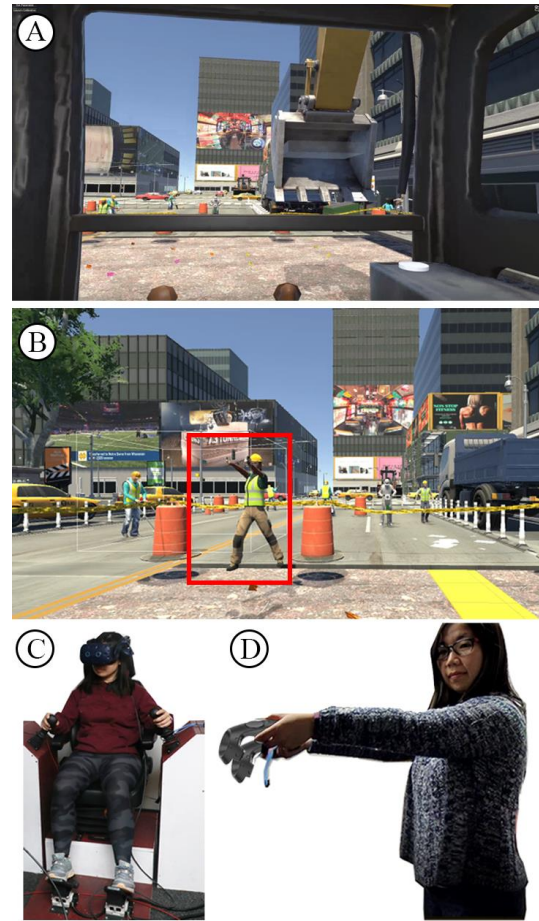


Figure 2. Immersive Multi-User Communication Environment:
 (A) Operator's view (B) Spotter's avatar (C) Real-person operator (D) Real-person Spotter

III. EXPERIMENT

We conducted a small group of user study by using the designed system prototype to examine three types of operator-spotters communication formats (hand signals, verbal signals, a mixture of hand-verbal signals), and two types of environmental conditions (baseline, challenging environment) on the tested subjects. A total of six participants were divided

into three groups based on hand signals, verbal signals, and a mixture of hand-verbal signals. Each subject repeatedly performed four trials of excavation tasks (three loads of soil per trial) in both baseline and challenging environments. To ensure the job completion quality, the tasks were monitored by the spotter. Dependent variables are defined as task-oriented performance variables including collision numbers (COLLI) and missed-signal rates (SGMR), as well as several cognitive responses variables including attention demand.

A. Experiment Procedures

On the experiment day, a total of six experimental sessions were conducted by each participant upon the completion (Fig. 3). In Session 1, participants were acknowledged by the consent form and given an introduction of the research. Participants completed a background questionnaire. Session 2 provided basic knowledge of operating an excavator. In Session 3, a 20-min practice in VR is provided. In Sessions 4, 5, 7, 8, participants were asked to perform tasks of excavating three loads of soil by following spotter's signals, as well as avoiding the collision with buried utility lines. In Session 6, a 5-min break is provided after Session 5. To counterbalance the learning effect, Sessions 4 and 8 are conducted in the baseline environment and Sessions 5 and 7 are in the challenging environment. In Session 9, participants were asked to complete post-experiment questionnaires.

B. Human Factor Measurements

Four types of measurements including performance, attention demand, mental workload, and awareness are assessed in the experiments. The number of collisions is recorded in a log file. Missed signals are counted from screen recording after the experiments. Participants' Signal Missing Rate (SGMR) per trial is calculated as below:

$\text{SGMR} = \frac{\text{the number of signals}}{\text{a total number of signals}} / \text{from spotter}$

Operator's attention demand is assessed by dynamic attention intensity and attention spatial density generated from eye tracking data.

Besides the instrument-based measurements, a set of subjective evaluation are collected, including NASA Task Load Index (NASA-TLX) to assess mental workload, 10-D SART Scale to evaluate the situation awareness, a 5-item environmental distraction questionnaire to evaluate the perceived distraction by different environmental elements, and

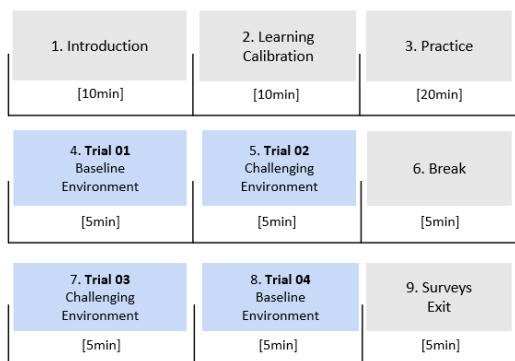


Figure 3. Experiment Procedure

a W&S presence questionnaire to access the sense of presence of the VR environment.

IV. RESULTS AND DISCUSSION

A. Performance Results (SGMR, COLLI)

Fig. 4 shows the results of signal-missing-rate (SGMR) and collision number (COLLI) of all subjects of two environments (B – baseline, C – challenging environment). For each subject, SGMR in challenging environment shows a higher value than SGMR in baseline environment. The average SGMR in challenging environment is 14.37%, which is higher than the average SGMR in baseline environment (3.77%). The results of SGMR indicate that all participants missed more signals from spotter when they performed the task in the challenging environment than they did in the baseline environment. Among different signal formats, a higher SGMR is occurred in the verbal signal group. In terms of collision number, Fig. 4 shows that, among all participants, COLLI in the challenging environment, with an average of 2.5, is higher than in the baseline environment in which the average COLLIS is 1. This result indicates that the operator tends to make more collisions in the challenging environment than in the baseline environment. Regarding the completion time of tasks, it was observed that participants completed the tasks faster in the baseline environment with verbal communication with spotter.

B. Attention Intensity and Attention Spatial Density

Fig. 5 shows the distribution of attention intensity. Visualizing attention intensity (heatmap) is commonly based on static 2D display on which the user has a static field of view. In an immersive VR environment, as the operator changes the view direction constantly and intuitively, i.e., look around by moving head positions, rotate the virtual excavator cabinet, it is necessary to categorize the dynamic view fields for analyzing attention demands. Therefore, operator's views are categorized into three classes: Trenching (TR), Rotating (RO), Dumping (DU). When performing task of each load, a static

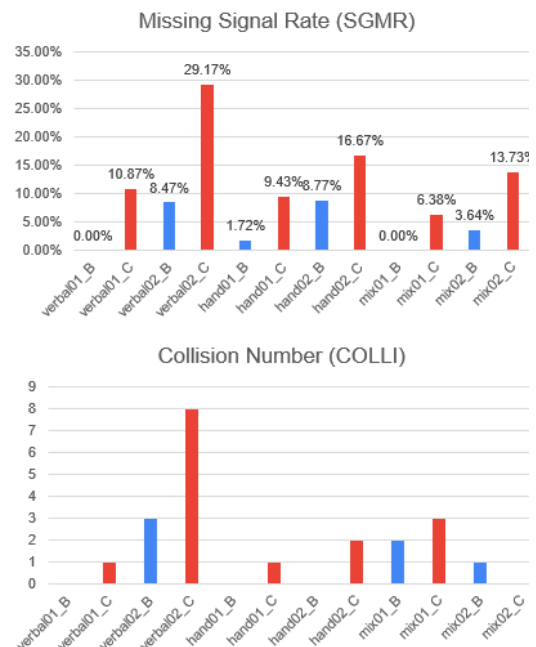


Figure 4. Performance Results



Figure 5. Dynamic Attention Intensity : (a) Attention heatmap in trial 1 (b) Attention heatmap in trial 2

scene with a short time interval for each view class is abstracted, the attention intensity of each static frame per load is rendered into a heatmap (Fig. 5). Fig.5 shows that in the challenging environment, a wider distributed attention is achieved than in the baseline environment. Fig. 6 shows that there is a higher fixation spatial density in challenging environments than in the baseline environment. These results indicate that in a challenging environment, the operator is more distracted than in the baseline environment, which strengthened the likelihood of accidents.



Figure 6. Attention spatial density : (a) Attention spatial density in trial 1 (b) Attention spatial density in trial 2

V. CONCLUSION

We proposed a multi-user immersive operation and communication system for excavation, and investigated how environment types and operator-spotters communication formats affect operator's performance and attention demand during human-excavator collaboration. In the user study, we found that in challenging environments, the operator tends to make more collisions and miss more signals from the spotters. Also, operator tends to have a wider distributed attention in the challenging environment. In the future work, we will conduct larger user studies and will analyze eye tracking and subjective evaluation results in a quantitative manner.

ACKNOWLEDGMENT

This work is supported by the National Science Foundation (NSF) under Grant No.2026574. Any opinions, findings, and conclusions or recommendations expressed in this material are those of the author(s) and do not necessarily reflect the views of the National Science Foundation.

REFERENCES

- [1] S.N. Naghshbandi, L. Varga, Y. Hu, Technologies for safe and resilient earthmoving operations: A systematic literature review, *Automation in Construction*. 125 (2021) 103632. <https://doi.org/10.1016/j.autcon.2021.103632>.
- [2] S. Talmaki, V.R. Kamat, H. Cai, Geometric modeling of geospatial data for visualization-assisted excavation, *Advanced Engineering Informatics*. 27 (2013) 283–298. <https://doi.org/10.1016/j.aei.2013.01.004>.
- [3] T. Çelik, S. Kamali, Y. Arayici, Social cost in construction projects, *Environmental Impact Assessment Review*. 64 (2017) 77–86. <https://doi.org/10.1016/j.eiar.2017.03.001>.
- [4] H. Jeong, C. Arboleda, D. Abraham, *Imaging and Locating Buried Utilities*, Purdue University, West Lafayette, IN, 2003. <https://doi.org/10.5703/1288284313237>.
- [5] S.A. Talmaki, S. Dong, V.R. Kamat, Geospatial Databases and Augmented Reality Visualization for Improving Safety in Urban Excavation Operations, (2012) 91–101. [https://doi.org/10.1061/41109\(373\)10](https://doi.org/10.1061/41109(373)10).
- [6] A.J. Al-Bayati, L. Panzer, Reducing Damage to Underground Utilities: Lessons Learned from Damage Data and Excavators in North Carolina, *Journal of Construction Engineering and Management*. 145 (2019) 04019078. [https://doi.org/10.1061/\(ASCE\)CO.1943-7862.0001724](https://doi.org/10.1061/(ASCE)CO.1943-7862.0001724).
- [7] DIRT Report, (n.d.). <https://commongroundalliance.com> (accessed April 12, 2022).
- [8] S. Li, H. Cai, V.R. Kamat, Uncertainty-aware geospatial system for mapping and visualizing underground utilities, *Automation in Construction*. 53 (2015) 105–119. <https://doi.org/10.1016/j.autcon.2015.03.011>.
- [9] X. Su, S. Talmaki, H. Cai, V.R. Kamat, Uncertainty-aware visualization and proximity monitoring in urban excavation: a geospatial augmented reality approach, *Vis. in Eng.* 1 (2013) 2. <https://doi.org/10.1186/2213-7459-1-2>.
- [10] S. Talmaki, V.R. Kamat, Real-Time Hybrid Virtuality for Prevention of Excavation Related Utility Strikes, *J. Comput. Civ. Eng.* 28 (2014) 04014001. [https://doi.org/10.1061/\(ASCE\)CP.1943-5487.0000269](https://doi.org/10.1061/(ASCE)CP.1943-5487.0000269).
- [11] CGA Best Practices Version 18.0, (n.d.). <https://bestpractices.commongroundalliance.com/> (accessed April 12, 2022).
- [12] Ohio Revised Code – OHIO811 | Call 811 Before You Dig | OHIO811, (n.d.). <https://www.oups.org/law/> (accessed April 12, 2022).

The effect of challenging work environment on human-robot interaction and cognitive load during teleoperation: a case study of teleoperated excavator in a virtual experiment*

Jin Sol Lee, and Youngjib Ham

Abstract— Construction sites typically involve a risky, dynamic, and challenging work environment. Despite numerous safety training programs and regulations, accidents still occur in construction sites, especially when working with construction robotics. To alleviate this problem in the most fundamental way, teleoperation that allows operators to work remotely has been studied. Teleoperated construction robots have the great potential to be used in various contexts for extreme and hazardous construction sites. Here, work conditions for human-robot interaction in construction differ from those in other structured and controlled environments like manufacturing factories, and thus there is a need for the associated studies. In this paper, we aim to measure and analyze the performance of human-robot interaction and the cognitive load of human operators in dynamic and challenging construction work environments (hazardous risks such as underground utility strikes and working under time constraints).

I. INTRODUCTION

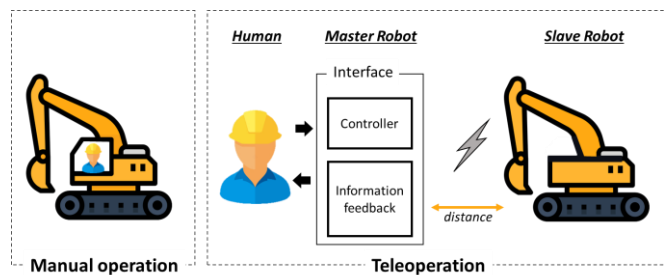
The construction site is known as a dynamic and challenging environment. Especially, construction excavation task has a high probability of fatal injuries and damages in the event of an accident [1]. Especially if a utility strike occurs during excavation, not only is damage and cost increased, but also the supply of water, gas, electricity, and commutation cable that is vital to people's everyday lives is negatively affected [1]. Despite the significance, it is not trivial to avoid these on construction sites. Providing a safe work environment for earthwork while reducing accidents is essential.

There has been increasing interest in automation in hazardous construction workplaces. Even with the most advanced technologies, achieving full autonomy for construction tasks still requires a great deal more research and development due to the extremely dynamic, complicated, and uncertain nature of construction jobs, as compared to manufacturing [2]. As a result, teleoperated construction robots have been studied in various contexts and become a promising solution for extreme and hazardous construction sites [3]. Teleoperation means operating a slave robot via a master robot by a human operator from a distance as illustrated in Fig. 1 [2]. Since the human operator cooperates with the robot system as a commander and takes advantage of human-

robot interactions, it has a wide range of capabilities and potential as a robotic application for construction tasks such as excavation [2].

Compared to a controlled and structured work environment (e.g., manufacturing), teleoperation in construction is typically obscured by open and changing environments [2]. These include dynamic flows of construction tasks, various work types, and different work and site conditions such as weather, soil conditions, and construction equipment that vary from site to site. Manually operating a construction robot by onboarding enables the human operator to directly sense and respond to the environment in which the robot is situated, whereas remotely operating a robot requires information feedback and awareness of the distanced situation via an interface, which can be a demanding job for the operators as illustrated in Fig. 1 [1]. In this regard, there is a need to carefully examine how the human operator's cognitive load and performance could be affected by challenging environments of construction sites in terms of human-robot interaction. This paper aims to investigate how the challenging work environments (e.g., hazardous risks such as underground utility strikes and work under time pressure) affect human-robot interaction during teleoperation situations in construction.

Figure 1. Teleoperation and human-robot interaction



This paper is organized as follows. In Section II, we look at relevant prior studies regarding human-robot interaction in challenging work environments in the construction domain and other disciplines. Section III and IV show the process and the results of the virtual experiments to explore the effect of the challenging work environment on human-robot interaction

*Research supported by National Science Foundation.

Jin Sol Lee is a Ph.D. student in the Department of Construction Science, Texas A&M University, College Station, TX 77843-3137 USA (e-mail: jinsollee@tamu.edu).

Youngjib Ham is a history maker home endowed associate professor in the Department of Construction Science and a director of smart construction, smart city, and smart building research lab, Texas A&M University, College Station, TX 77843-3137 USA (corresponding author; phone: 979-458-0184; e-mail: yham@tamu.edu).

in construction. In Section V, we summarized the preliminary outcomes of the proposed studies and discuss the possibilities and the impact of our work.

II. LITERATURE REVIEW

A. Theoretical background

According to the Adaptive Decision Maker theory, human decision behavior is determined by an individual considering various task conditions or environments [4]. In other words, even if the same person performs the same task, the final decision or behavior may change if the task condition or environment is different. Decision-makers try to balance their effort with the accuracy of performance by considering multiple task constraints [5]. Depending on the level of difficulty of these task conditions, stress or cognitive load increases when people perform a task, which affects the decision and performance in the course of the task. However, an increase in stress or cognitive load does not necessarily imply a decrease in performance or decision quality. According to the Yerkes-Dodson Law, task performance is an inverted U-shaped function of attention [6]. In other words, the performance level may increase as the arousal level go up, and it drops after reaching the fatigue point. Thus, in order to achieve the most optimal human performance and minimize the risk of injury and task failure during excavation, the operator's attention needs to be managed within a certain range in a challenging environment.

B. Task performance under time pressure

Time pressure is one of the major stresses that affect decision-making, behavior, and task performance [7], and make the work environment more challenging. There have been studies regarding time pressure in various disciplines such as the automotive and aviation industry to understand the performance and cognitive load of drivers and pilots. Time pressure may cause excessive stress, productivity demands, negative emotional reactions, anger, and aggressive performance [8], [9]. This would lead to risk-taking behaviors or decisions to achieve goals in time, just like a driver may not be able to pay close attention to their surroundings and neglect safety when speeding [8]. In contrast, when the appropriate amount of time pressure is applied, it can enable an individual to work optimally, as well as have positive emotions, and increase job satisfaction [10]. Time pressure has become a routine phenomenon in construction by site managers or clients or by unexpected risks such as weather. There have been studies on time pressure in the construction industry. Under time pressure, some researchers looked at the electrical line workers' risk-taking behavior and cognitive demand [11], and others conducted experiments in a virtual reality environment to find how time pressure affects the hazard recognition, analysis, and decision making of construction site workers [5].

Since operators play a significant role in efficient construction robot manipulation [12], our study examines how time pressure affects human-robot interaction performance and cognitive load in teleoperation when conducting hazardous construction tasks and how these factors correlate with each other.

III. METHODOLOGY

Experimental tasks in this study were designed to understand how human-robot interaction performance and operator's cognitive load change in a dangerous work environment depending on the level of time pressure.

A. Environment design and apparatus

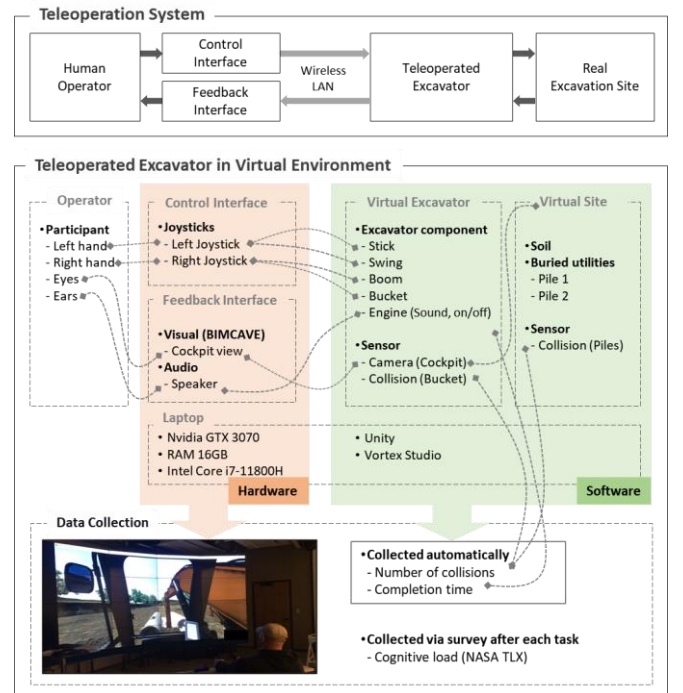
The site scenario in the virtual environment was built upon the site visit of actual construction sites and advice from excavation experts (Fig. 2).

Figure 2. Virtual site scene setup



We developed a challenging site scenario that requires participants to dig the soil delicately while avoiding two hazardous buried utilities. In the experiment, participants manipulated the excavator with two joysticks, the control interfaces of the excavator, while observing the movement of the excavator and the surrounding situation in the computer aided virtual environment (CAVE). During the experiment, performance data of operators were automatically collected (Fig. 3).

Figure 3. Human-robot interaction in a virtual environment



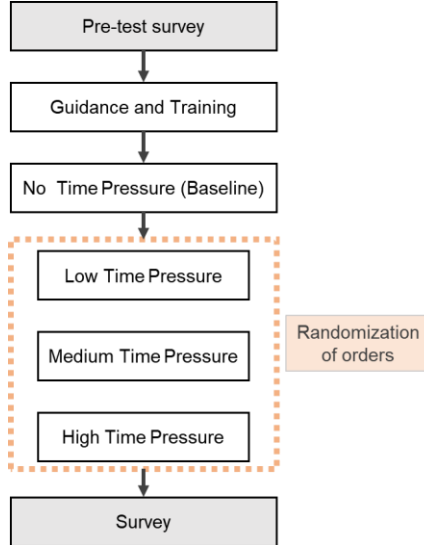
B. Experiment

- Task description

In the experimental task, we had participants excavate the soil between two utility lines and dump the soil by swinging the excavator body to the left, repeating a total of 5 times. Each time the soils were dug, participants were asked to fill the bucket with soil as much as possible in the 'Guidance and Training' session. Graduate students majoring in architecture and construction engineering participated in the pilot experiments.

- Procedure

Figure 4. Procedure of experiment



Step 1. Pre-test questionnaires (gender, age, 3D game experience, and work experience in the AEC industry) were provided to the participant before the virtual experiment begin.

Step 2. Guidance and training session. Participants were trained not to hit the utilities during their task. Basic excavator control such as arm out/in, swing left/right, boom down/up, curl/uncurl bucket were requested. Only if they succeeded without making a mistake more than 15 times in a row, the participants could move onto the next session so that they could adapt to the basic manipulation as much as possible before the experiment task with time pressure levels.

Step 3. Task experiment session. At first, all participants performed excavation in the absence of time pressure. This measured time with no time pressure (NTP) was used as the reference time when applying the time pressure. In the low time pressure (LTP) task, participants were asked to finish the task at 90 percent of NTP time, 80 percent of NTP time for the medium time pressure (MTP) task, and 70 percent of NTP time for the high time pressure (HTP) task. During the experiments with time pressure, we tried to reduce the learning effect bias by randomizing the orders of time pressure levels for each participant (Fig. 4).

Step 4. After each task, the NASA TLX questionnaire was used to measure the cognitive load depending on the time pressure levels [13].

- Performance and cognitive load assessment

Performance related to human-robot interaction in a challenging environment was measured by the number of collisions and completion time. The participants were asked to rate their cognitive load with a 0 to 10 scales in six aspects (Mental Demand, Physical Demand, Temporal Demand, Self-rated Performance, Effort, and Frustration level).

IV. RESULT AND DISCUSSION

Given the relatively small number of participants in the pilot study, the mean of the preliminary outcomes may involve an interpretation error due to an outlier or a skewed distribution. Therefore, the analysis of the results was conducted with the median known as a better measure of central tendency rather than the mean.

A. Human-Robot Interaction (HRI) Performance

- Number of collisions

The number of collisions is a metric to measure the performance accuracy of manipulation. Collision refers to the case where the bucket of the excavator hit buried utilities during the experiment. Therefore, if the number of collisions is high, it means that more utility strikes have occurred, and in turn it means that the probability of leading to a dangerous accident increase. The smaller the number of collisions means the better human-robot interaction performance. When it comes to analyze the HRI performance depending on the time pressure level with a median value, it was observed that the HRI performance was the highest at low time pressure based on the collision number in the experiment result (Fig. 5). This is consistent with the Yerkes-Dodson Law that appropriate stress or arousal levels may improve performance [6].

Figure 5. Number of collisions under time pressure

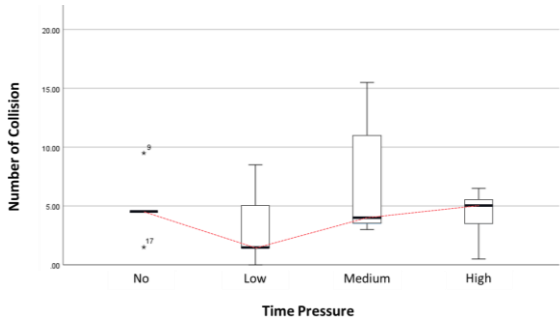
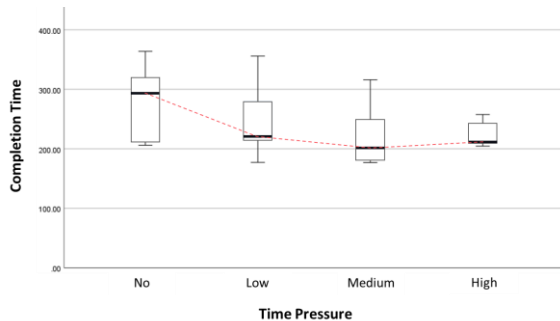


Figure 6. Completion time under time pressure



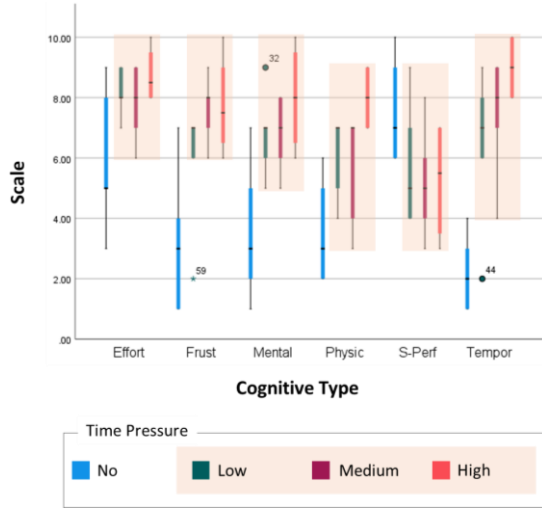
- *Completion time*

The completion time for the given tasks in the presence of time pressure (LTP, MTP, HTP) was relatively lower than that with NTP (Fig. 6). Especially the results of the LTP showed not only an improvement in HRI performance, but also a reduction in completion time in comparison with NTP. The participants in HTP got pressure to complete the task as fast as possible compared to other sessions with time pressure (LTP, MTP), however, it was observed that the completed time between MTP and HTP did not differ significantly (Fig. 6).

B. Cognitive load of the human operator

Participants were asked to answer the following questions after each task during the experiment. **Mental Demand** - Was the task easy or demanding, simple or complex? **Physical Demand** - How much physical activity was required (e.g., pushing, pulling, controlling, manipulating)? **Temporal Demand** - How much time pressure did you feel performing the task? **Self-rated Performance** - How successful or satisfied did you feel upon the performance or completion of the 0 to 10 given task? **Effort** - How hard did you have to work (mentally and physically) to accomplish your level 0 to 10 of performance? **Frustration Level** - How insecure, discouraged, stressed, and annoyed versus content, relaxed, and 0 to 10 complacent did you feel during the task? Overall, with time pressure, it was observed that the cognitive load is higher in proceeding with the excavation task near buried utilities compared to without time pressure (Fig. 7).

Figure 7. Cognitive load under time pressure (NASA-TLX)



V. CONCLUSION

In this study, we investigated how challenging work environments in construction sites (hazardous safety risks such as underground utilities and time pressures) affect human-robot interactions and the cognitive load of human operators during teleoperation. Such a challenging environment is a work environment frequently encountered by construction workers in the case of excavation. In particular, most of the safety accidents related to construction are accidents caused by less-skilled workers with less than 2 years of work experience in construction. Accordingly, in this study, human-robot interaction performance and cognitive load of novice operators were primarily investigated the case of teleoperation in a

challenging environment in a virtual environment. Overall experiments show that the challenging work environment with time pressure increases the individual's cognitive load and lowers the performance compared to working under no time pressure. Interestingly, the performance related to human-robot interaction has been improved given a reasonable time pressure (low time pressure). Therefore, for future research, it is necessary to conduct more in-depth studies taking into account the risk of the task, the difficulty of the task, and the different levels of time pressure. By doing so, we anticipate that this research will significantly contribute to the body of knowledge for human-robot interaction in a challenging environment during teleoperation.

ACKNOWLEDGMENT

This material is based upon work supported by the National Science Foundation under Grant No. 2026574. Any opinions, findings, and conclusions or recommendations expressed in this material are those of the author(s) and do not necessarily reflect the views of the National Science Foundation.

REFERENCES

- [1] J. S. Lee and Y. Ham, "Exploring Human-Machine Interfaces for Teleoperation of Excavator," pp. 757–765, Mar. 2022, doi: 10.1061/9780784483961.079.
- [2] J. S. Lee, Y. Ham, H. Park, and J. Kim, "Challenges, tasks, and opportunities in teleoperation of excavator toward human-in-the-loop construction automation," *Automation in Construction*, vol. 135, p. 104119, Mar. 2022, doi: 10.1016/j.autcon.2021.104119.
- [3] M. Ito, C. Raima, S. Saiki, Y. Yamazaki, and Y. Kurita, "Effects of machine instability feedback on safety during digging operation in teleoperated excavators," *IEEE Access*, vol. 9, pp. 28987–28998, 2021.
- [4] J. W. Payne, J. R. Bettman, and E. J. Johnson, *The Adaptive Decision Maker*. Cambridge: Cambridge University Press, 1993. doi: 10.1017/CBO9781139173933.
- [5] Y. Han, Y. Diao, Z. Yin, R. Jin, J. Kangwa, and O. J. Ebohon, "Immersive technology-driven investigations on influence factors of cognitive load incurred in construction site hazard recognition, analysis and decision making," *Advanced Engineering Informatics*, vol. 48, p. 101298, Apr. 2021, doi: 10.1016/j.aei.2021.101298.
- [6] R. M. Yerkes and J. D. Dodson, "The relation of strength of stimulus to rapidity of habit-formation," *J. Comp. Neurol. Psychol.*, vol. 18, no. 5, pp. 459–482, Nov. 1908, doi: 10.1002/cne.920180503.
- [7] G. Phillips-Wren and M. Adya, "Decision making under stress: the role of information overload, time pressure, complexity, and uncertainty," *Journal of Decision Systems*, vol. 29, no. sup1, pp. 213–225, Aug. 2020, doi: 10.1080/12460125.2020.1768680.
- [8] S. Coegnet, J. Navet, P. Antoine, and F. Anceaux, "Time pressure and driving: Work, emotions and risks," *Transportation Research Part F: Traffic Psychology and Behaviour*, vol. 20, pp. 39–51, Sep. 2013, doi: 10.1016/j.trf.2013.05.002.
- [9] A. Szollos, "Toward a psychology of chronic time pressure: Conceptual and methodological review," *Time & Society*, vol. 18, no. 2–3, pp. 332–350, Sep. 2009, doi: 10.1177/0961463X09337847.
- [10] R. A. Karasek, "Job Demands, Job Decision Latitude, and Mental Strain: Implications for Job Redesign," *Administrative Science Quarterly*, vol. 24, no. 2, pp. 285–308, 1979, doi: 10.2307/2392498.
- [11] S. Pooladvand, B. Kiper, A. Mane, and S. Hasanzadeh, "Effect of Time Pressure and Cognitive Demand on Line Workers' Risk-Taking Behaviors: Assessment of Neuro-Psychophysiological Responses in a Mixed-Reality Environment," pp. 759–769, Mar. 2022, doi: 10.1061/9780784483985.077.
- [12] Y. Fang, Y. K. Cho, F. Durso, and J. Seo, "Assessment of operator's situation awareness for smart operation of mobile cranes," *Automation in Construction*, vol. 85, pp. 65–75, Jan. 2018, doi: 10.1016/j.autcon.2017.10.007.
- [13] S. G. Hart, "NASA task load index (TLX)," 1986.